SUPPLEMENTAL MATERIALS

ASCE *Journal of Sustainable Water in the Built Environment*

Effects of Design and Climate on Bioretention Effectiveness for Watershed-Scale Hydrologic Benefits

Roderick W. Lammers, Laura Miller, and Brian P. Bledsoe

DOI: 10.1061/JSWBAY.0000993

Supplemental Material for

Effects of design and climate on bioretention effectiveness for watershed-scale hydrologic benefits

Table of Contents

Rainfall Regions

Table S1 summarizes the nine precipitation metrics used in the rainfall region analysis. Briefly, monthly average PET was calculated based on (Hamon, 1960):

$$E_p = 25.4 * CD^2 P_t$$

Where E_p is the potential ET in mm (converted from inches by multiplying by 25.4), C is a coefficient (0.0055 after Hamon), D is the hours of daily sunshine in units of 12 hours, and P_t is the saturated water vapor concentration at the mean temperature in g/m^3:

$$P_t = 216.7 * \frac{E_{sat}}{T_{mean} + 273.3}$$

$$E_{sat} = 6.108 * exp(17.26939 * \frac{T_{mean}}{T_{mean} + 237.3})$$

Where E_{sat} is the saturated vapor pressure (mb) and T_{mean} is the daily mean temperature (C) (Lu et al., 2005). D was calculated for each point based on latitude using the *insol* R package (Corripio, 2019).

Each parameter was calculated for each of the 481,631 4x4 km grid cells from the PRISM database. These rasters were then aggregated to a 20x20 km grid. We then used cluster analysis to separate the conterminous US into regions based on similarity in these precipitation parameters. Clustering attempts to group data so that differences within groups are small and differences between groups are large. We used the Clustering Large Applications (clara) algorithm implemented in the *cluster* R package (Maechler et al., 2019). This is similar to traditional kmeans clustering approaches, but is better suited for large datasets and is less sensitive to outliers. The main difference is that clara uses the medoids of repeated samples of data to create clusters, whereas kmeans uses the mean of the full dataset. We used the clara method to create a series of 8 clusters. This number was based off iterations with different clustering sizes, and was chosen to maximize cluster dissimilarity while being small enough for

interpretation. The performance of the clustering algorithm was also not ideal, with an average silhouette width of 0.3. Values closer to one indicate better performance. However, these regions still represent broad trends in precipitation patterns that are useful for stormwater design.

Figure S1 shows the spatial variability in the precipitation metrics used in the clustering analysis. Figure S2 shows violin plots illustrating differences in precipitation metrics between different regions.

Table S1. Precipitation metrics used the regional precipitation analysis. All metrics were calculated using PRISM monthly climate normals data or daily precipitation data from 1981-2010.

Metric	Description	Source/Methods
Annual PPT	Average annual precipitation (1981-2010 climate normals) in mm	PRISM monthly climate normals precipitation
PPT - PET	Annual PPT – average annual potential evapotranspiration	PRISM monthly climate normals precipitation and average temperature, PET estimated using the Hamon (1960) method
Snow PPT / Annual PPT	Fraction of average annual precipitation that fell as snow	PRISM monthly climate normal PPT and temp (assumed snow if temp < 0 C)
Seasonality index	An index describing the seasonality of precipitation (0 – 1.83), where higher values indicate higher seasonality	Walsh and Lawler (1981): $SI = \frac{1}{\bar{R}} \sum_{n=1}^{12} \lvert \bar{p}_n - \bar{R}/12 \rvert$ $\bar{R}$ = mean annual rainfall $\bar{p}_n$= mean monthly rainfall PRISM monthly normals
Summer PPT / Annual PPT	Fraction of annual precipitation that fell in June – August (a value of 0.25 would mean precipitation is relatively uniform seasonally)	PRISM monthly normals
Num Days w/ PPT	Average number of days per year with precipitation >1 mm	PRISM daily precipitation (1981-2010)
Num Days Intense PPT	Average number of days per year with 25.4 mm < precipitation < 76.2 mm*	PRISM daily precipitation (1981-2010)
Num Days Very Intense PPT	Average number of days per year with precipitation >= 76.2 mm*	PRISM daily precipitation (1981-2010)
Inter-storm Dur. [days]	Annual average length of time between days with >1 mm of precipitation	PRISM daily precipitation (1981-2010)

*Intensity thresholds from (Dourte et al., 2015)

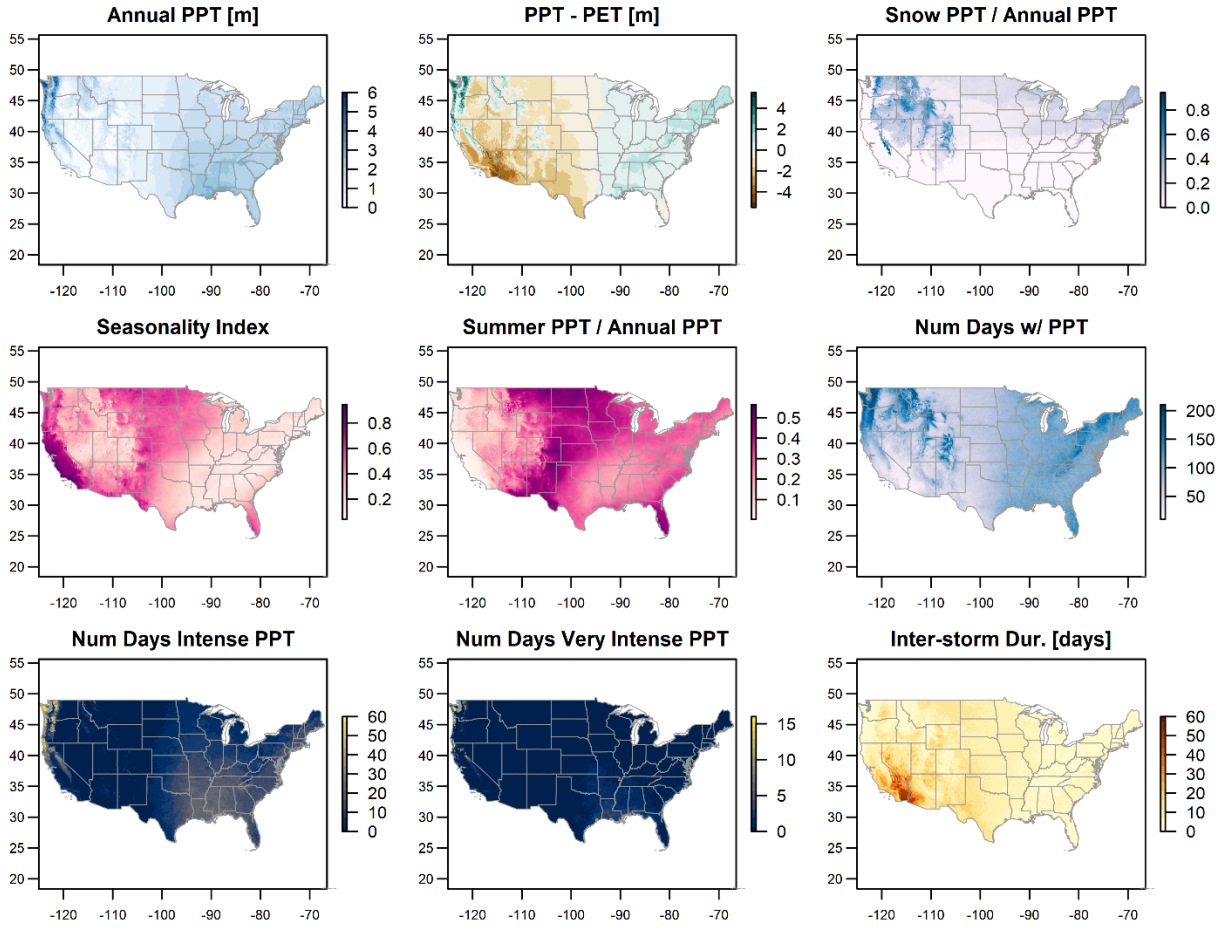

Figure S1. Various quantified precipitation metrics on a 20x20 km grid for the conterminous US. All metrics (see Table S1) were quantified using PRISM data.

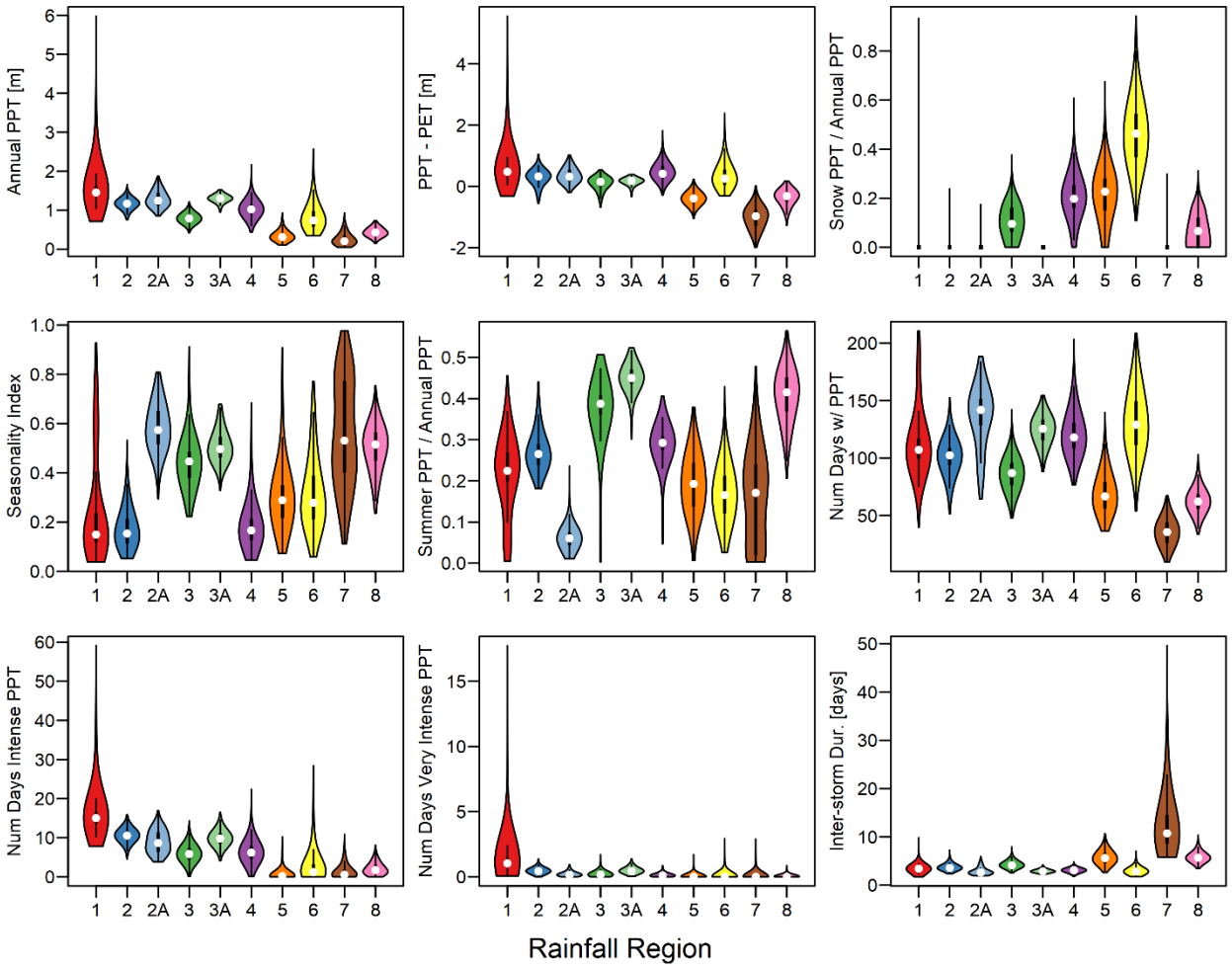

Figure S2. Violin plots of how each precipitation metric varies by region.

Modifications to Lee et al. SWMM Model

We made several modifications to the SWMM model provided by Lee et al. (2018). The primary changes were made to prevent errors in the model mass balance for both flooding and groundwater modeling.

To prevent water loss from flooding, we allowed ponding in the SWMM model and extended the depth-discharge relationships of the existing stormwater control ponds. In addition, we deepened the trapezoidal stream channels to prevent excess flooding loss.

The model provided by Lee et al. had some significant groundwater mass balance errors. To remedy this, we changed several parameters:

- We set the minimum depth for groundwater flow to occur to the bottom elevation of each sub-basin's outlet junction
- We set the depth of evaporation for the saturated zone to zero
- We set the groundwater flow parameters A1 and B1 to 10 and 2, respectively

We also set all pervious areas to drain to the sub-basin outlet, rather than draining to the impervious portion of the sub-basin. For the continuous simulation modeling, we allowed the model to calculated evapotranspiration using daily temperature and wind speed data. We also allowed snowfall (if air temperature was below 34 degrees F). All other snowfall parameters were set to model defaults. There was no snow removal modeled. These changes reduced mass balance errors in the model to close to zero and only slightly reduced the accuracy of the model calibration.

We determined the accuracy of the modified model by comparing simulated and observed flows at the watershed outlet for July 2009 – August 2009 (using the same observed rainfall and streamflow data used by Lee et al. (2018) in the original model calibration). Overall performance was essentially unchanged (Figure S3). We found a Nash-Sutcliffe coefficient of 0.853 and R^2 of 0.861, compared to Lee et al. (2018)'s values of 0.852 and 0.871. Our model underpredicted total runoff volume by 11.6%.

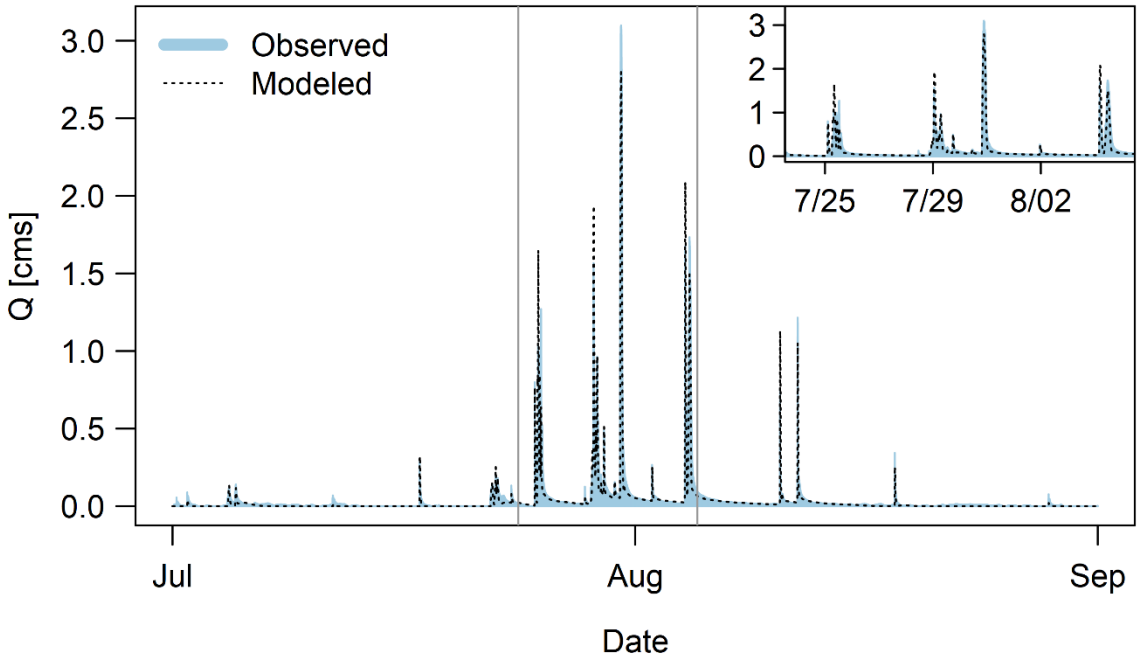

Figure S3. Observed and modeled flow rate at the watershed outlet for 1 July 2009 through 31 August 2009. Observed precipitation and flow data from Lee et al. (2018). Inset graph shows flows from 24 July through 05 August to better see differences in observe and modeled hydrographs during these large runoff events.

Bioretention Modeling

Table S2 shows the details of the bioretention areas modeled in SWMM. Figure S4 shows the conceptual modeling layout for each sub-basin.

Table S2. Bioretention model parameters.

	High soil (loamy sand)	Med soil (loam)	Low soil (clay loam)	Source
Surface parameters				
Surface berm height ($d_{ponding}$)	7.6 cm (3 in)	--	--	Assumed
Vegetation volume fraction	0	--	--	Assumed
Surface Manning's n	0	--	--	Assumed
Surface slope	0	--	--	Assumed
Soil parameters				
Thickness (d_{soil})	45.7 cm (18 in)	--	--	Assumed
Porosity (θ)	0.437	0.463	0.464	SWMM Users Guide
Field capacity (FC)	0.105	0.232	0.31	SWMM Users Guide
Wilting point (WP)	0.047	0.116	0.187	SWMM Users Guide
Conductivity	3.0 cm/hr (1.18 in/hr)	0.33 cm/hr (0.13 in/hr)	0.10 cm/hr (0.04 in/hr)	SWMM Users Guide
Conductivity Slope	46.9	36.2	46.6	SWMM Users Guide
Suction head	6.1 cm (2.4 in)	8.9 cm (3.5 in)	21 cm (8.27 in)	SWMM Users Guide
Storage parameters				
Thickness ($d_{storage}$)	30.5 cm (12 in)	--	--	Assumed
Void ratio (VR)	0.75	--	--	SWMM Users Guide
Seepage rate	0.089 cm/hr (0.035 in/hr)	--	--	Underlying soil infiltration rate
Clogging factor	0	--	--	Assumed
Drain parameters				
Flow coefficient	0.1273	--	--	Calculated to drain in 72 hrs
Flow exponent	0.5	--	--	SWMM Users Guide
Offset	30.5 cm (12 in)	--	--	Assumed
Total Water Storage Depth	38.6 cm (15.2 in)	36.6 cm (14.4 in)	33.3 cm (13.1 in)	Calculated*

*Water storage depth calculated as: $d_{ponding} + d_{storage} * \left(\frac{VR}{1+VR}\right) + d_{soil} * (\theta - WP)$

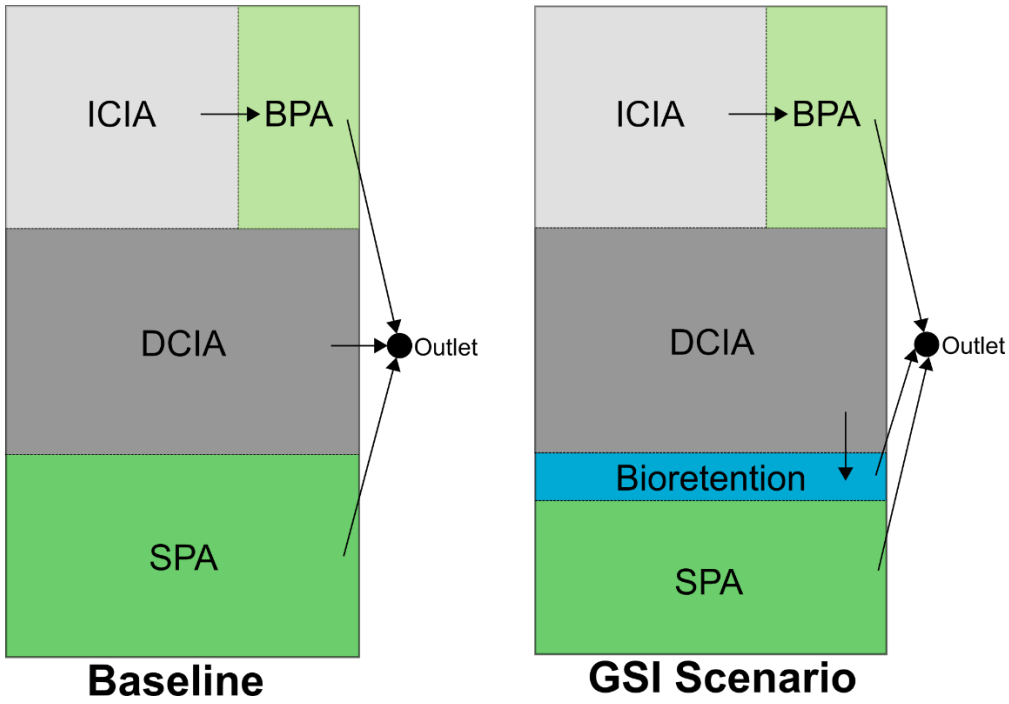

Figure S4. Schematic of the basic modeling structure for each sub-basin in the baseline scenarios (left) and GSI scenarios (right). Arrows denote flow direction. ICIA: indirectly-connected impervious area, BPA: buffering pervious area, DCIA: directly-connected impervious area, SPA: stand-alone pervious area. For the GSI scenarios, the size of the bioretention area varies but always results in a reduction in the size of the SPA. Figure adapted from Lee et al. (2018).

Additional Results

Figure S5 shows difference in peak flow and volume reduction for the design storm analysis. Volume reduction is generally larger than peak flow reduction, especially for larger storm events. For high infiltration soils, there are more instances where peak reduction is greater. Figure S6 shows that adding GSI in the continuous simulations consistently increased groundwater flow into surface channels, helping explain why we did not see as large of reductions in runoff volume at the watershed scale as at the sub-basin scale. Infiltrating water mostly went to this groundwater flow or was evaporated from the soil. Less than 1% in all simulations percolated to deep groundwater. Subsequent figures show detailed results by city for the design storm (Figures S7-S42) and continuous simulation analyses (Figures S43-S60).

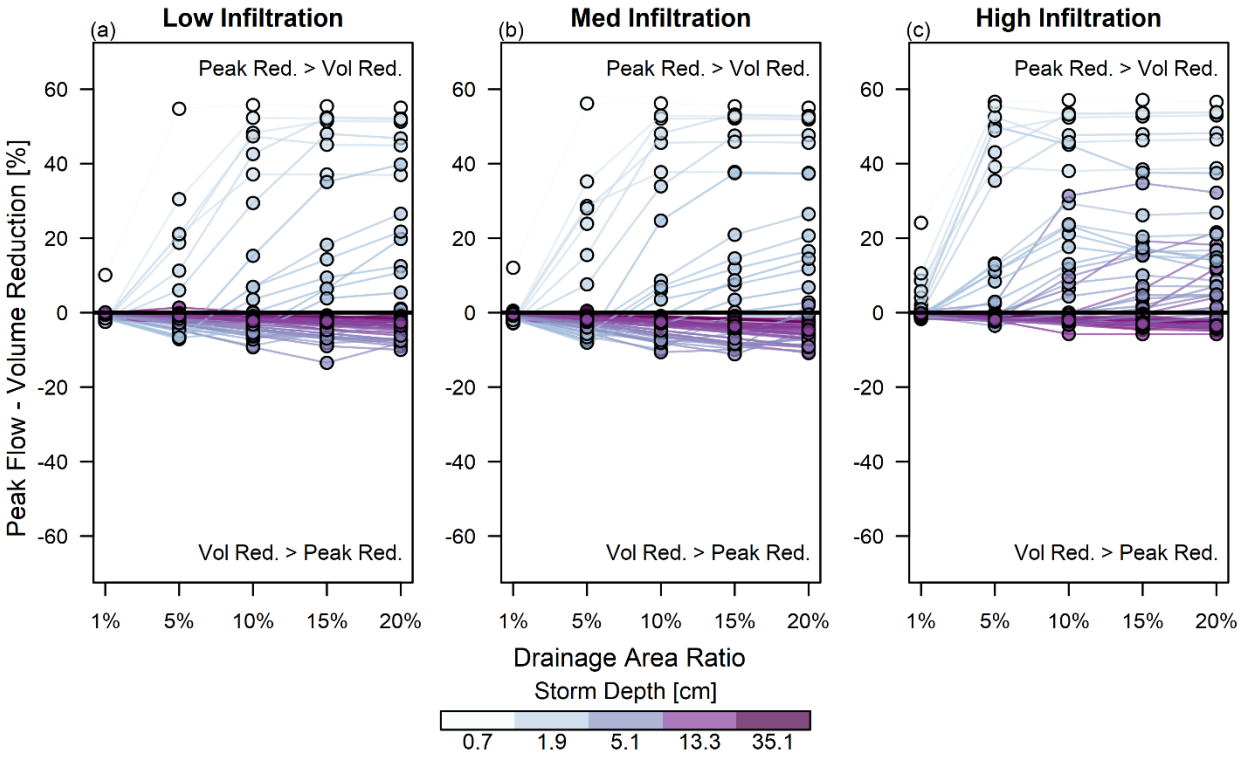

Figure S5. Summary plot of the difference between reduction in peak flow and runoff volume by DAR and storm event depth.

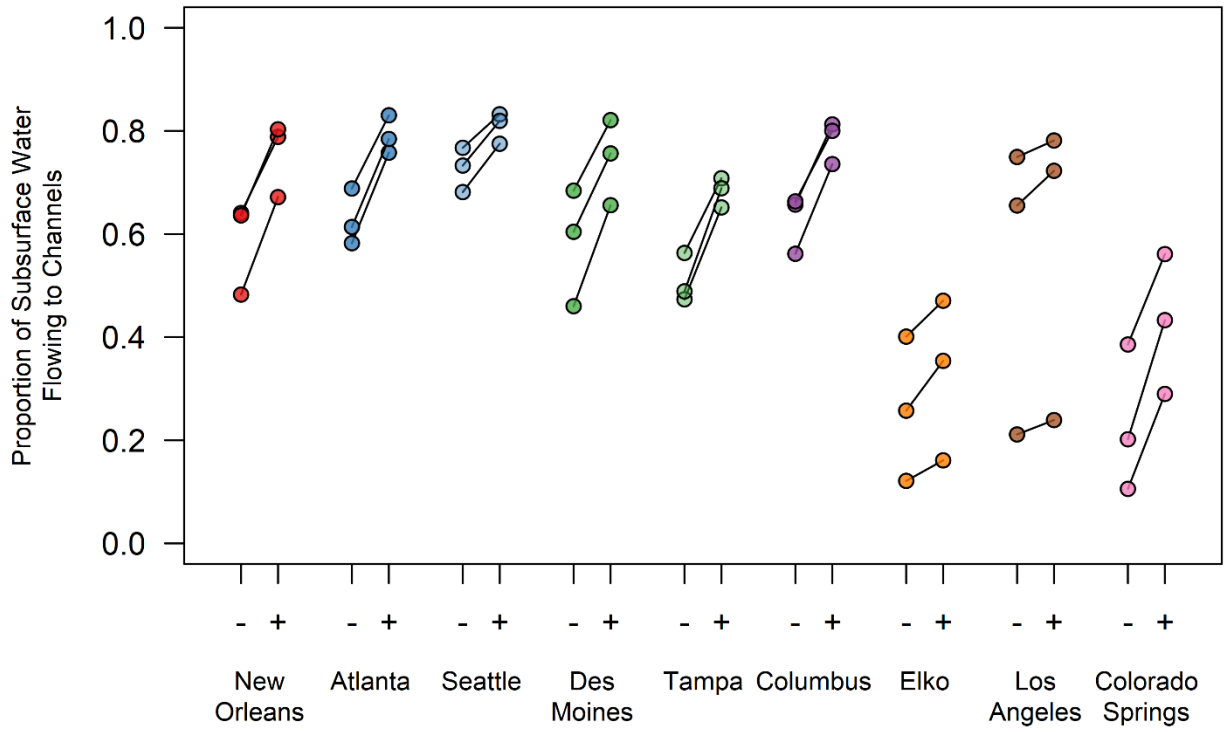

Figure S6. Increase in the proportion of subsurface water flowing to surface channels with (+) versus without (-) GSI for continuous simulations in all cities (points are for wet, normal, and dry years). Only GSI scenarios with high infiltration soils are shown, although there was little difference between soil types.

Additional Results from Design Storm Simulations

Results from event-scale analysis of GSI scenarios for nine cities from different rainfall regions in the continental US. Individual hydrographs are shown for each rainfall event with lines for different GSI scenarios (bioretention drainage area ratios). Three sets of hydrographs are produced - one for high, medium, and low bioretention soil infiltration rates. Furthermore, performance plots for each city and soil type are included, showing the reductions in peak flows and runoff volumes for the different rainfall events and different GSI scenarios.

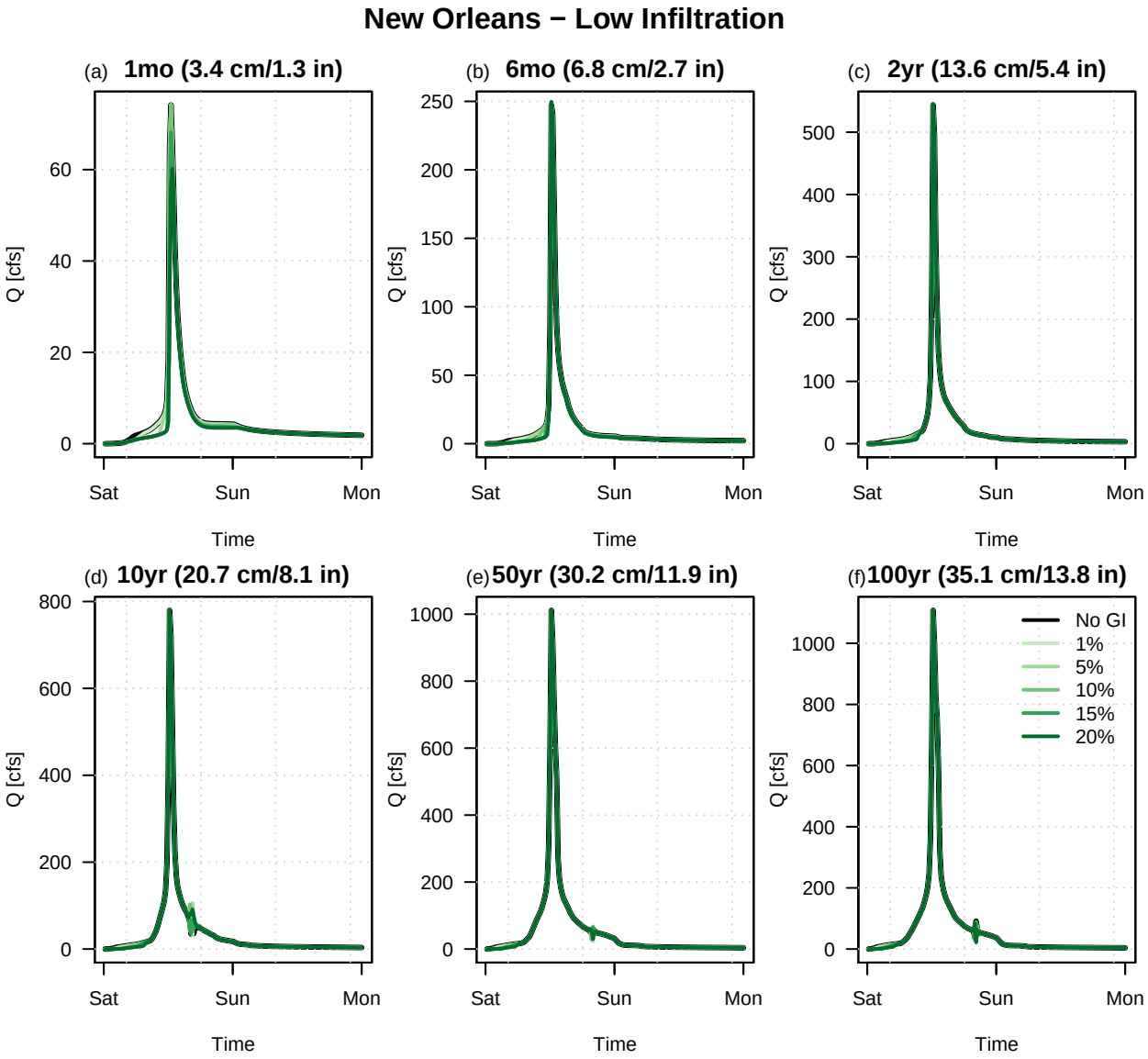

Figure S7: Simulated hydrographs at the watershed outlet for the baseline and GSI scenarios for the 1-month (a), 6-month (b), 2-year (c), 10-yr (d), 50-yr (e), and 100-yr (f) storm events.

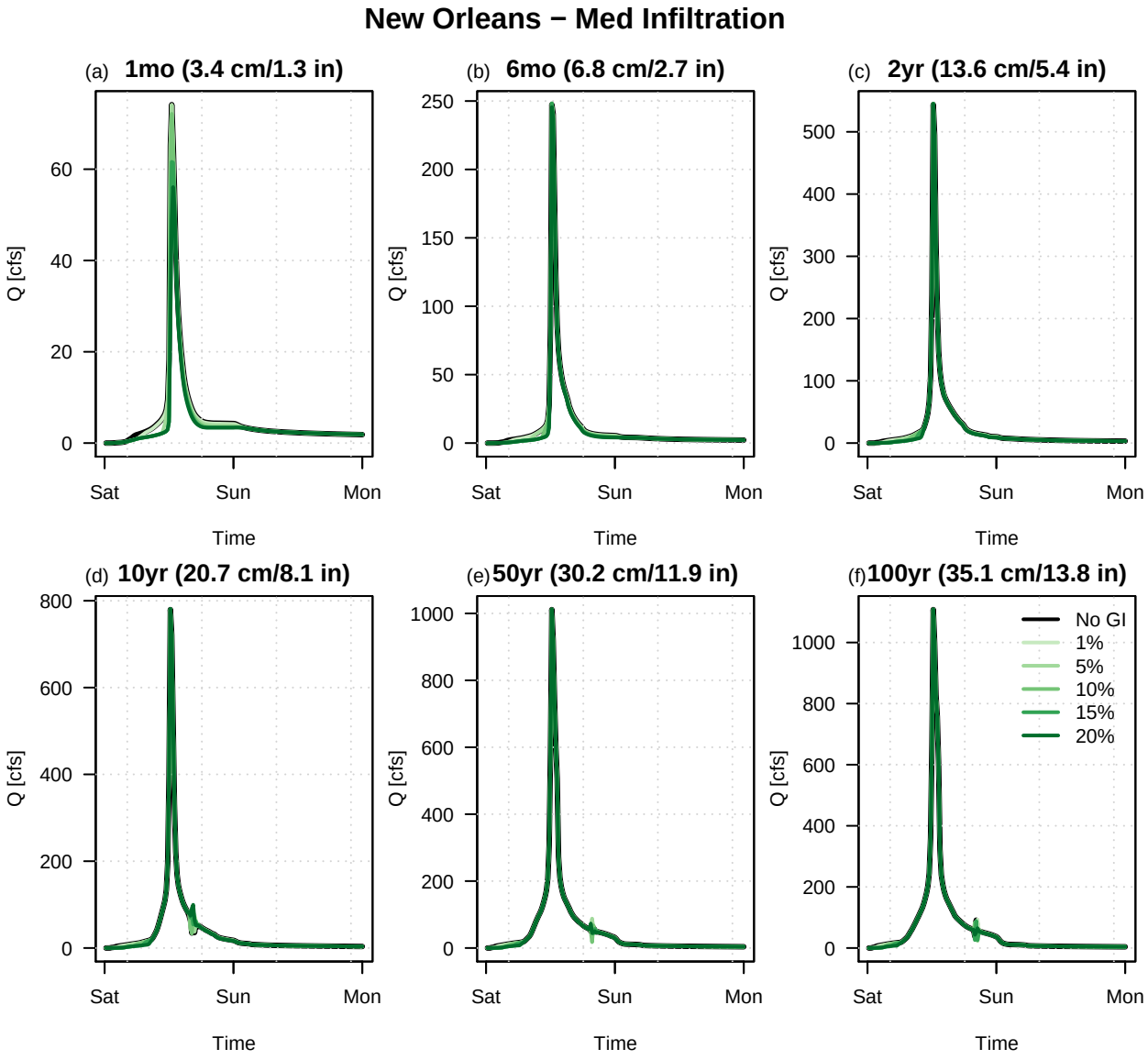

Figure S8: Simulated hydrographs at the watershed outlet for the baseline and GSI scenarios for the 1-month (a), 6-month (b), 2-year (c), 10-yr (d), 50-yr (e), and 100-yr (f) storm events.

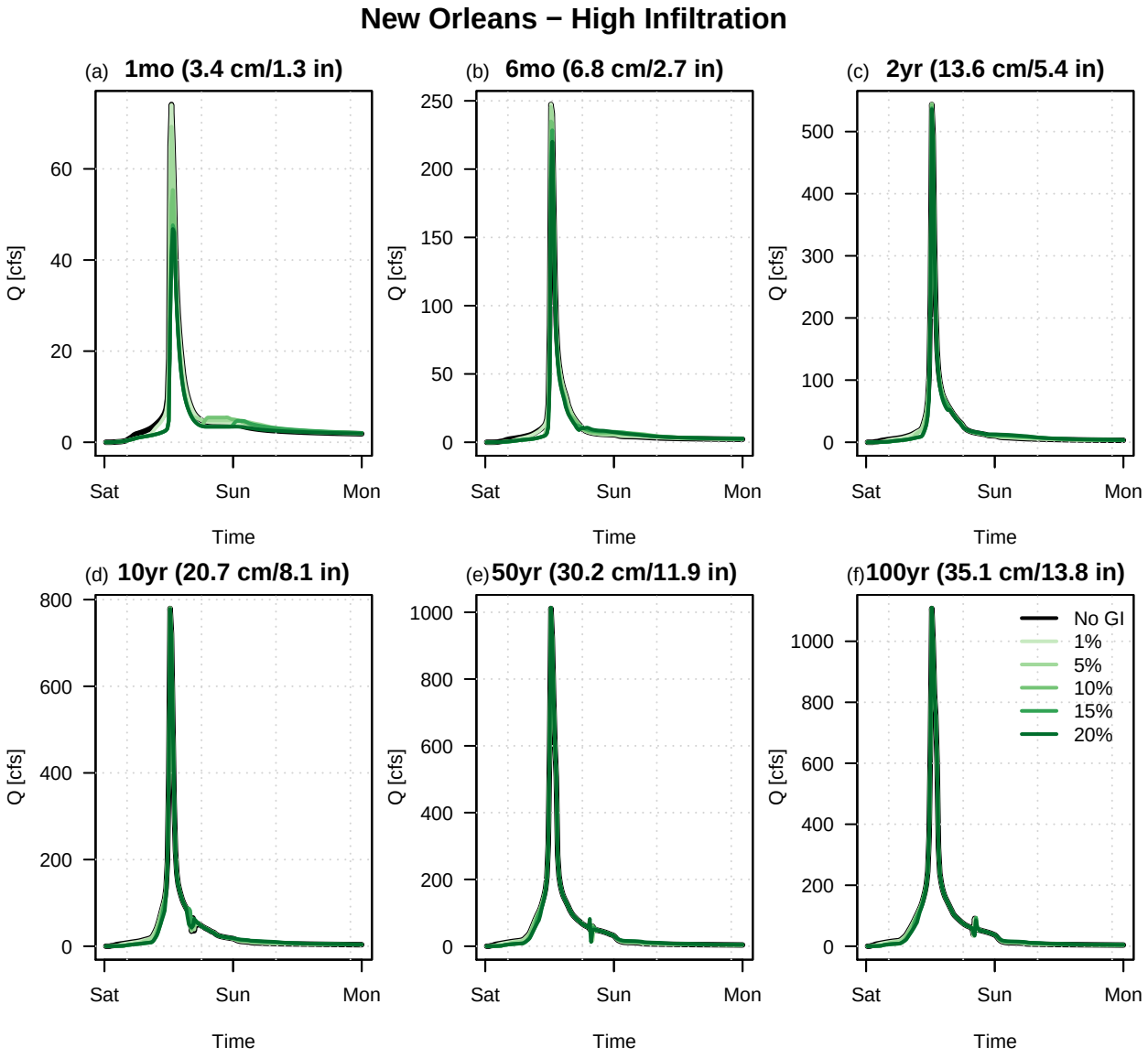

Figure S9: Simulated hydrographs at the watershed outlet for the baseline and GSI scenarios for the 1-month (a), 6-month (b), 2-year (c), 10-yr (d), 50-yr (e), and 100-yr (f) storm events.

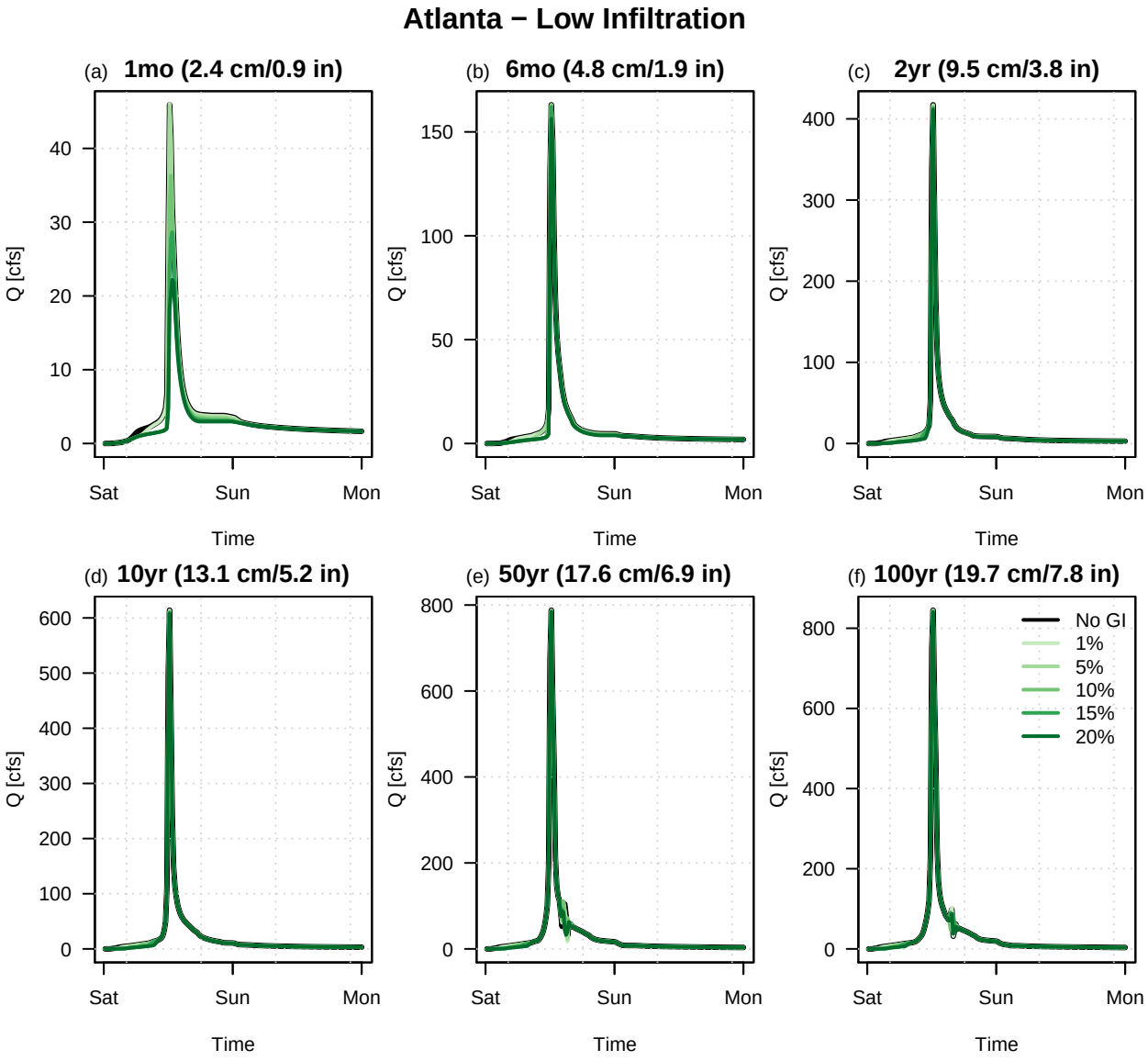

Figure S10: Simulated hydrographs at the watershed outlet for the baseline and GSI scenarios for the 1-month (a), 6-month (b), 2-year (c), 10-yr (d), 50-yr (e), and 100-yr (f) storm events.

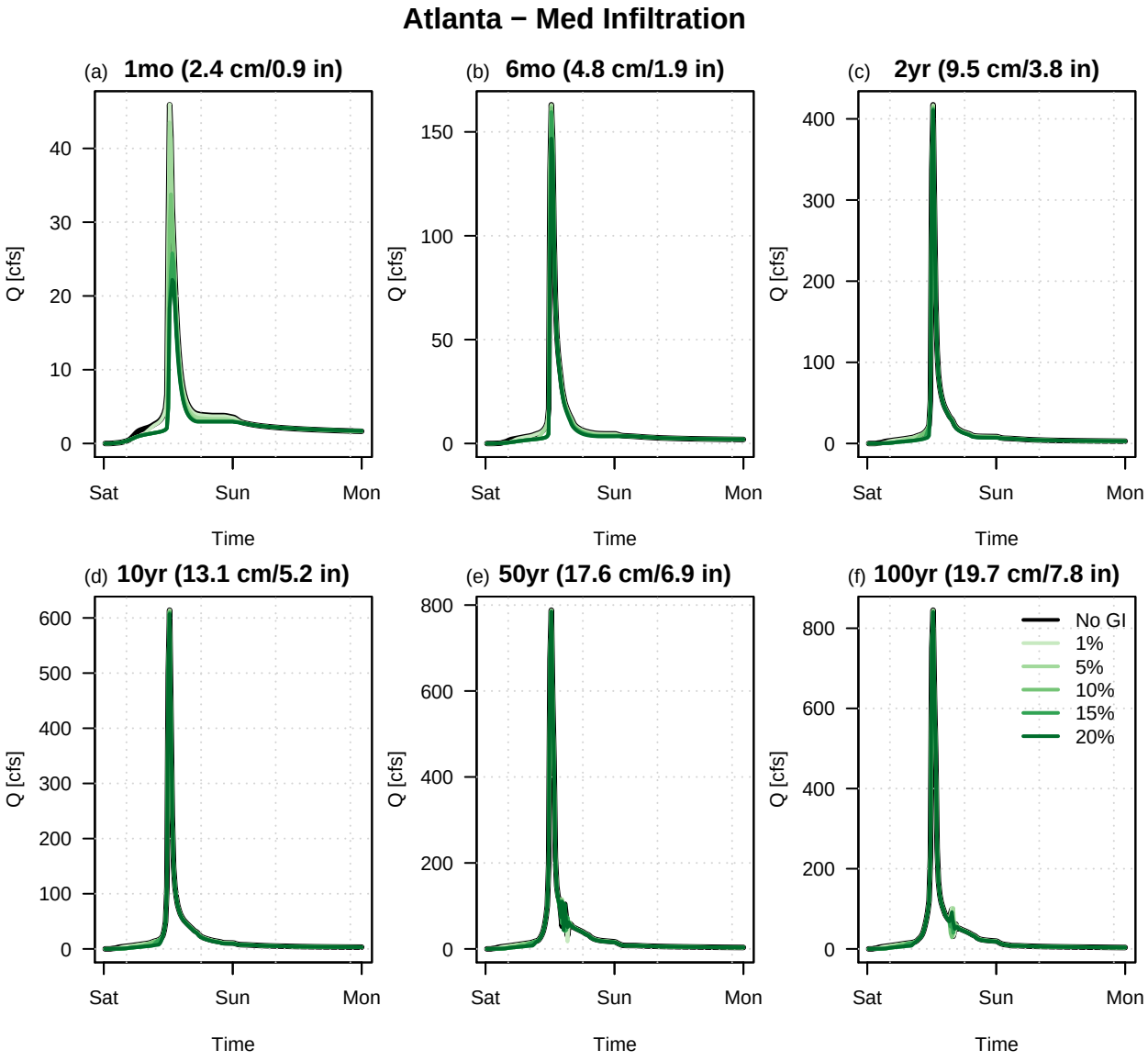

Figure S11: Simulated hydrographs at the watershed outlet for the baseline and GSI scenarios for the 1-month (a), 6-month (b), 2-year (c), 10-yr (d), 50-yr (e), and 100-yr (f) storm events.

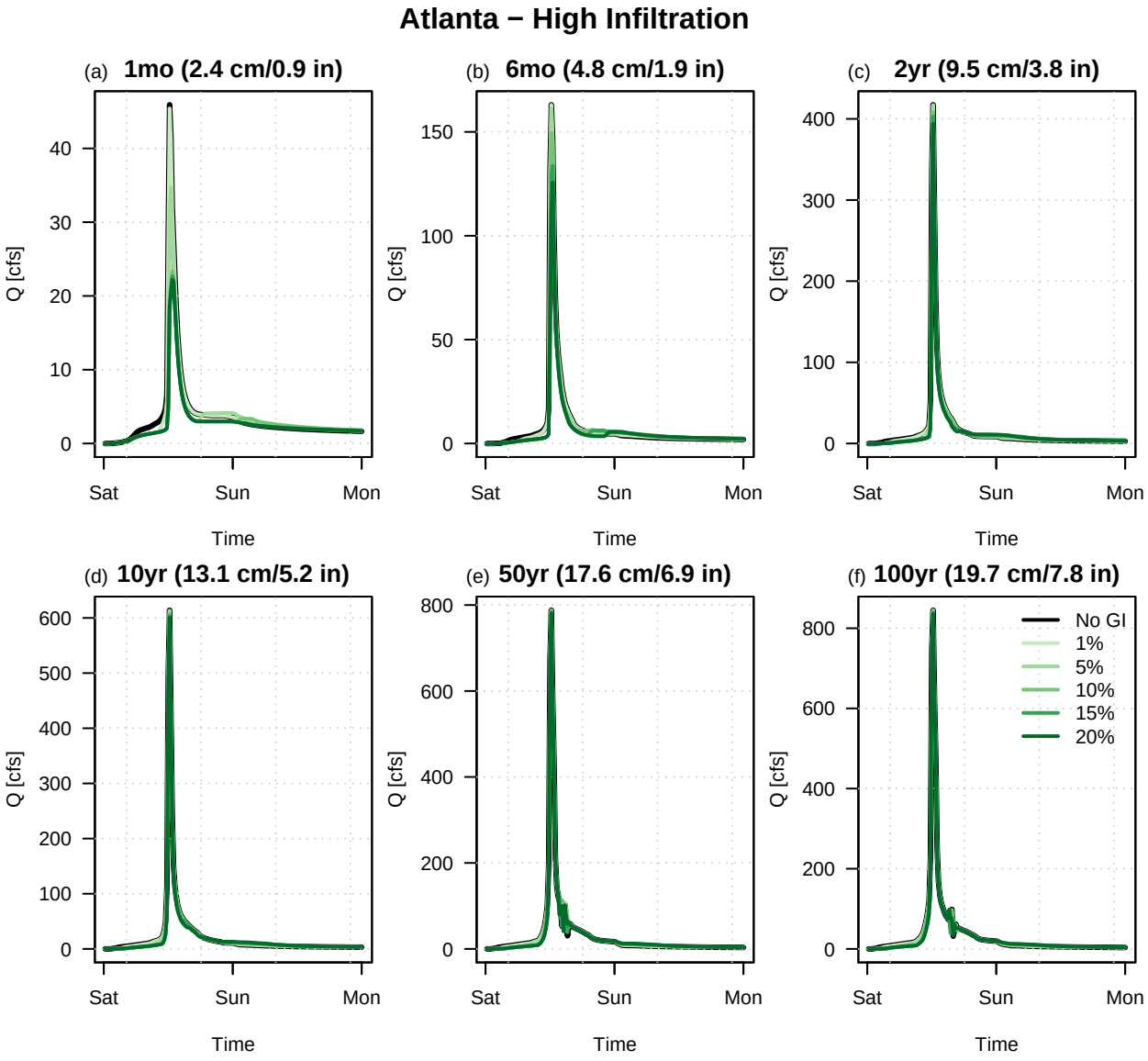

Figure S12: Simulated hydrographs at the watershed outlet for the baseline and GSI scenarios for the 1-month (a), 6-month (b), 2-year (c), 10-yr (d), 50-yr (e), and 100-yr (f) storm events.

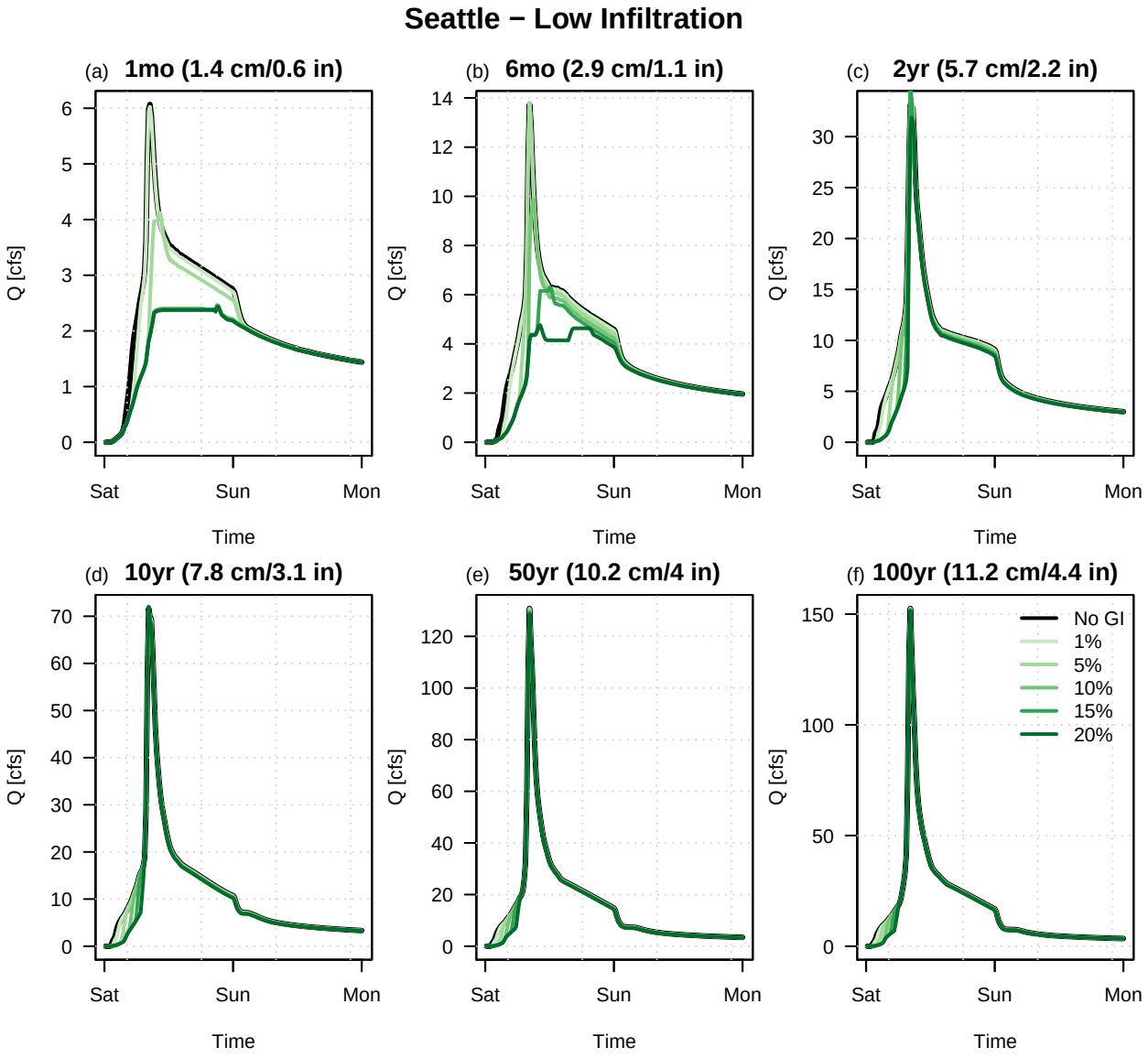

Figure S13: Simulated hydrographs at the watershed outlet for the baseline and GSI scenarios for the 1-month (a), 6-month (b), 2-year (c), 10-yr (d), 50-yr (e), and 100-yr (f) storm events.

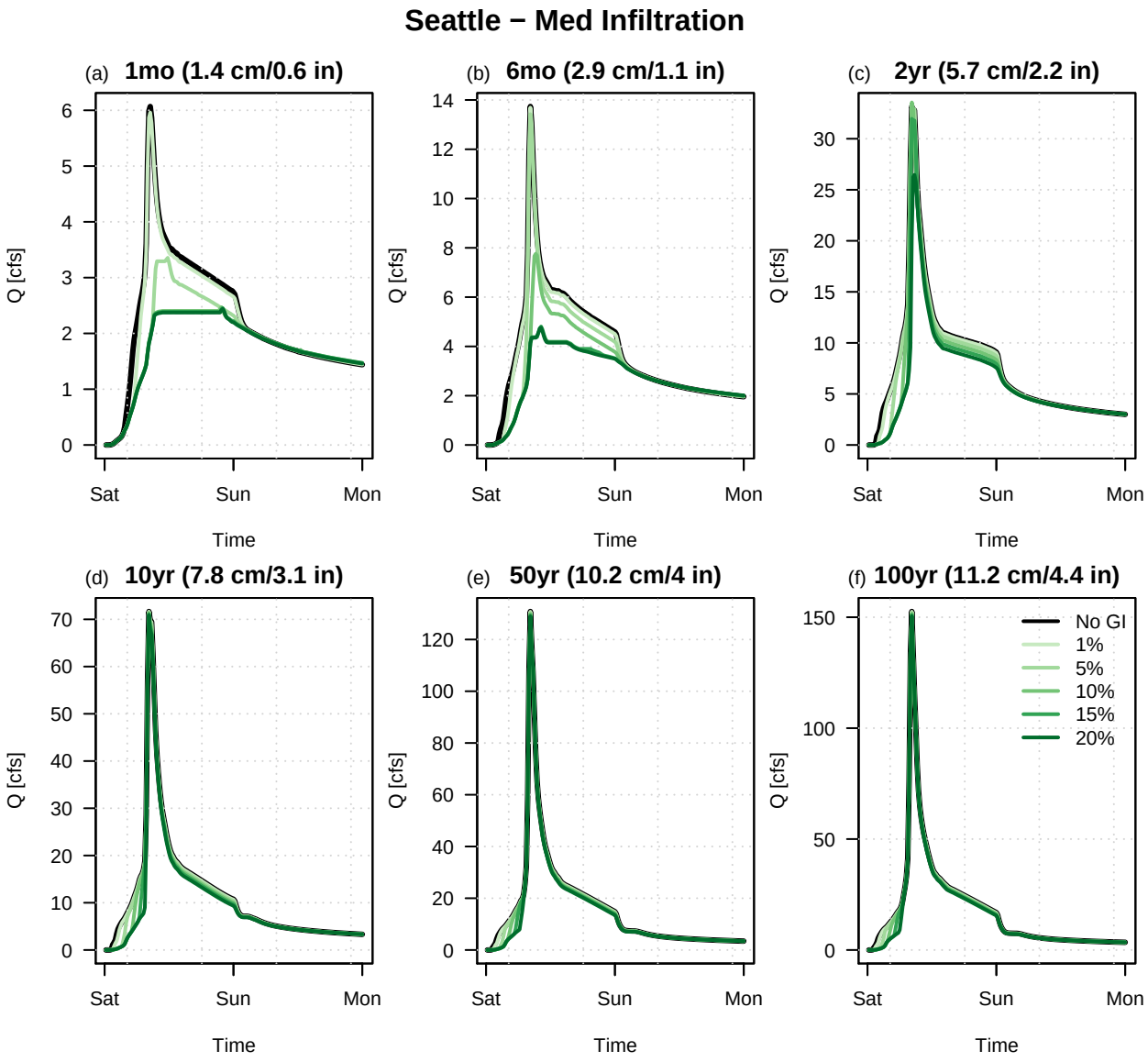

Figure S14: Simulated hydrographs at the watershed outlet for the baseline and GSI scenarios for the 1-month (a), 6-month (b), 2-year (c), 10-yr (d), 50-yr (e), and 100-yr (f) storm events.

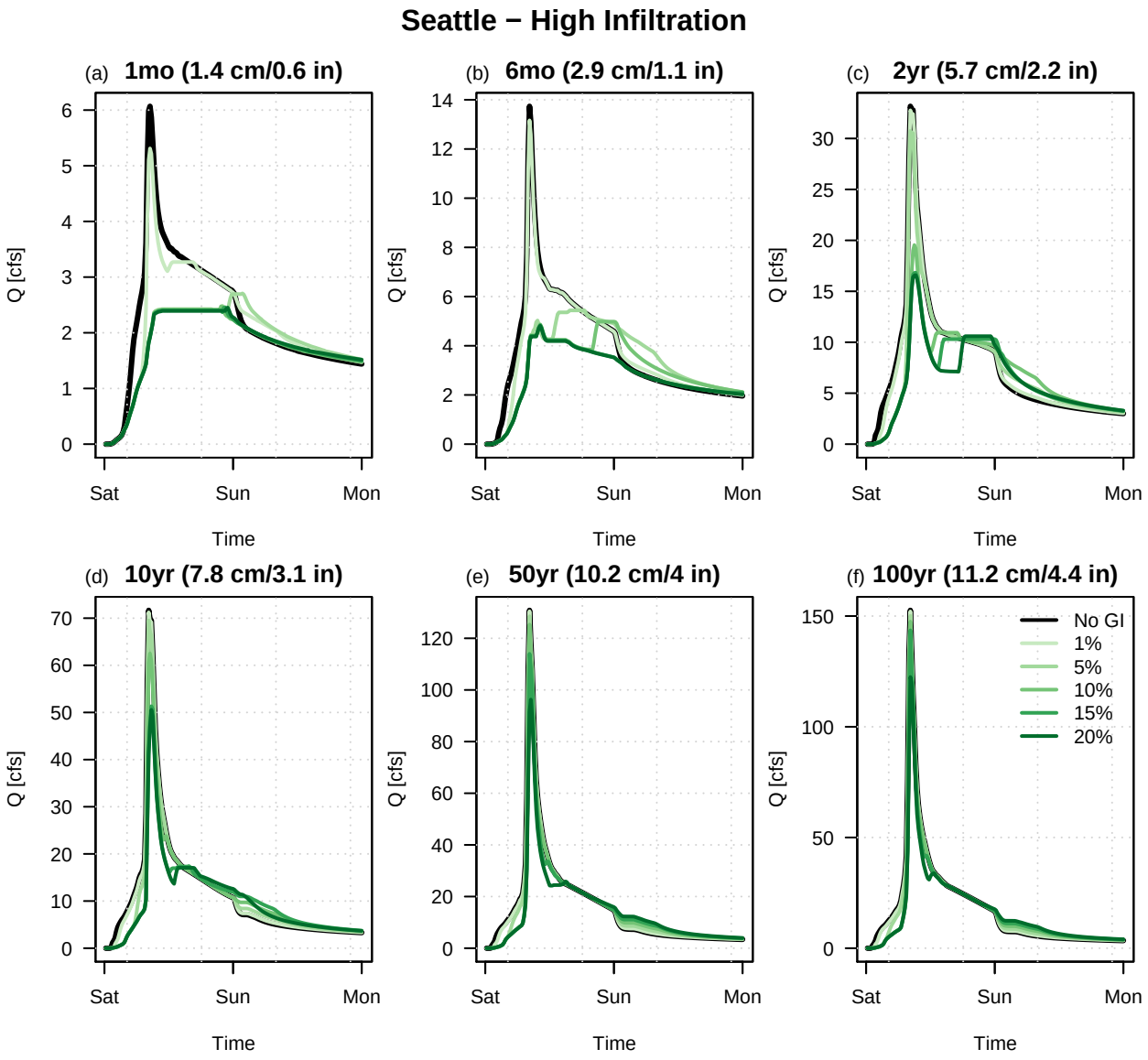

Figure S15: Simulated hydrographs at the watershed outlet for the baseline and GSI scenarios for the 1-month (a), 6-month (b), 2-year (c), 10-yr (d), 50-yr (e), and 100-yr (f) storm events.

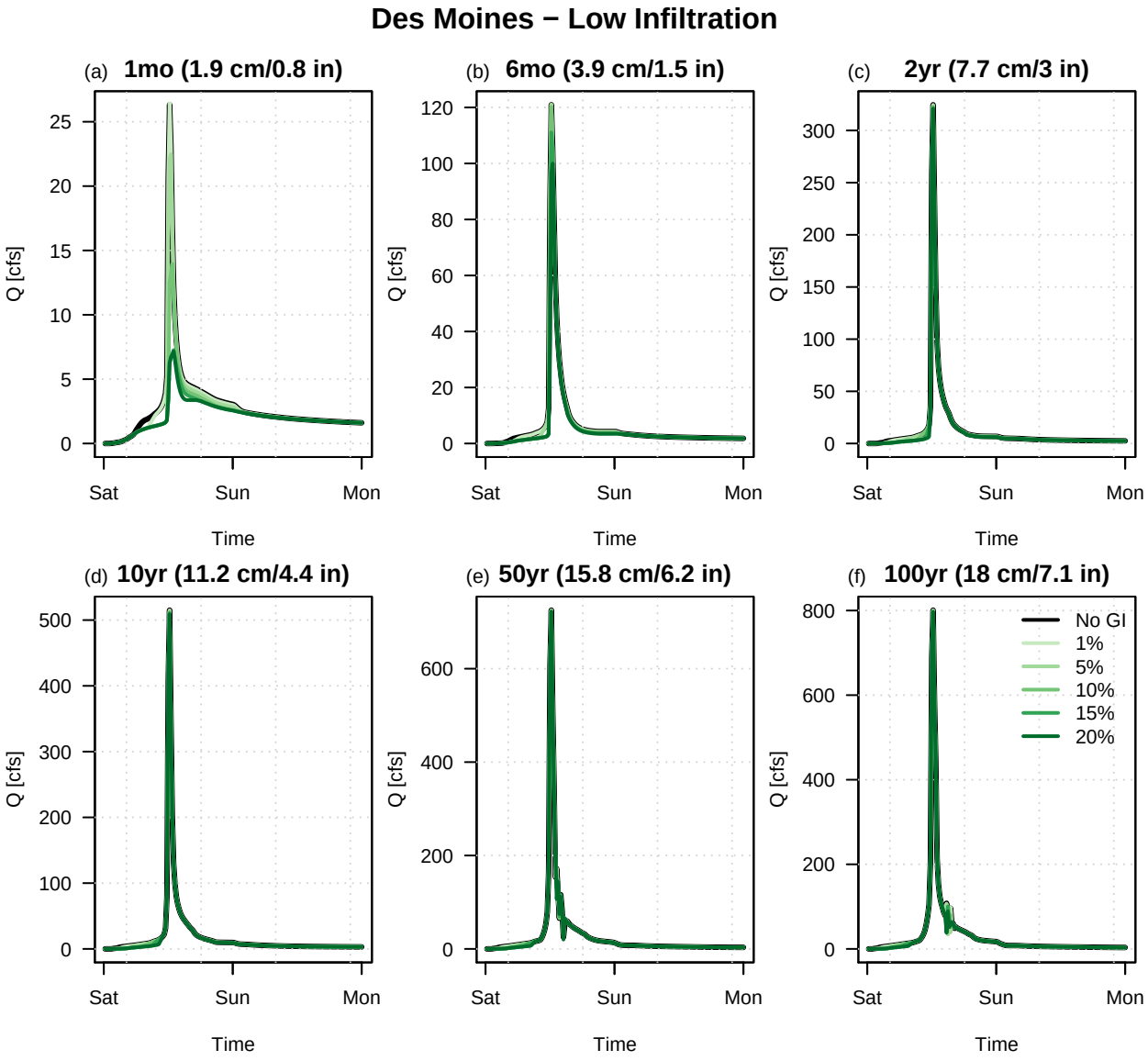

Figure S16: Simulated hydrographs at the watershed outlet for the baseline and GSI scenarios for the 1-month (a), 6-month (b), 2-year (c), 10-yr (d), 50-yr (e), and 100-yr (f) storm events.

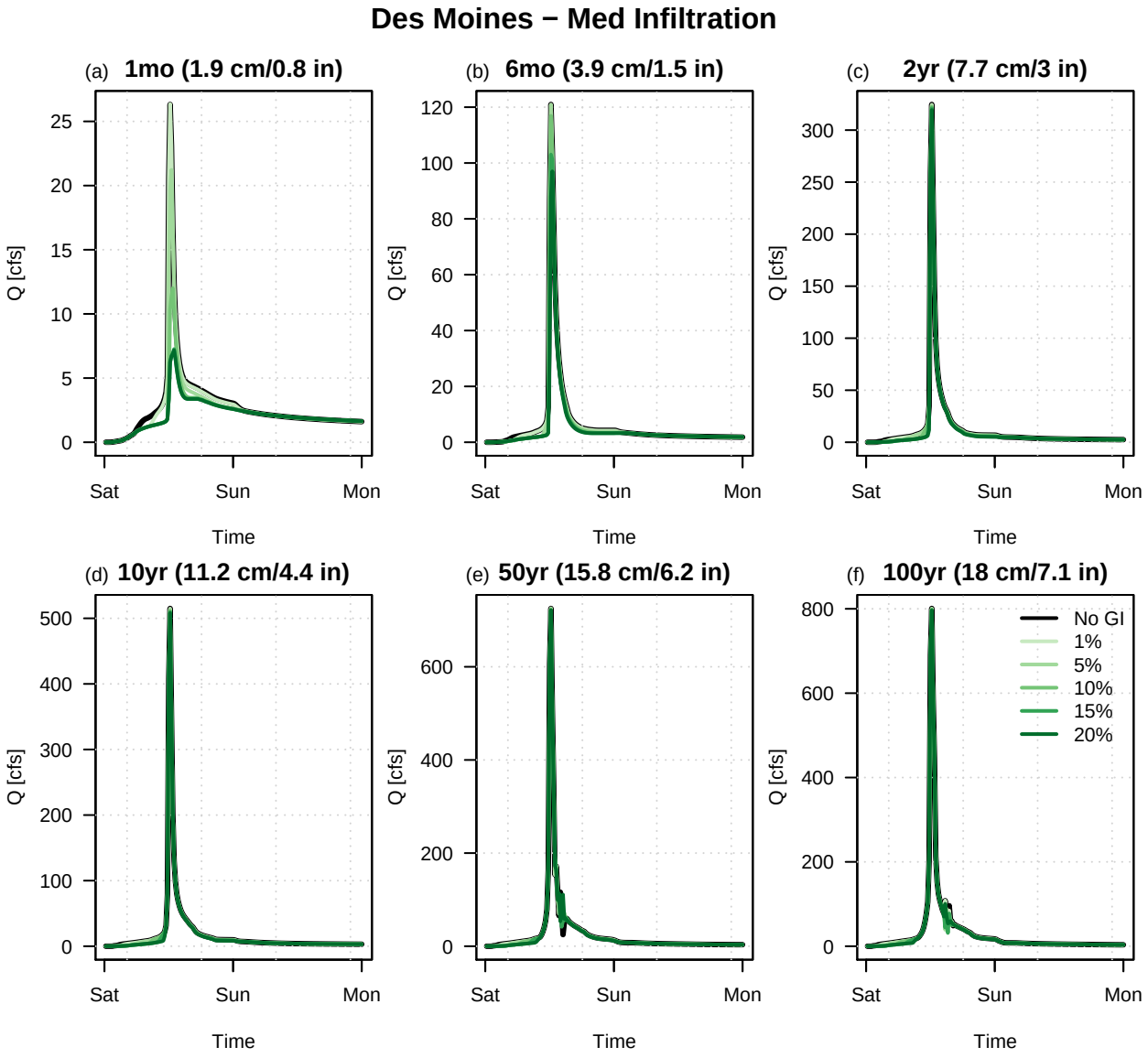

Figure S17: Simulated hydrographs at the watershed outlet for the baseline and GSI scenarios for the 1-month (a), 6-month (b), 2-year (c), 10-yr (d), 50-yr (e), and 100-yr (f) storm events.

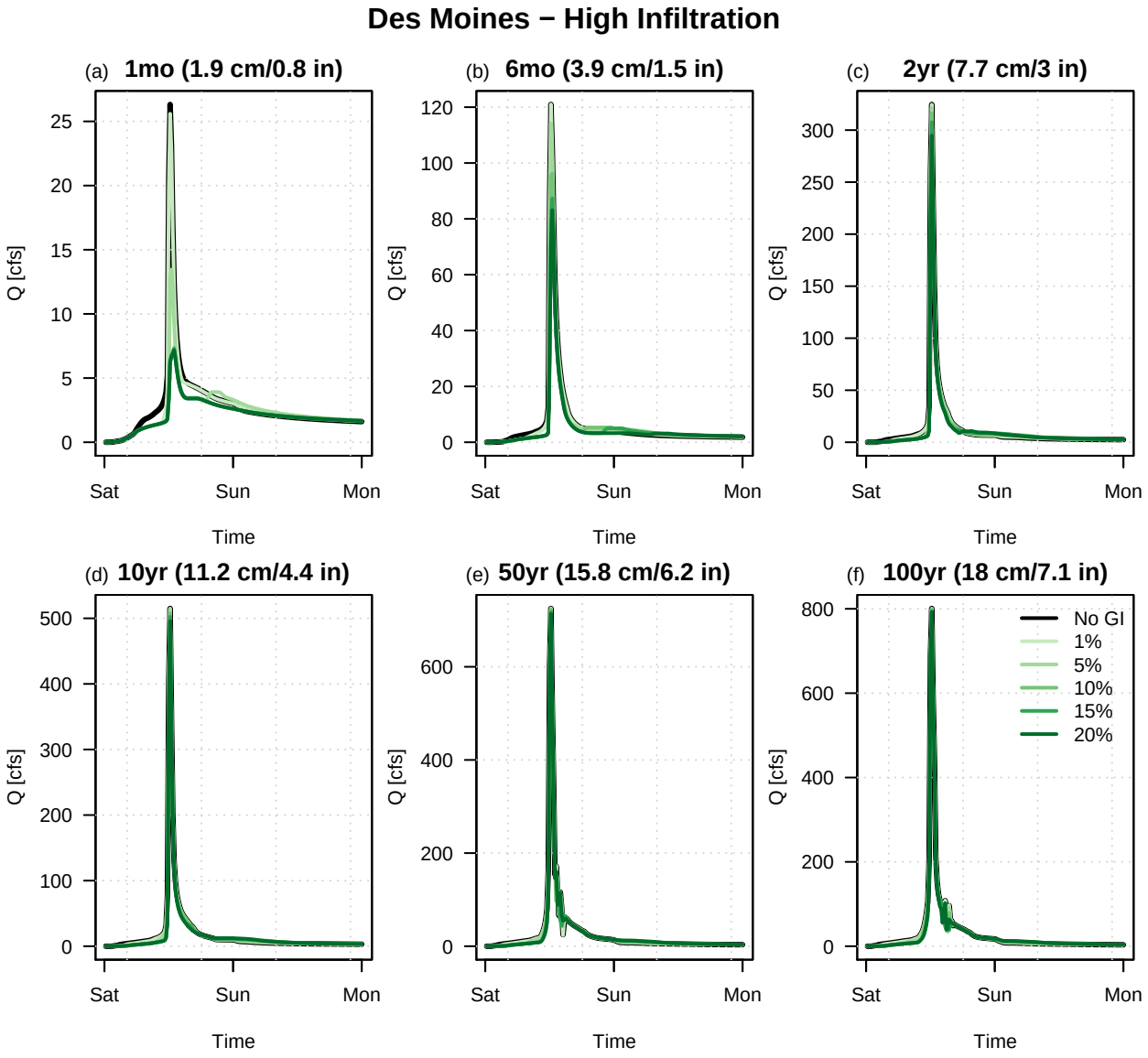

Figure S18: Simulated hydrographs at the watershed outlet for the baseline and GSI scenarios for the 1-month (a), 6-month (b), 2-year (c), 10-yr (d), 50-yr (e), and 100-yr (f) storm events.

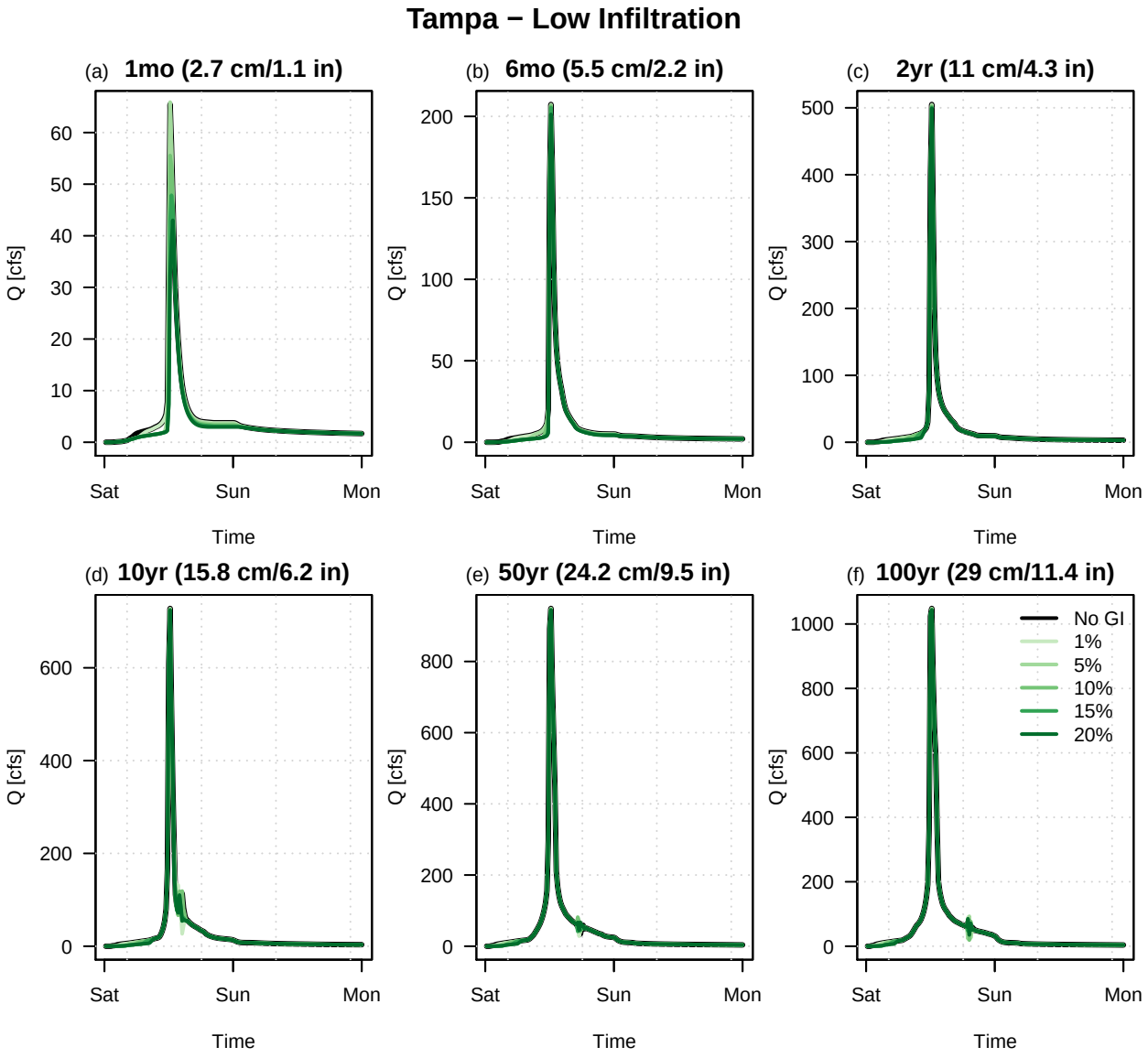

Figure S19: Simulated hydrographs at the watershed outlet for the baseline and GSI scenarios for the 1-month (a), 6-month (b), 2-year (c), 10-yr (d), 50-yr (e), and 100-yr (f) storm events.

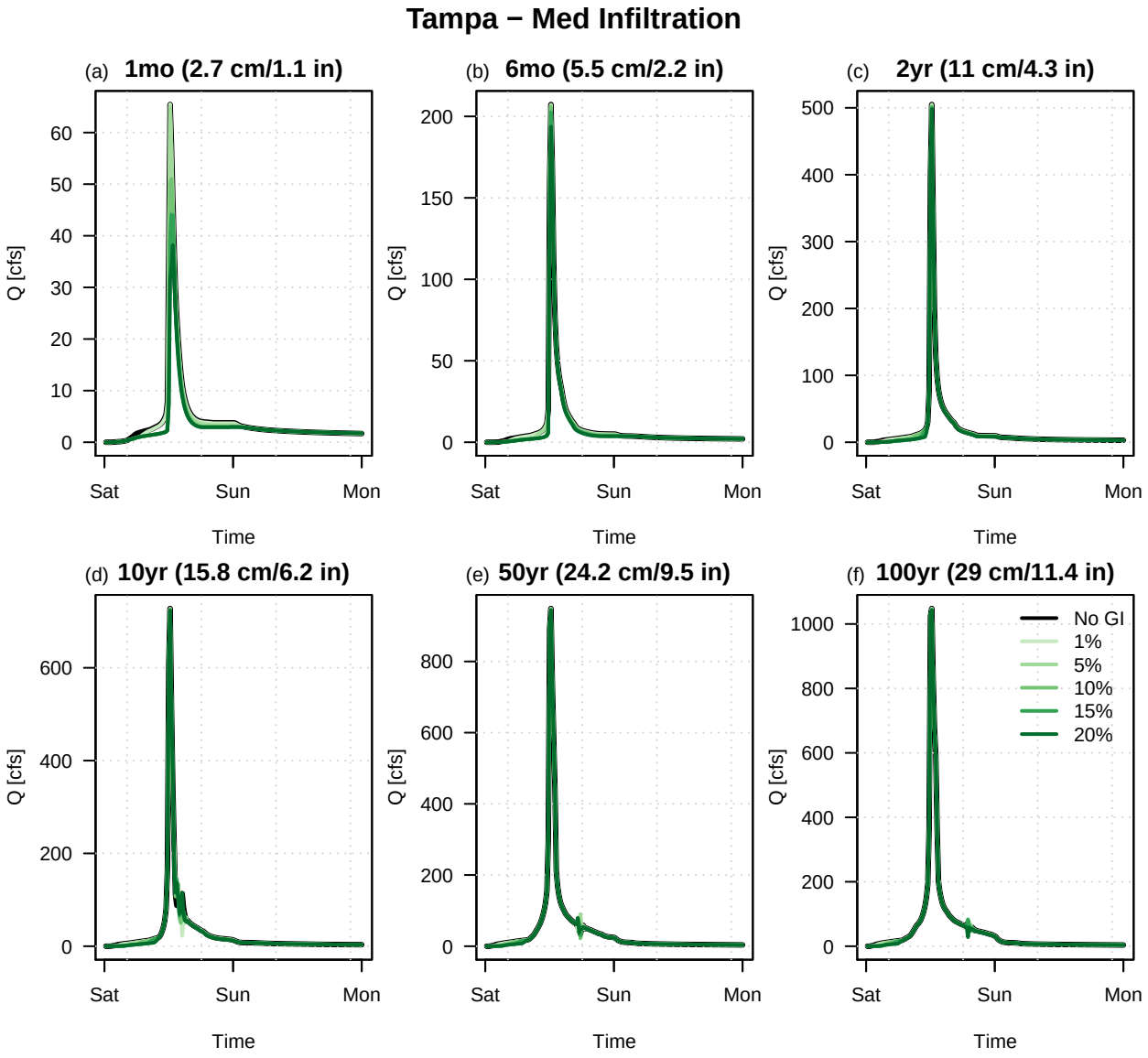

Figure S20: Simulated hydrographs at the watershed outlet for the baseline and GSI scenarios for the 1-month (a), 6-month (b), 2-year (c), 10-yr (d), 50-yr (e), and 100-yr (f) storm events.

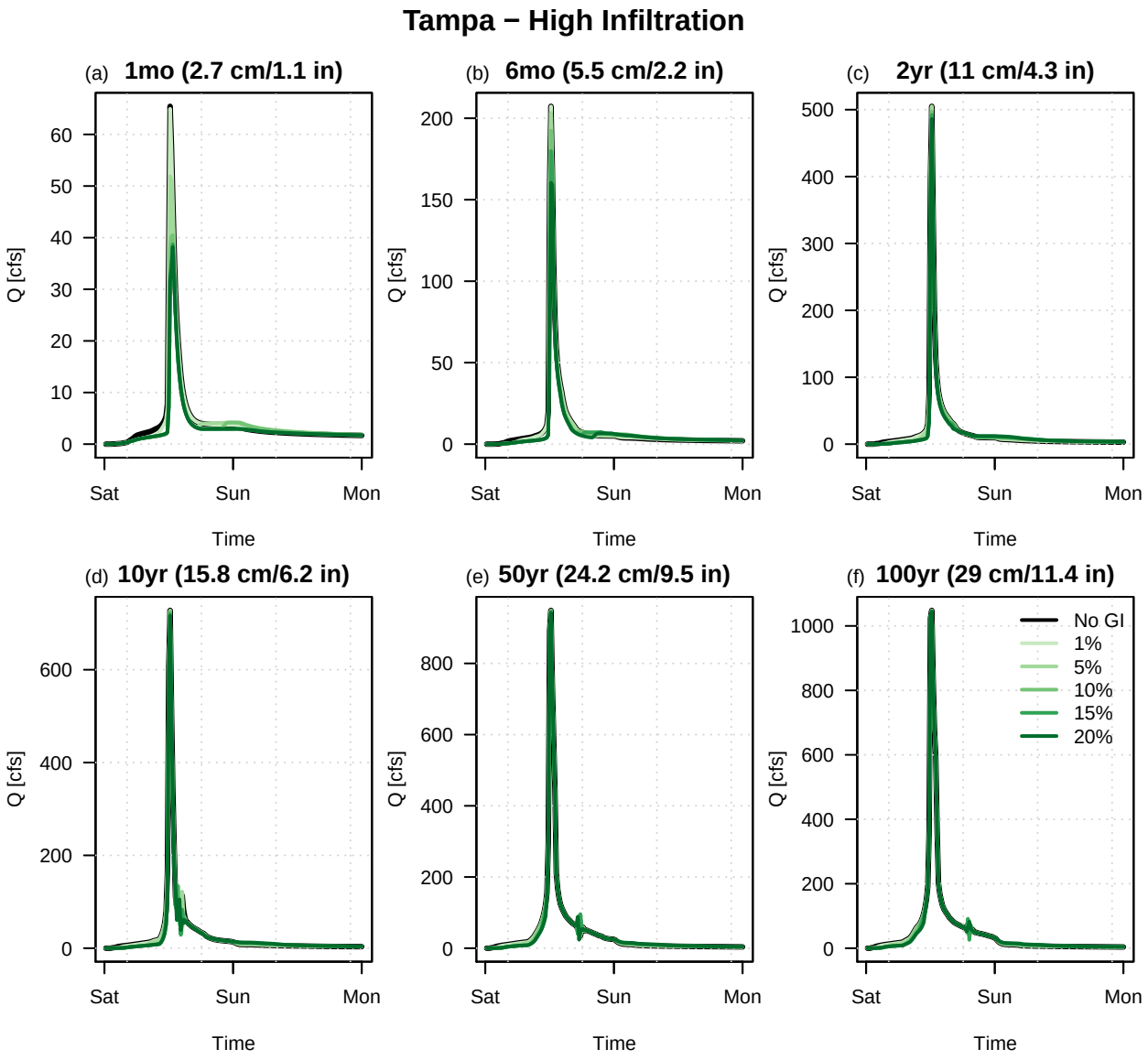

Figure S21: Simulated hydrographs at the watershed outlet for the baseline and GSI scenarios for the 1-month (a), 6-month (b), 2-year (c), 10-yr (d), 50-yr (e), and 100-yr (f) storm events.

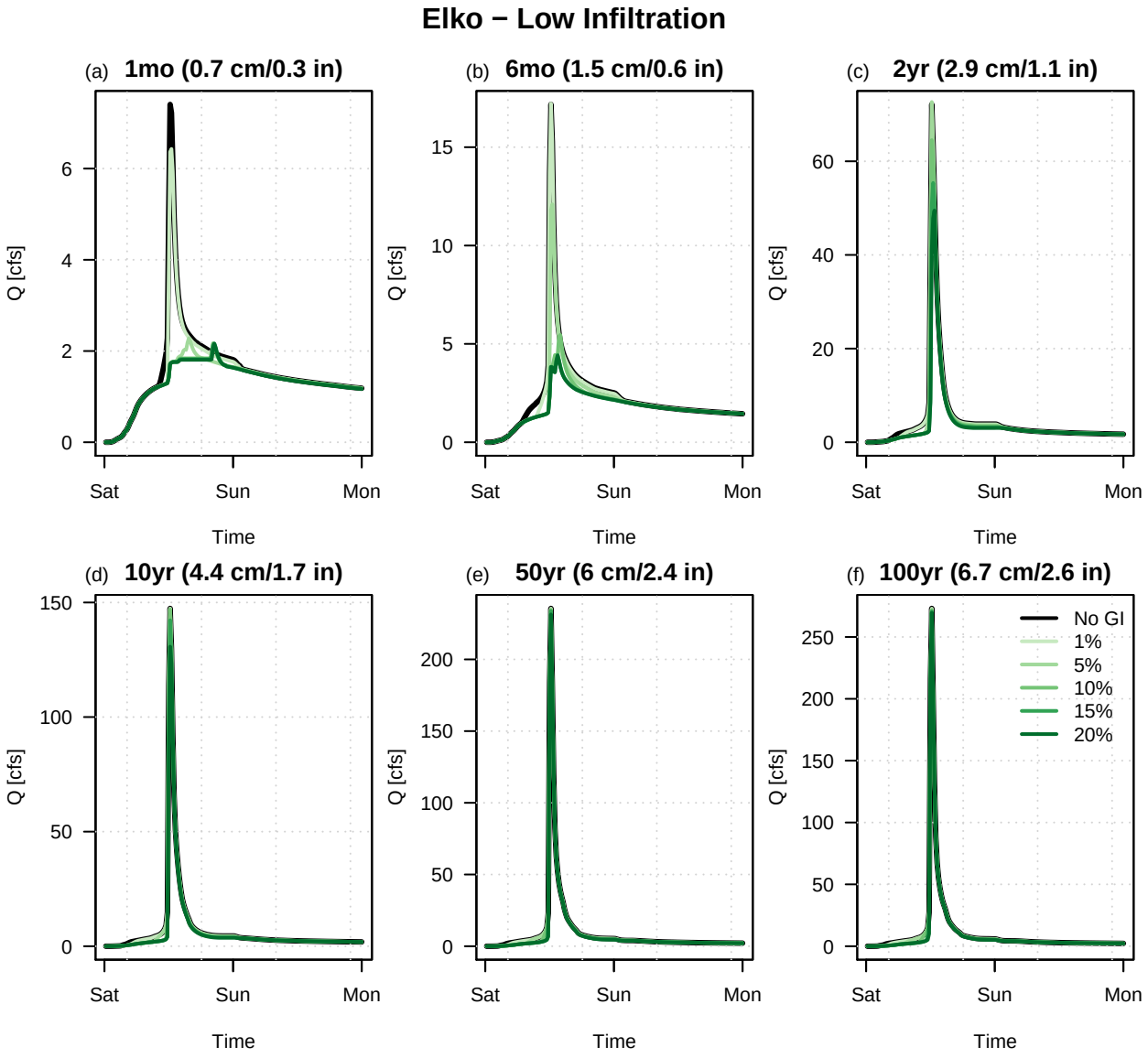

Figure S22: Simulated hydrographs at the watershed outlet for the baseline and GSI scenarios for the 1-month (a), 6-month (b), 2-year (c), 10-yr (d), 50-yr (e), and 100-yr (f) storm events.

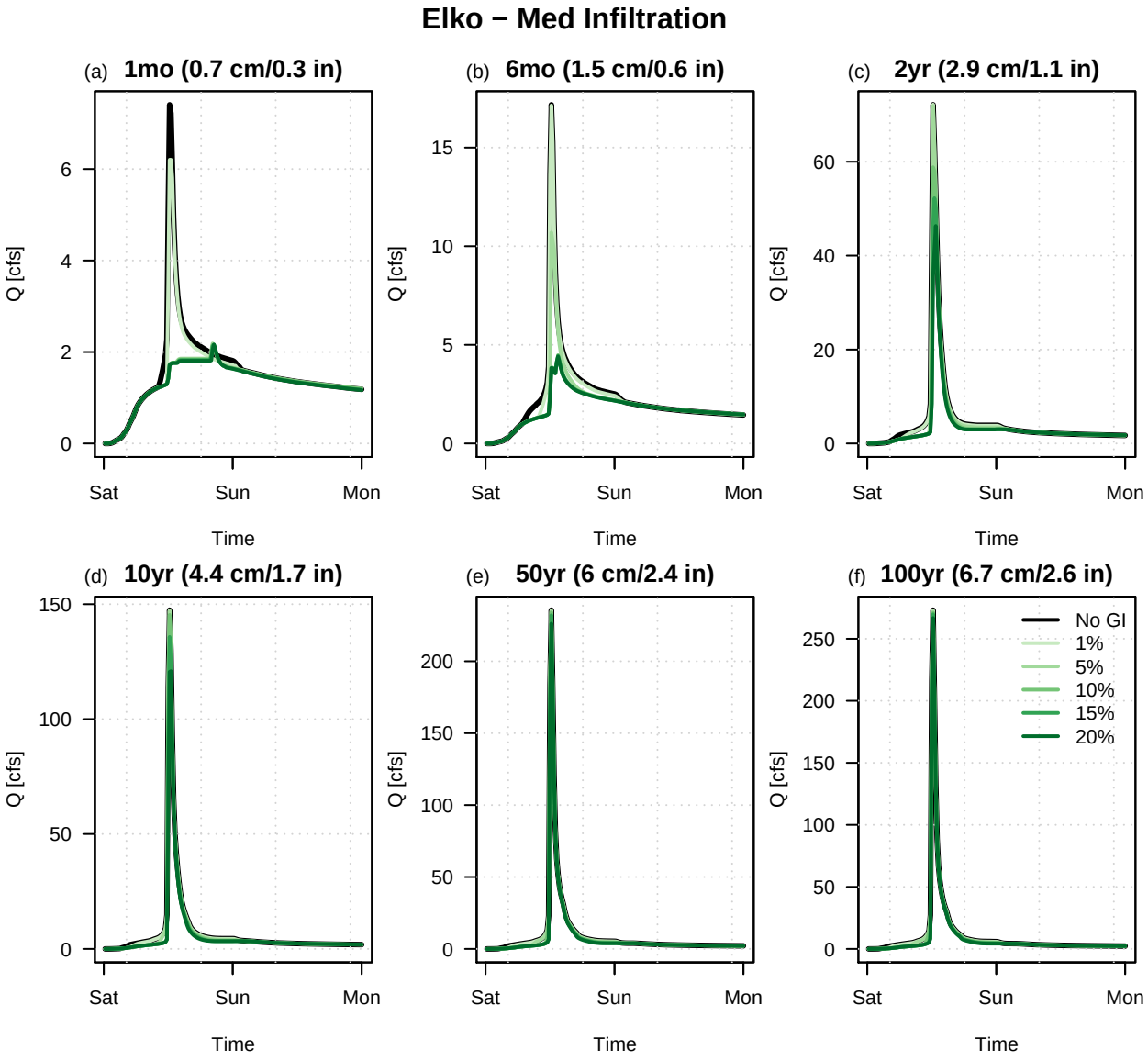

Figure S23: Simulated hydrographs at the watershed outlet for the baseline and GSI scenarios for the 1-month (a), 6-month (b), 2-year (c), 10-yr (d), 50-yr (e), and 100-yr (f) storm events.

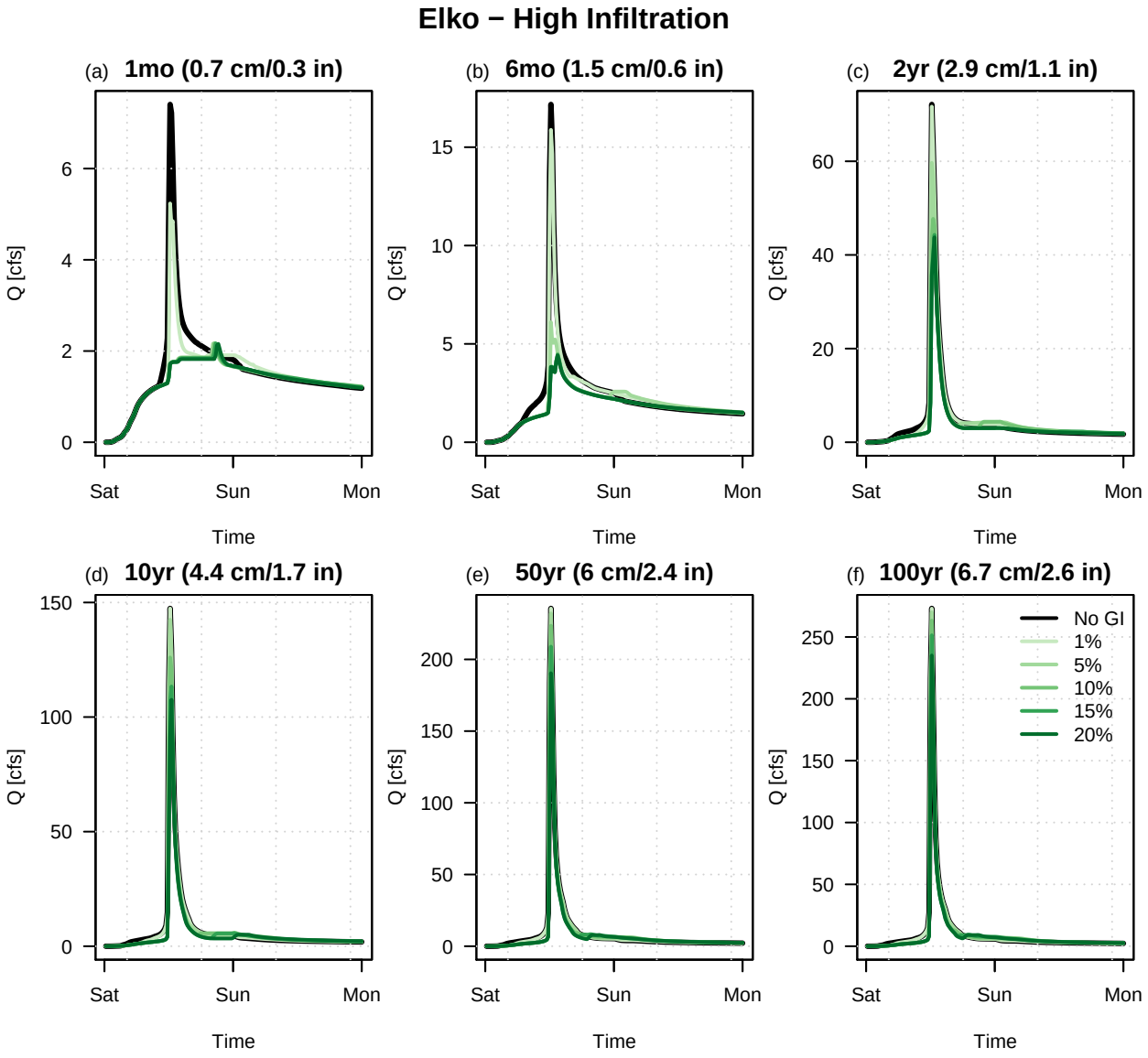

Figure S24: Simulated hydrographs at the watershed outlet for the baseline and GSI scenarios for the 1-month (a), 6-month (b), 2-year (c), 10-yr (d), 50-yr (e), and 100-yr (f) storm events.

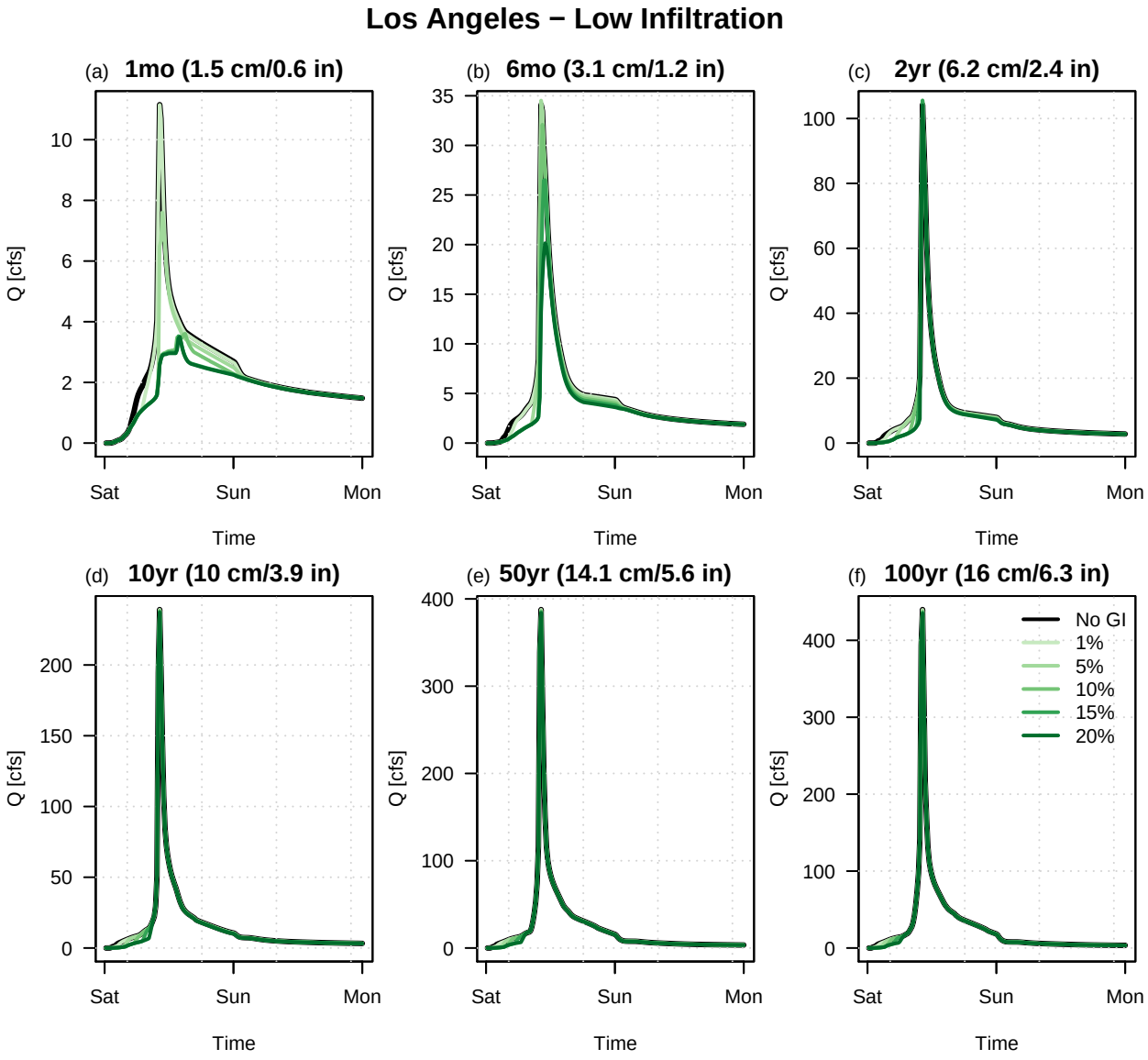

Figure S25: Simulated hydrographs at the watershed outlet for the baseline and GSI scenarios for the 1-month (a), 6-month (b), 2-year (c), 10-yr (d), 50-yr (e), and 100-yr (f) storm events.

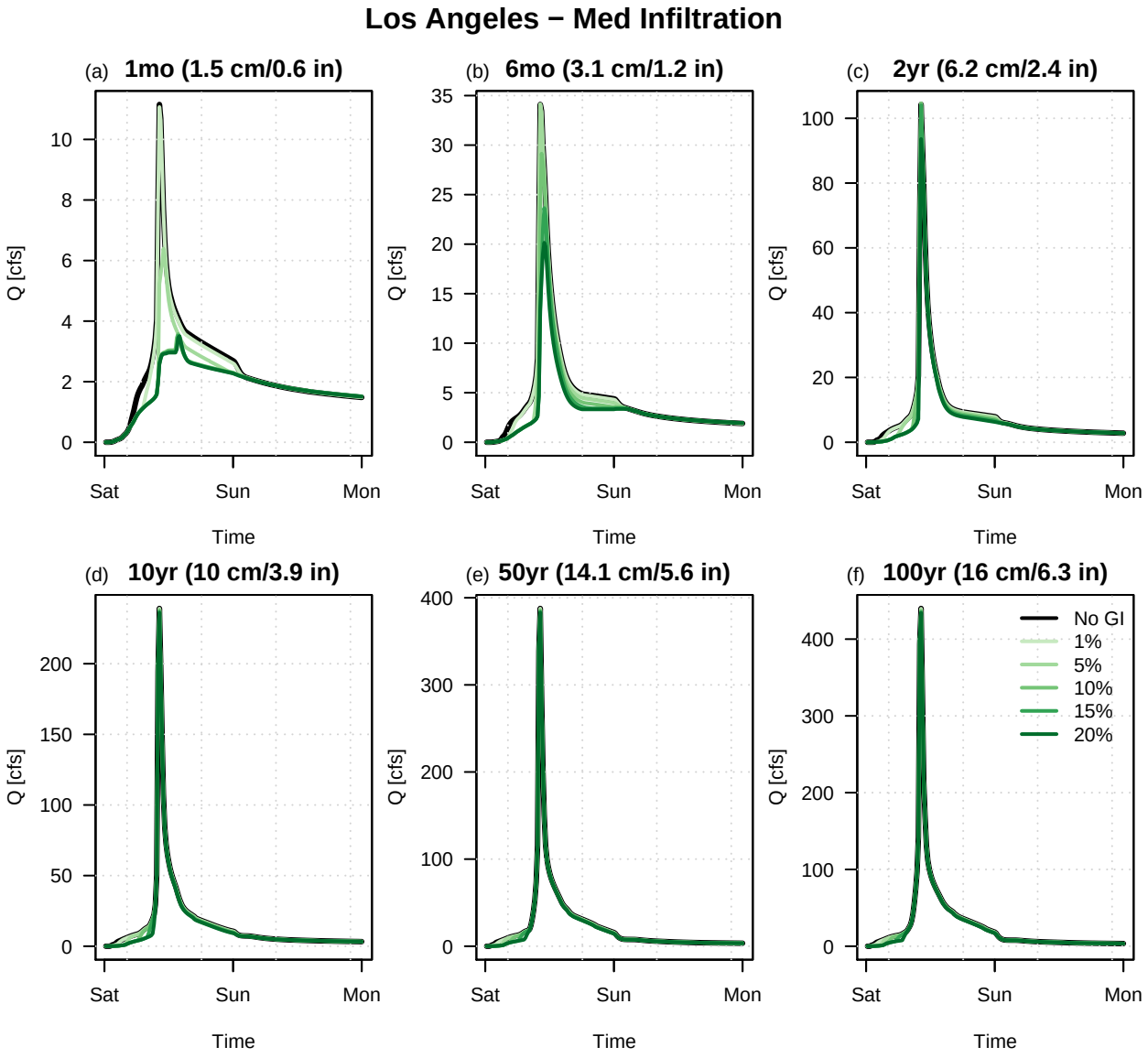

Figure S26: Simulated hydrographs at the watershed outlet for the baseline and GSI scenarios for the 1-month (a), 6-month (b), 2-year (c), 10-yr (d), 50-yr (e), and 100-yr (f) storm events.

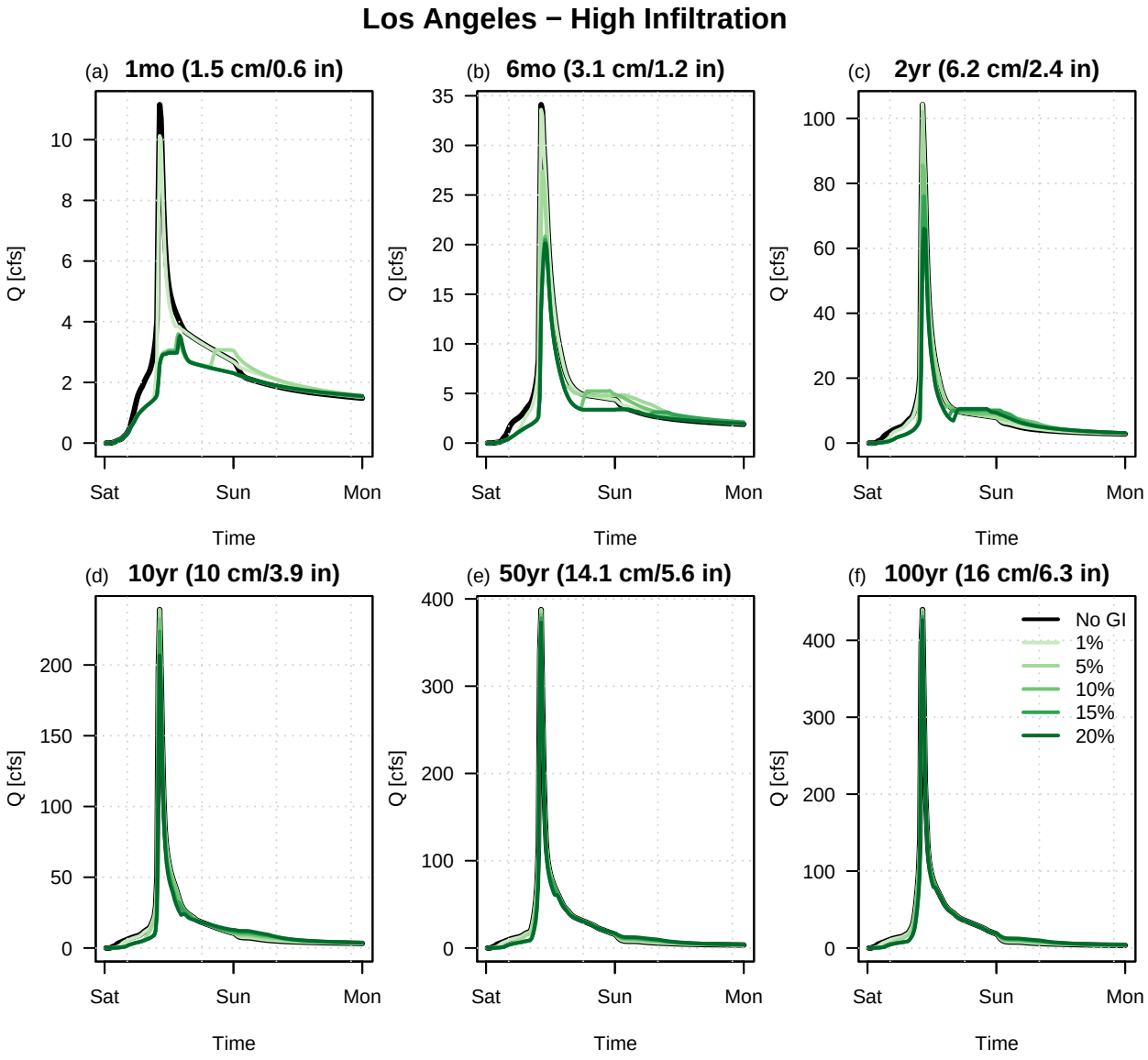

Figure S27: Simulated hydrographs at the watershed outlet for the baseline and GSI scenarios for the 1-month (a), 6-month (b), 2-year (c), 10-yr (d), 50-yr (e), and 100-yr (f) storm events.

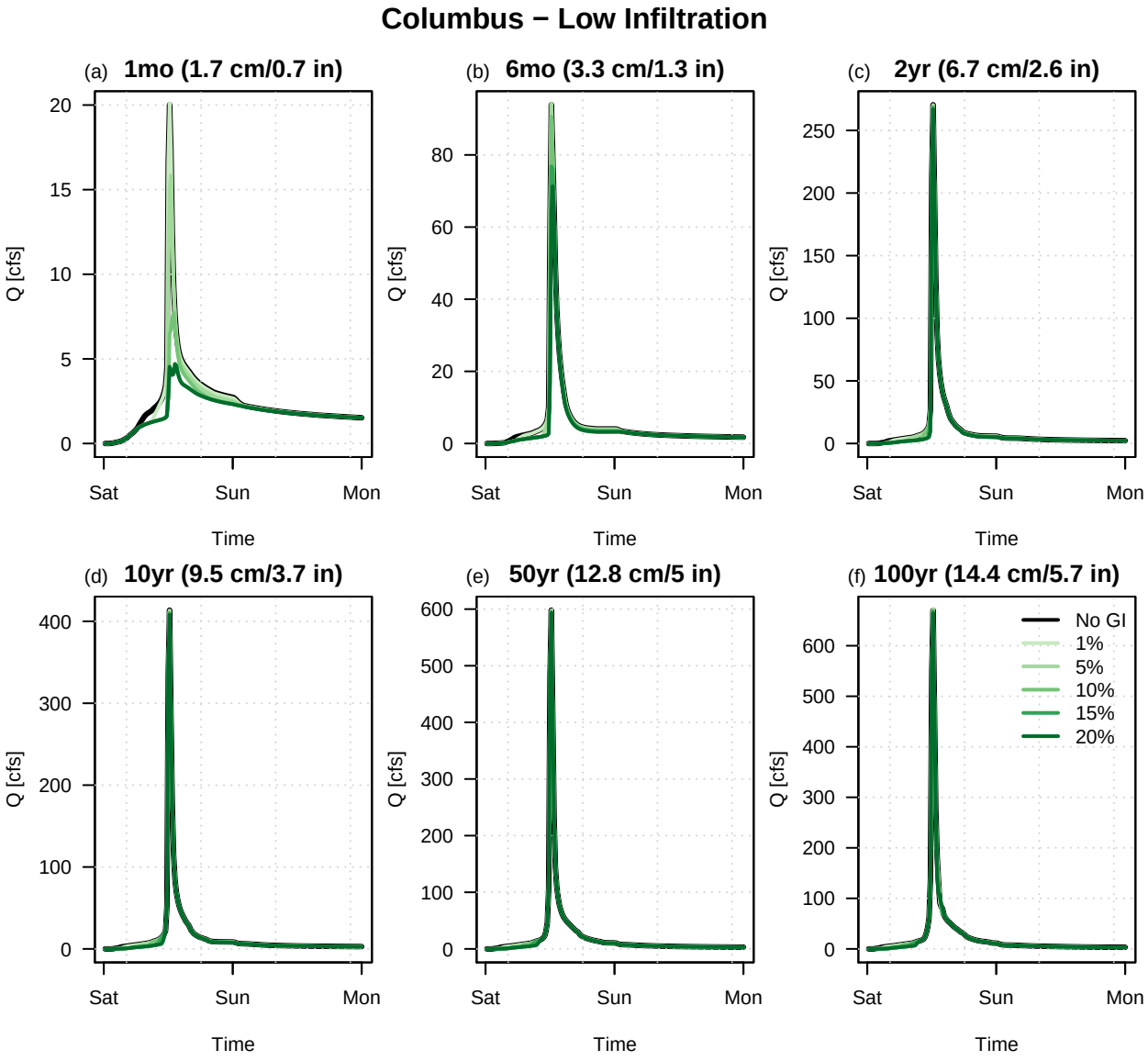

Figure S28: Simulated hydrographs at the watershed outlet for the baseline and GSI scenarios for the 1-month (a), 6-month (b), 2-year (c), 10-yr (d), 50-yr (e), and 100-yr (f) storm events.

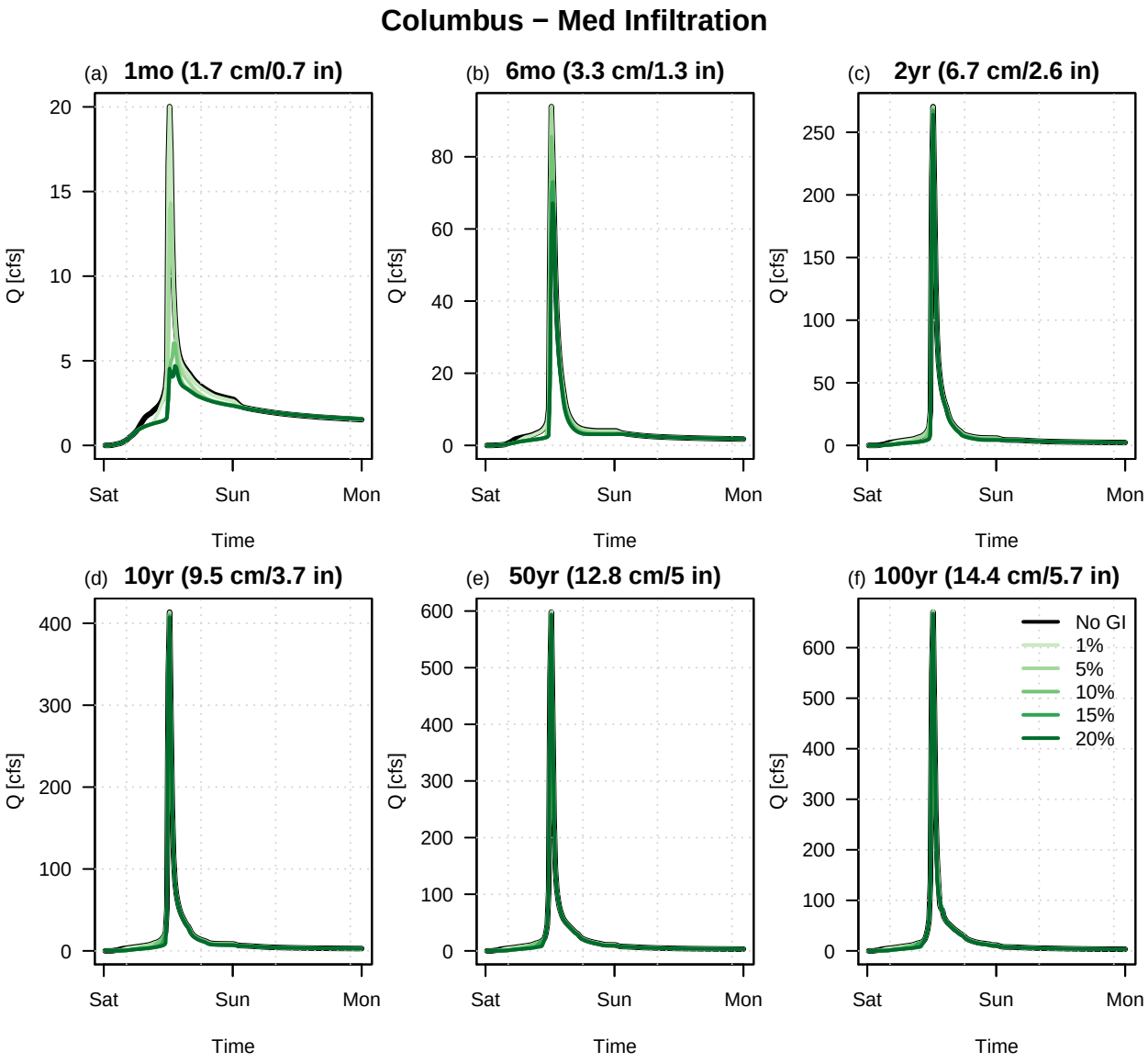

Figure S29: Simulated hydrographs at the watershed outlet for the baseline and GSI scenarios for the 1-month (a), 6-month (b), 2-year (c), 10-yr (d), 50-yr (e), and 100-yr (f) storm events.

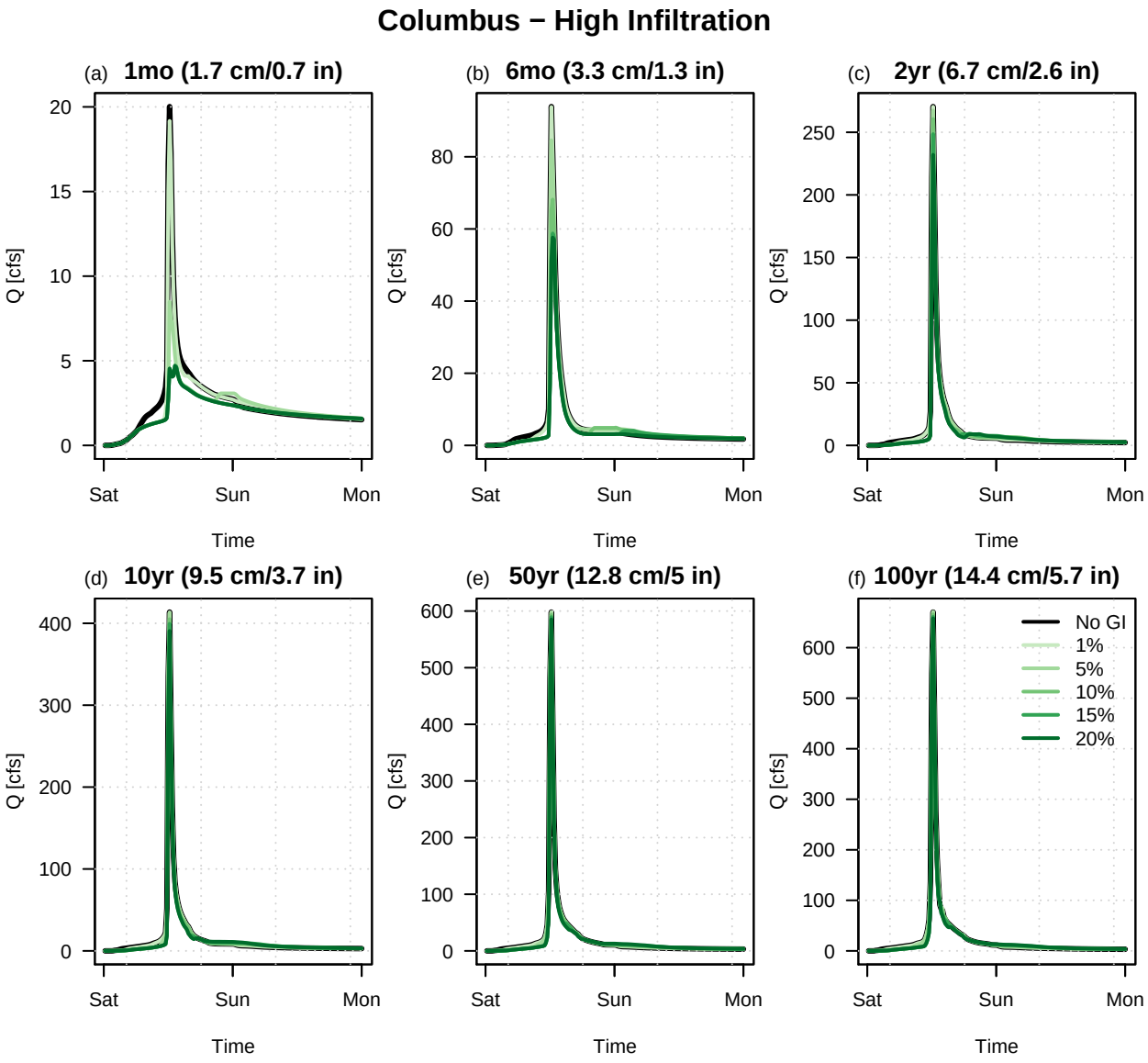

Figure S30: Simulated hydrographs at the watershed outlet for the baseline and GSI scenarios for the 1-month (a), 6-month (b), 2-year (c), 10-yr (d), 50-yr (e), and 100-yr (f) storm events.

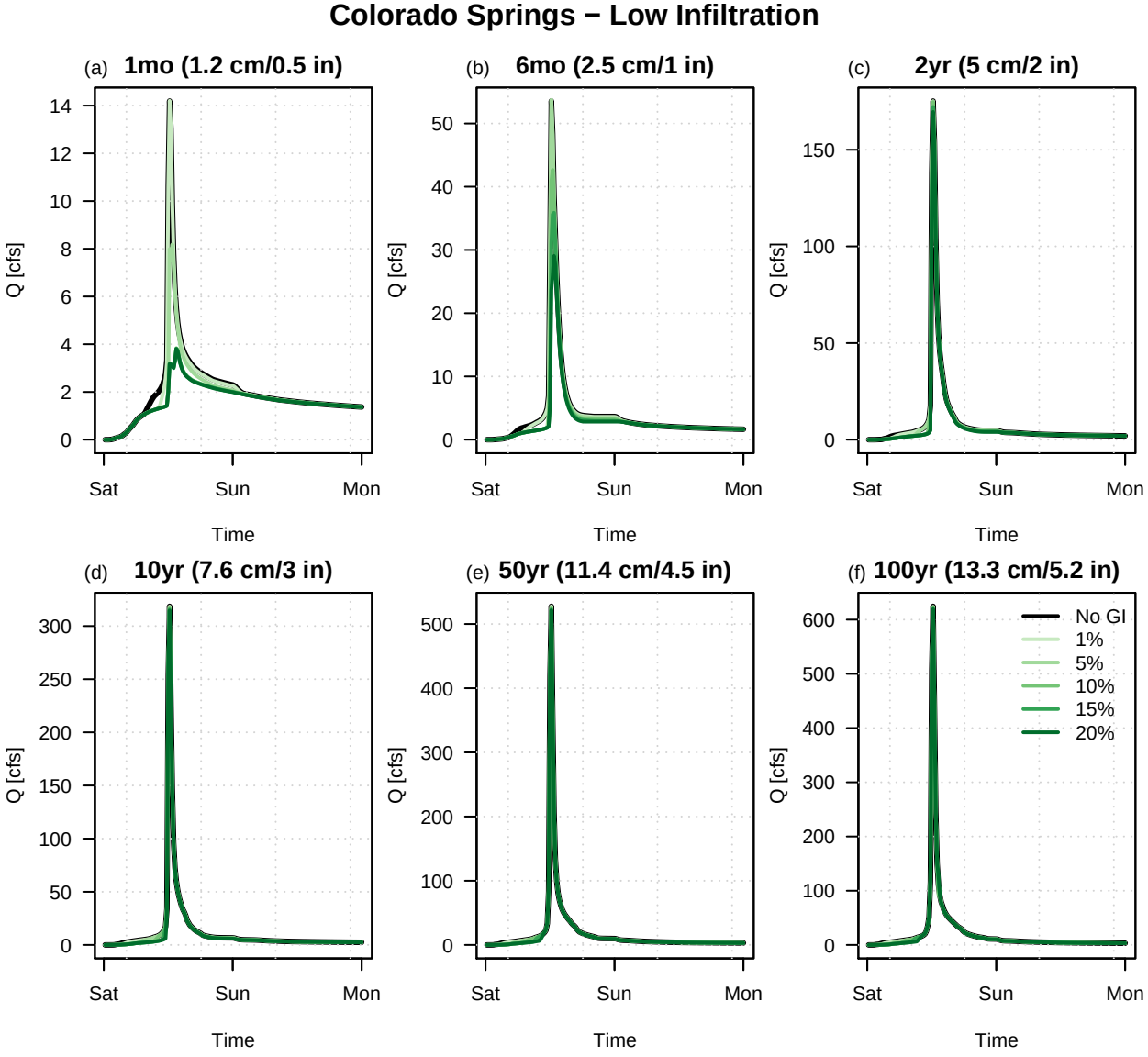

Figure S31: Simulated hydrographs at the watershed outlet for the baseline and GSI scenarios for the 1-month (a), 6-month (b), 2-year (c), 10-yr (d), 50-yr (e), and 100-yr (f) storm events.

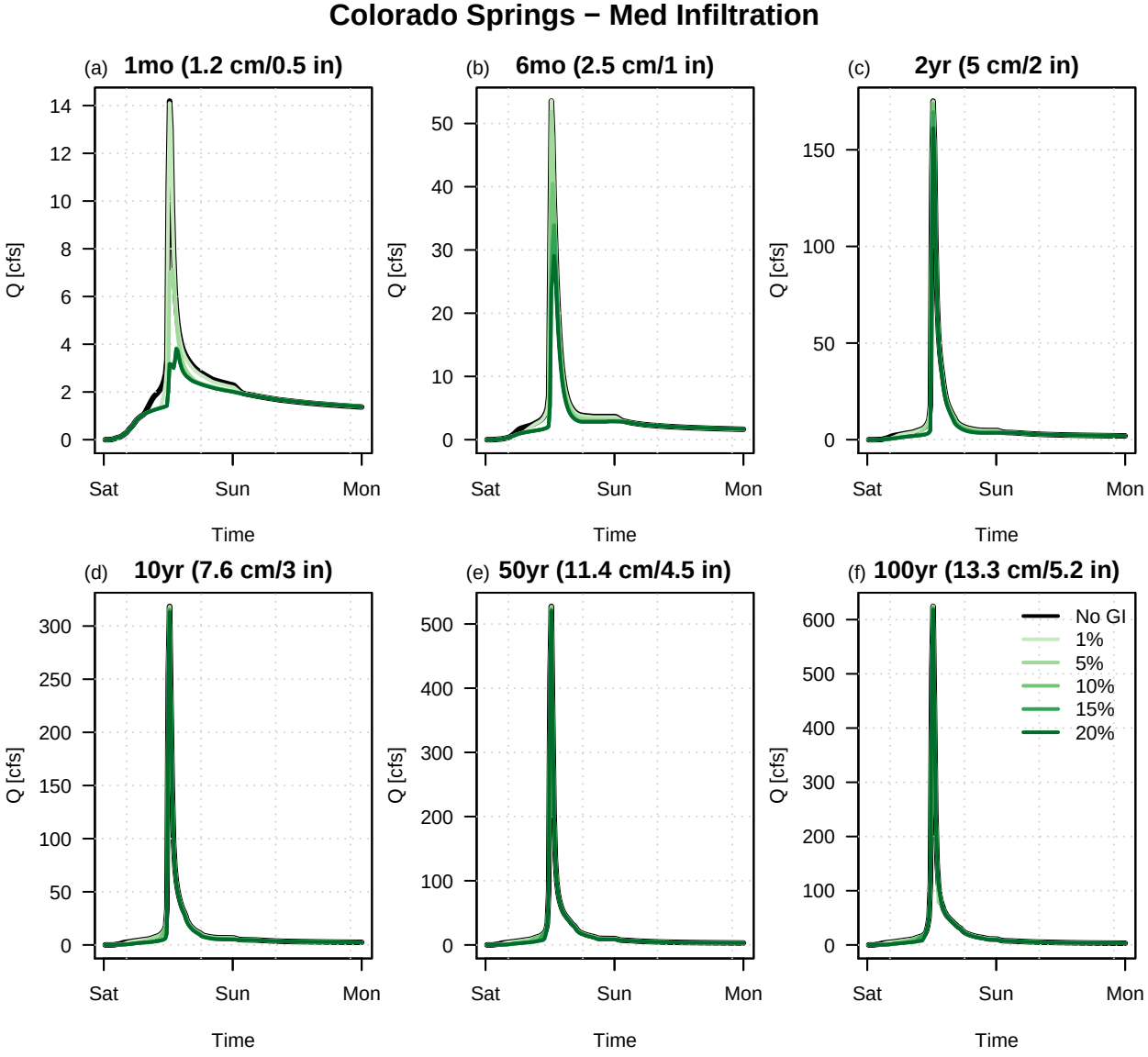

Figure S32: Simulated hydrographs at the watershed outlet for the baseline and GSI scenarios for the 1-month (a), 6-month (b), 2-year (c), 10-yr (d), 50-yr (e), and 100-yr (f) storm events.

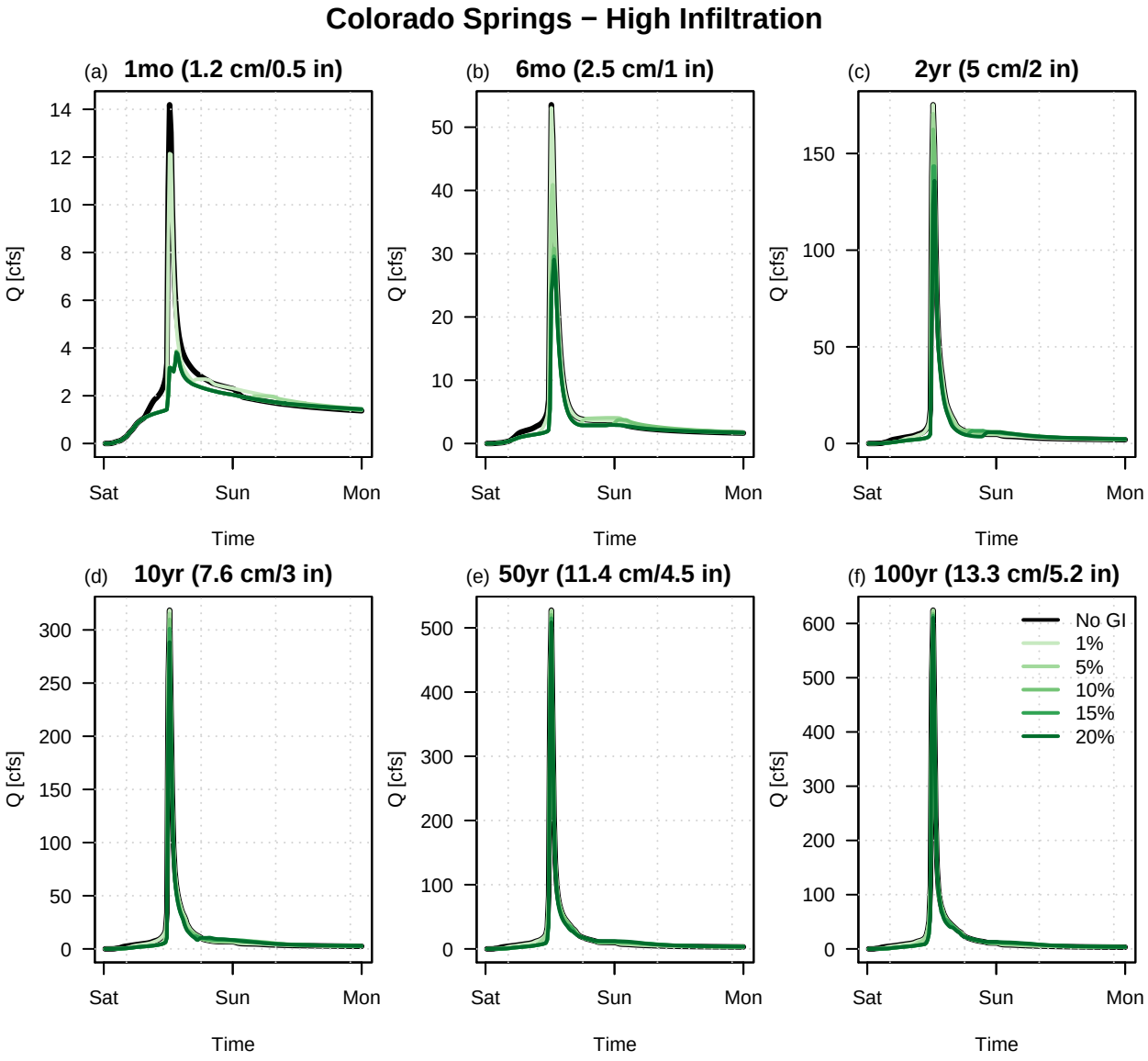

Figure S33: Simulated hydrographs at the watershed outlet for the baseline and GSI scenarios for the 1-month (a), 6-month (b), 2-year (c), 10-yr (d), 50-yr (e), and 100-yr (f) storm events.

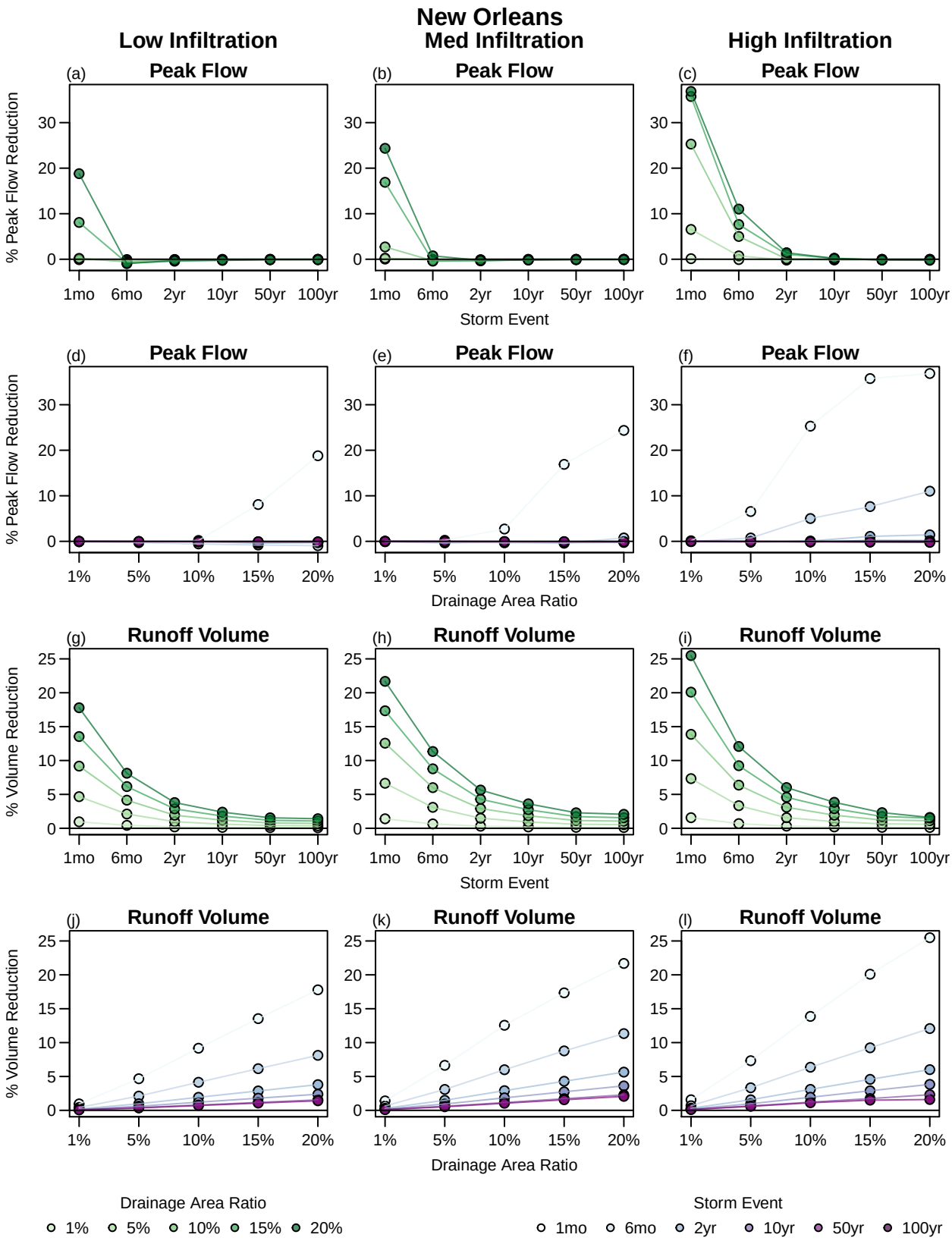

Figure S34: Reduction in peak flow rate and total runoff volume measured at the watershed outlet for all design storm scenarios for New Orleans. Data are shown twice, once as performance vs. storm depth (points colored by DAR; a-c and g-i) and once as performance vs. DAR (points colored by storm depth; d-f and j-l).

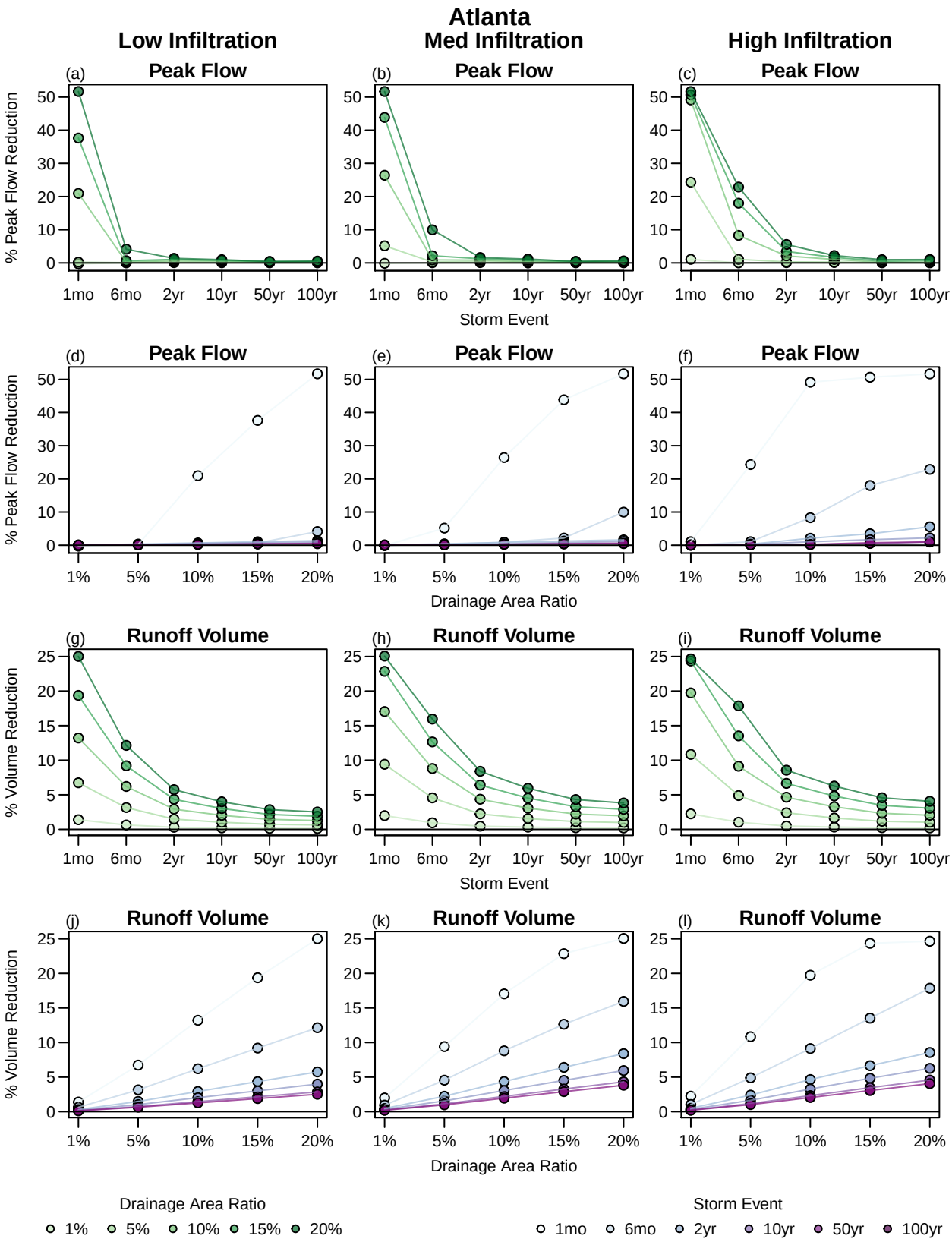

Figure S35: Reduction in peak flow rate and total runoff volume measured at the watershed outlet for all design storm scenarios for Atlanta. Data are shown twice, once as performance vs. storm depth (points colored by DAR; a-c and g-i) and once as performance vs. DAR (points colored by storm depth; d-f and j-l).

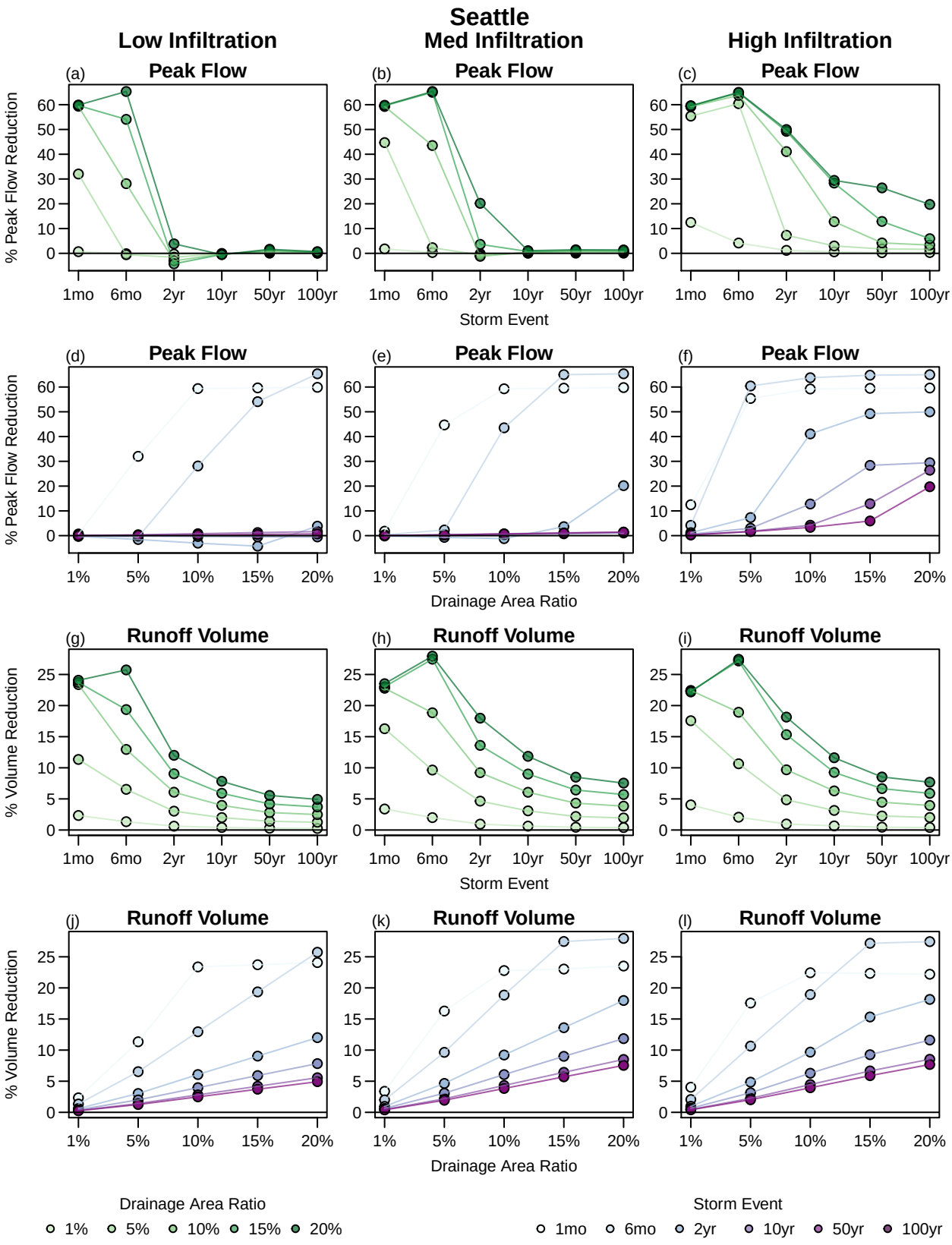

Figure S36: Reduction in peak flow rate and total runoff volume measured at the watershed outlet for all design storm scenarios for Seattle. Data are shown twice, once as performance vs. storm depth (points colored by DAR; a-c and g-i) and once as performance vs. DAR (points colored by storm depth; d-f and j-l).

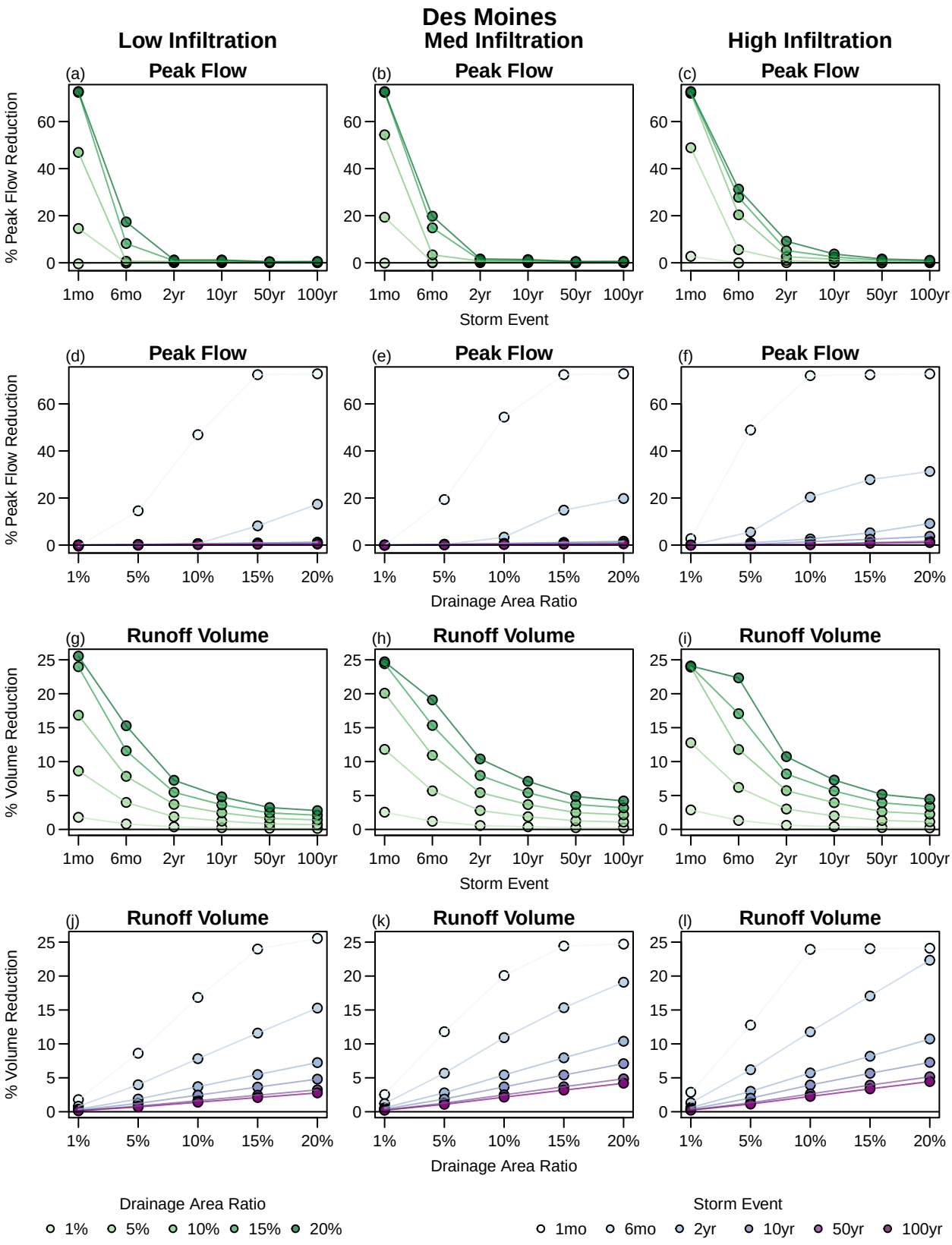

Figure S37: Reduction in peak flow rate and total runoff volume measured at the watershed outlet for all design storm scenarios for Des Moines. Data are shown twice, once as performance vs. storm depth (points colored by DAR; a-c and g-i) and once as performance vs. DAR (points colored by storm depth; d-f and j-l).

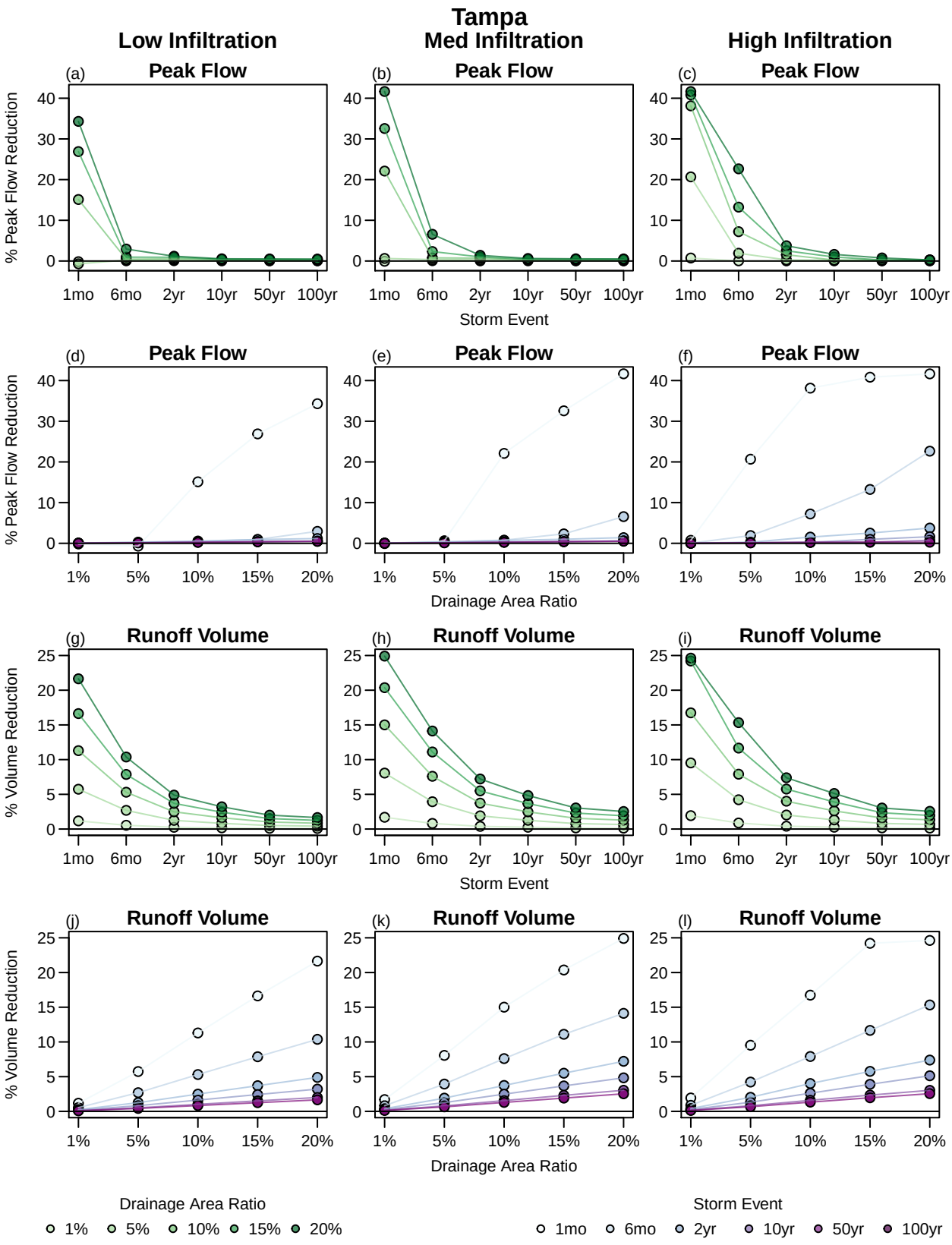

Figure S38: Reduction in peak flow rate and total runoff volume measured at the watershed outlet for all design storm scenarios for Tampa. Data are shown twice, once as performance vs. storm depth (points colored by DAR; a-c and g-i) and once as performance vs. DAR (points colored by storm depth; d-f and j-l).

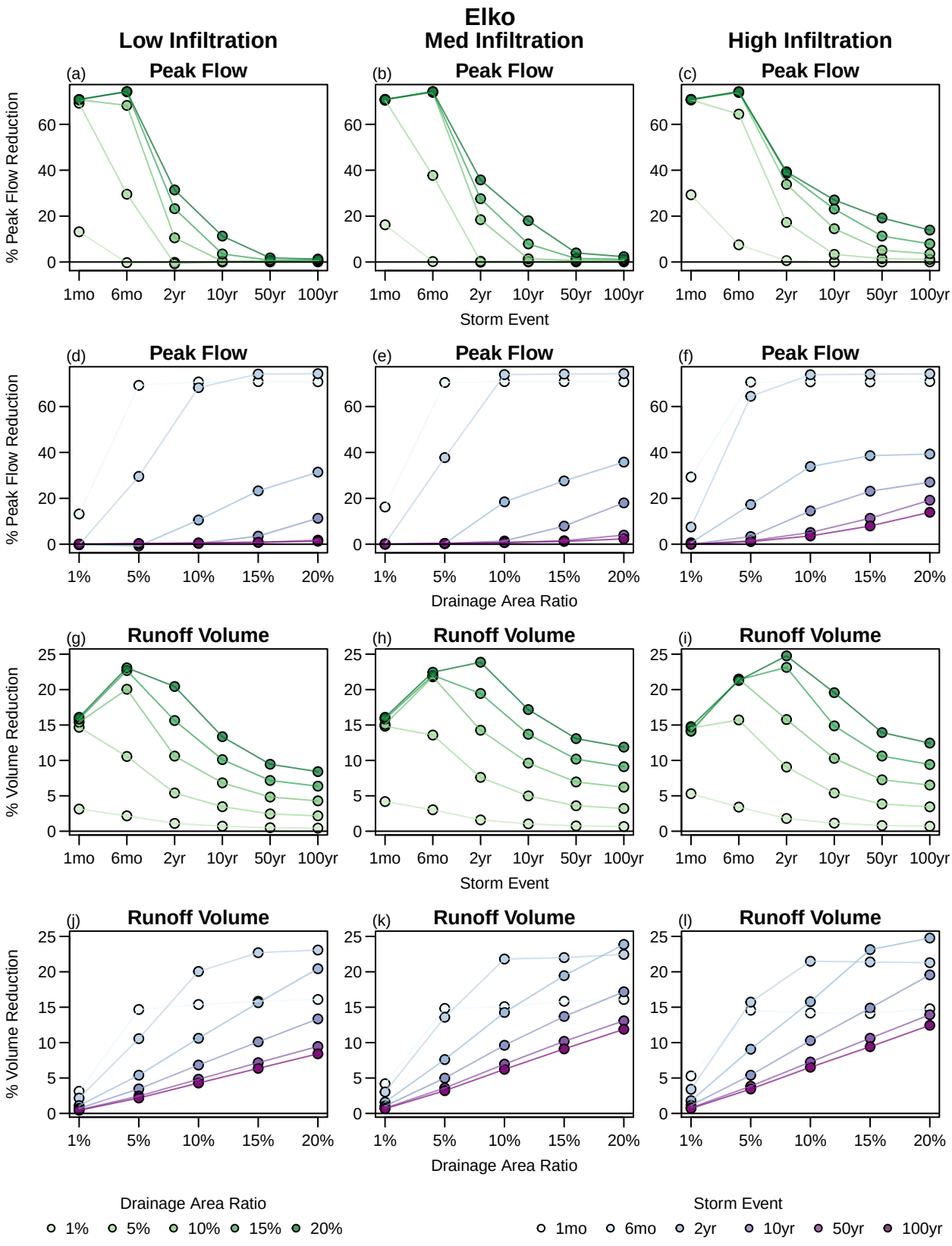

Figure S39: Reduction in peak flow rate and total runoff volume measured at the watershed outlet for all design storm scenarios for Elko. Data are shown twice, once as performance vs. storm depth (points colored by DAR; a-c and g-i) and once as performance vs. DAR (points colored by storm depth; d-f and j-l).

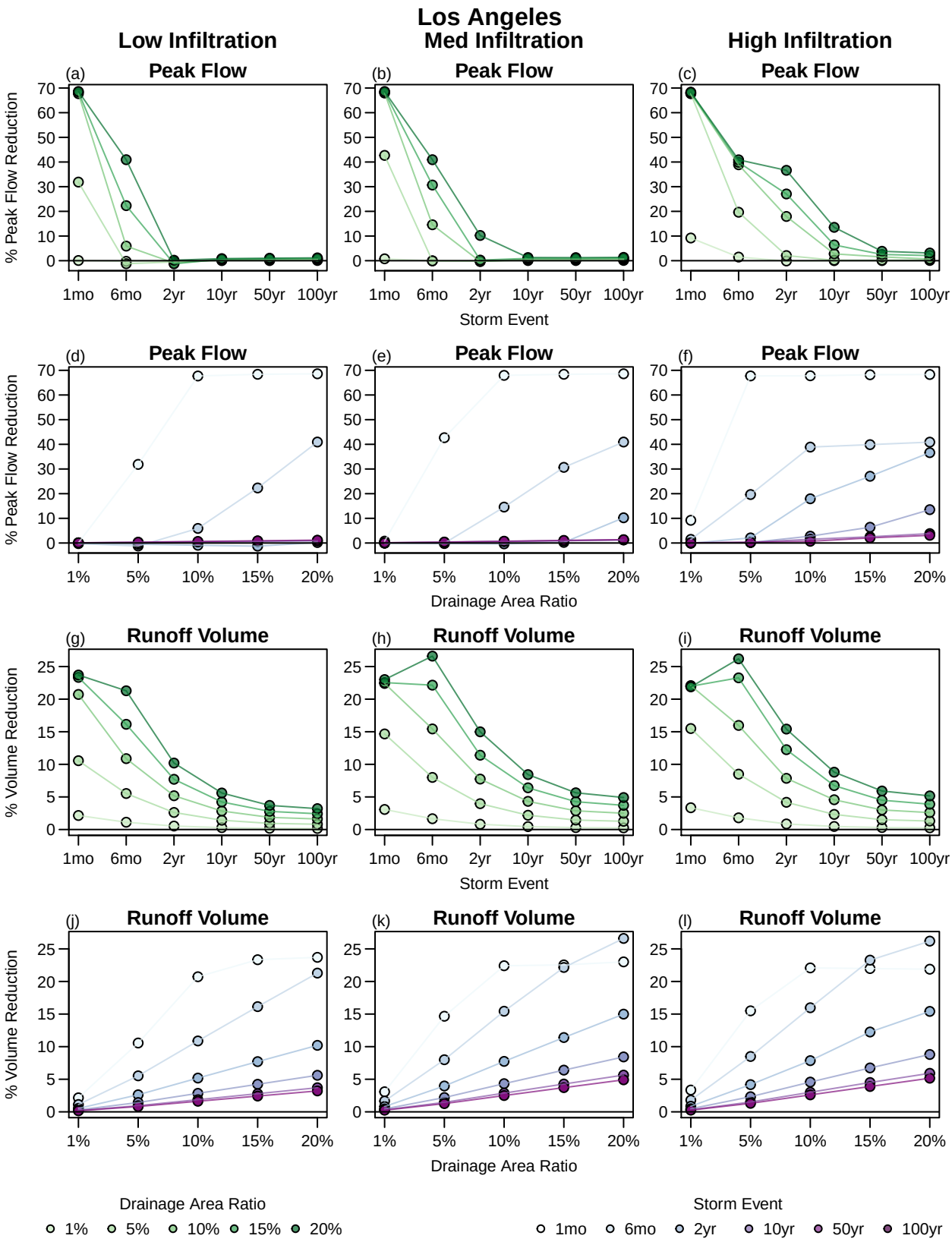

Figure S40: Reduction in peak flow rate and total runoff volume measured at the watershed outlet for all design storm scenarios for Los Angeles. Data are shown twice, once as performance vs. storm depth (points colored by DAR; a-c and g-i) and once as performance vs. DAR (points colored by storm depth; d-f and j-l).

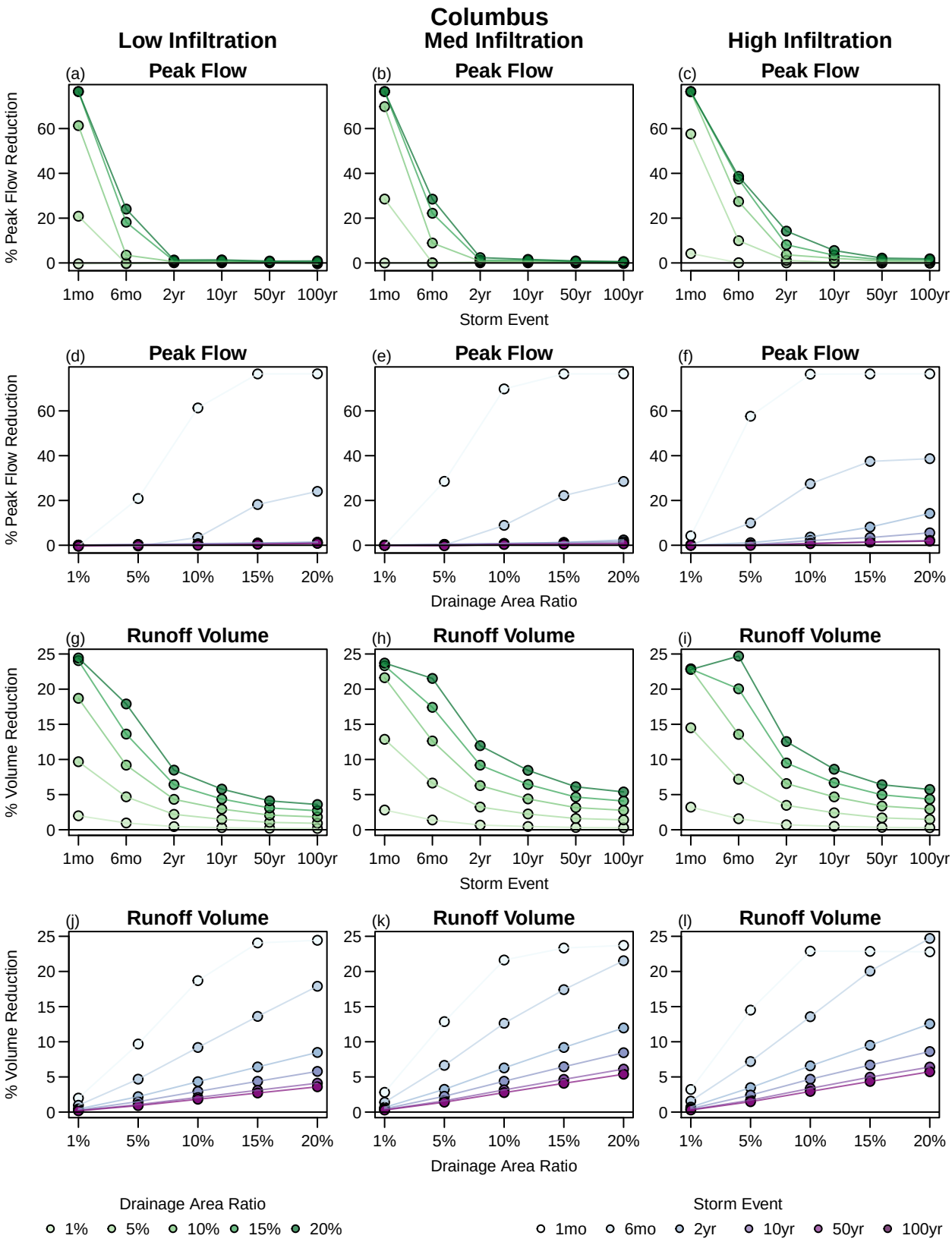

Figure S41: Reduction in peak flow rate and total runoff volume measured at the watershed outlet for all design storm scenarios for Columbus. Data are shown twice, once as performance vs. storm depth (points colored by DAR; a-c and g-i) and once as performance vs. DAR (points colored by storm depth; d-f and j-l).

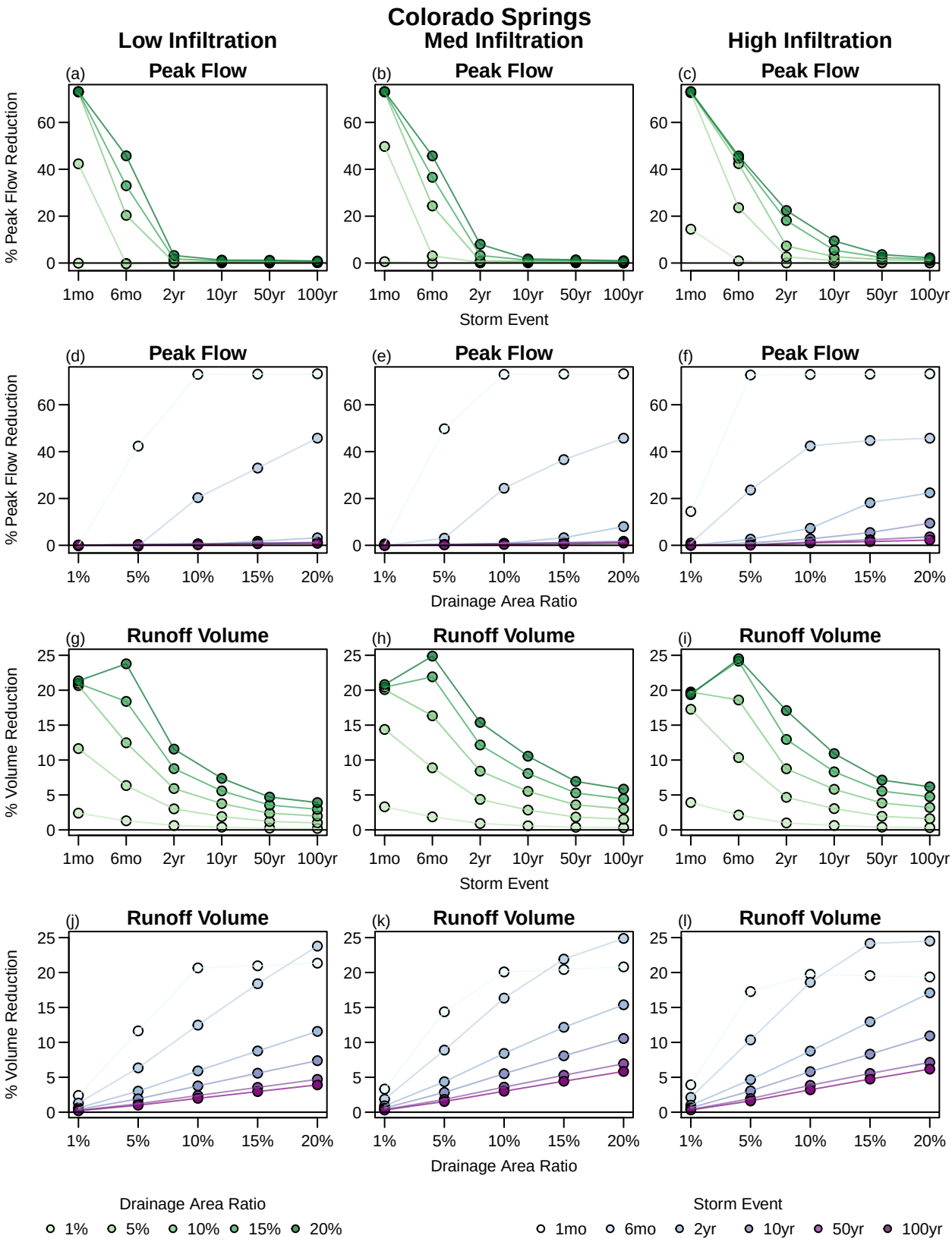

Figure S42: Reduction in peak flow rate and total runoff volume measured at the watershed outlet for all design storm scenarios for Colorado Springs. Data are shown twice, once as performance vs. storm depth (points colored by DAR; a-c and g-i) and once as performance vs. DAR (points colored by storm depth; d-f and j-l).

Additional Results from Continuous Simulations

Summary plots

Summary results for each city for all three years (wet, normal, and dry) and three GSI soil types (high, medium, and low infiltration capacity). Plots show percent reduction in peak flow rates and runoff volume by event, as well as annual summaries of high pulse count, high pulse duration, % reduction in surface runoff volume, and Richards-Baker Flashiness index.

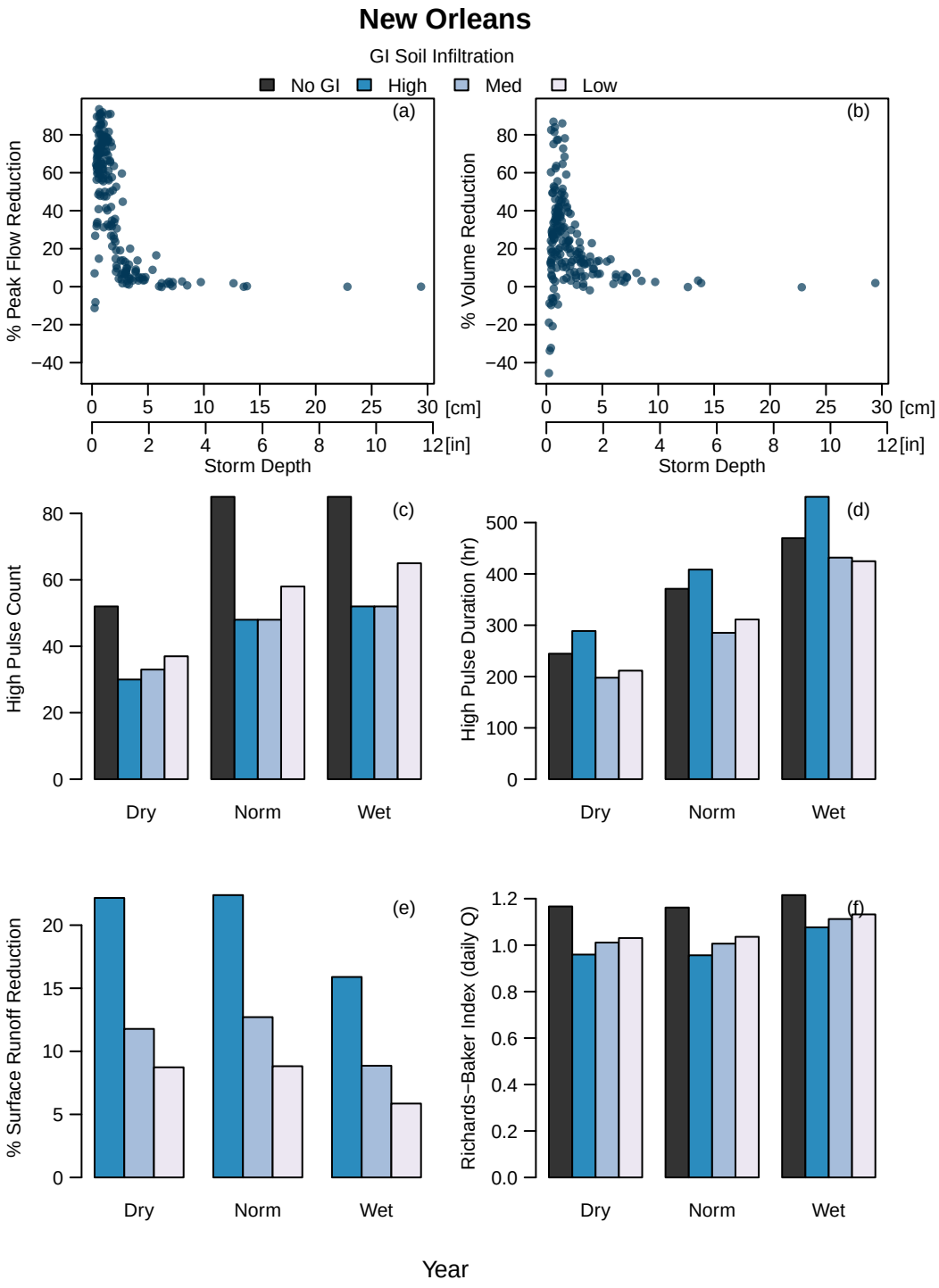

Figure S43: Peak flow reduction (a) and runoff volume reduction (b) by event, high pulse count (c), high pulse duation (d), surface runoff volume reduction (e), and flow flashiness (RBI calculated using 15-min flow data; f) for New Orleans. Plots (a) and (b) show only results for high infiltration soils to improve readability.

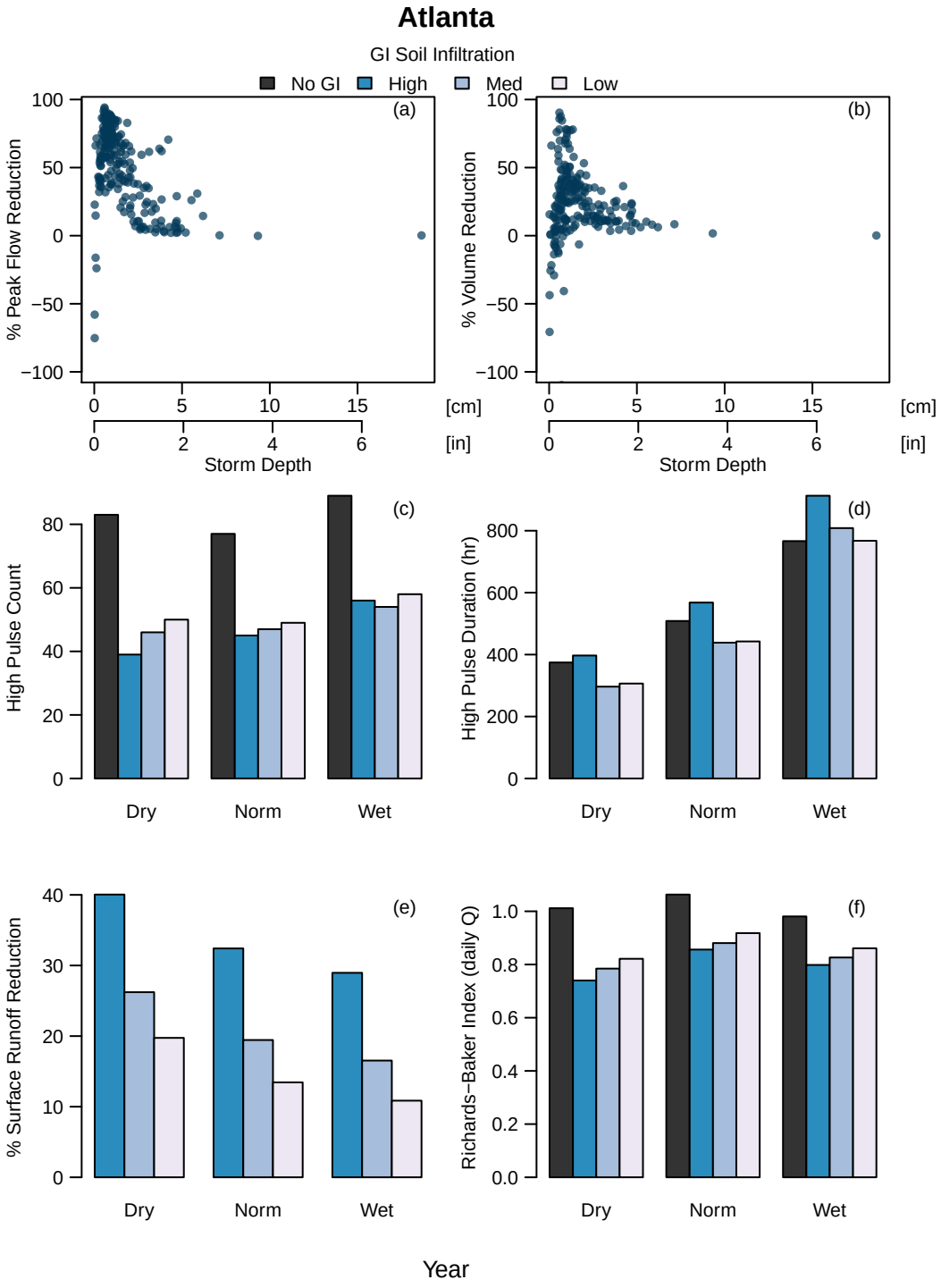

Figure S44: Peak flow reduction (a) and runoff volume reduction (b) by event, high pulse count (c), high pulse duation (d), surface runoff volume reduction (e), and flow flashiness (RBI calculated using 15-min flow data; f) for Atlanta. Plots (a) and (b) show only results for high infiltration soils to improve readability.

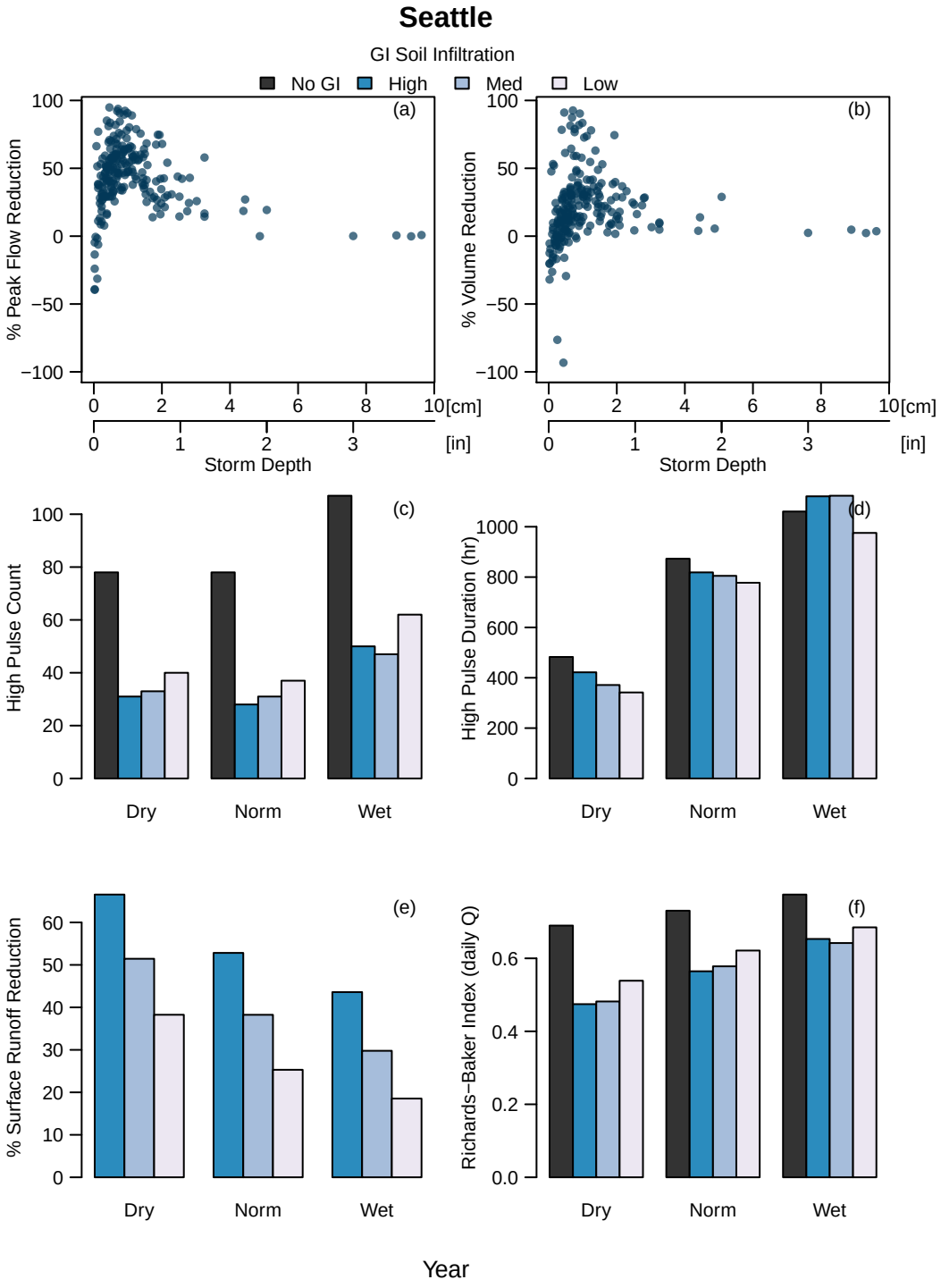

Figure S45: Peak flow reduction (a) and runoff volume reduction (b) by event, high pulse count (c), high pulse duation (d), surface runoff volume reduction (e), and flow flashiness (RBI calculated using 15-min flow data; f) for Seattle. Plots (a) and (b) show only results for high infiltration soils to improve readability.

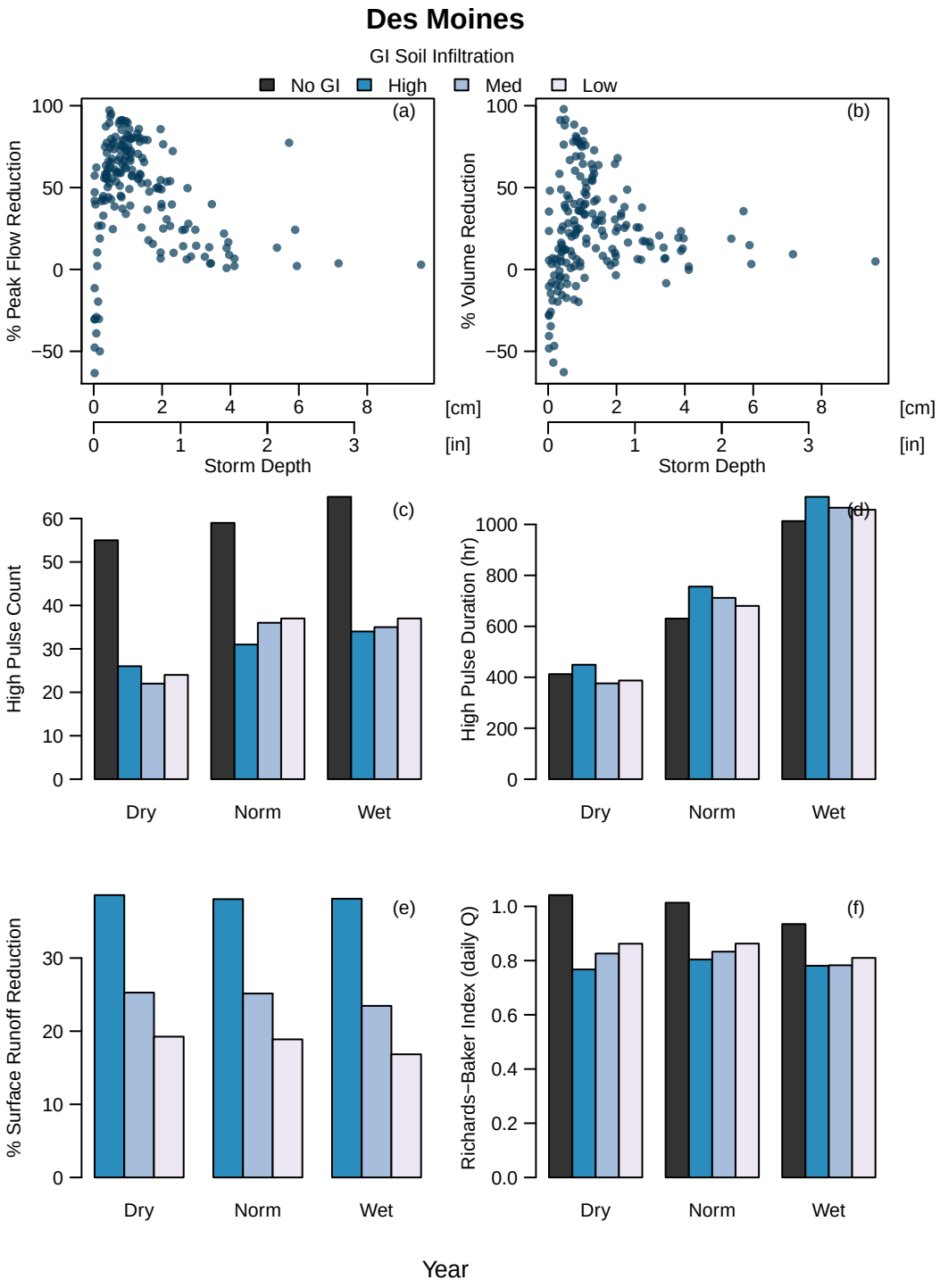

Figure S46: Peak flow reduction (a) and runoff volume reduction (b) by event, high pulse count (c), high pulse duation (d), surface runoff volume reduction (e), and flow flashiness (RBI calculated using 15-min flow data; f) for Des Moines. Plots (a) and (b) show only results for high infiltration soils to improve readability.

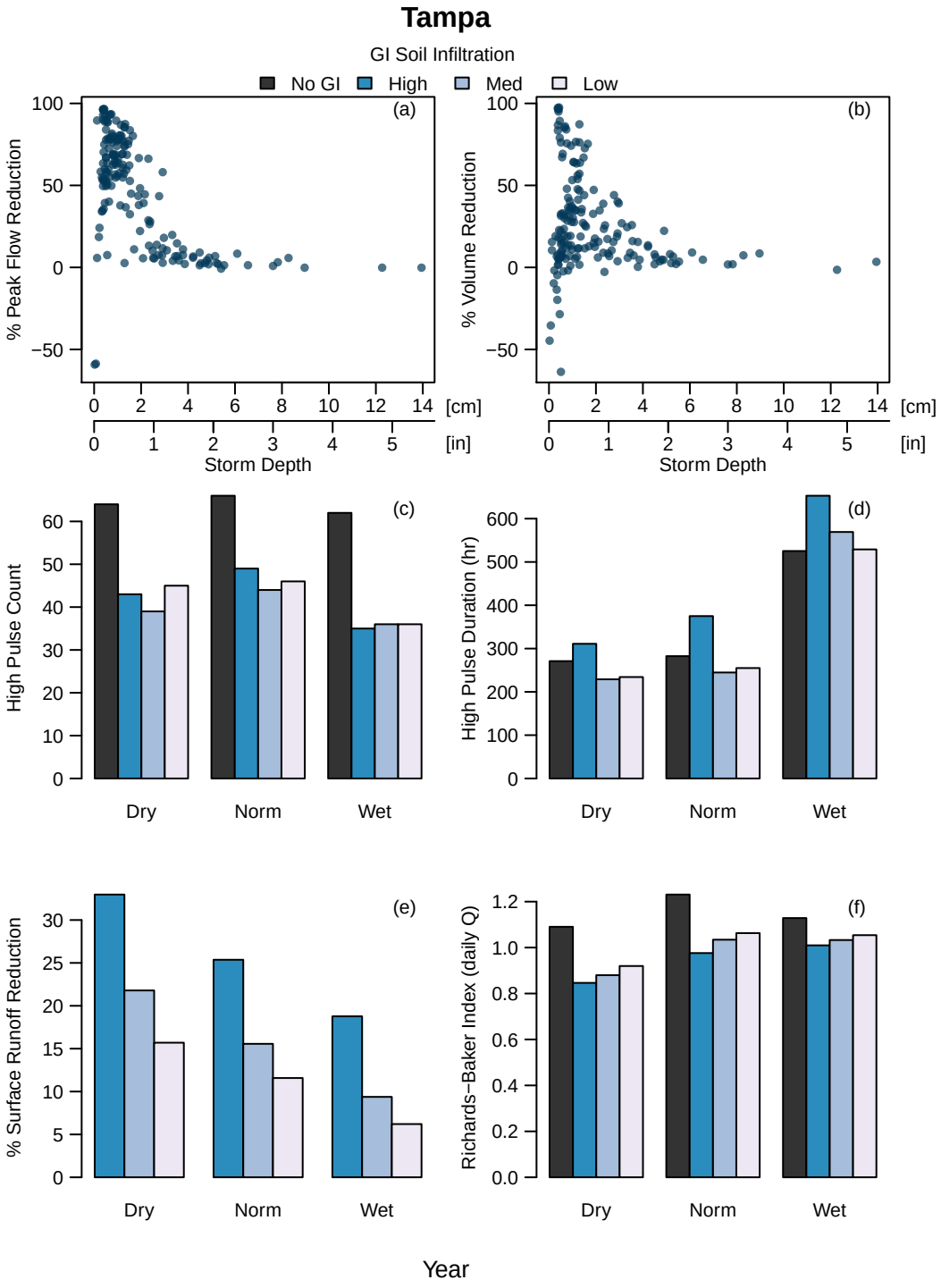

Figure S47: Peak flow reduction (a) and runoff volume reduction (b) by event, high pulse count (c), high pulse duation (d), surface runoff volume reduction (e), and flow flashiness (RBI calculated using 15-min flow data; f) for Tampa. Plots (a) and (b) show only results for high infiltration soils to improve readability.

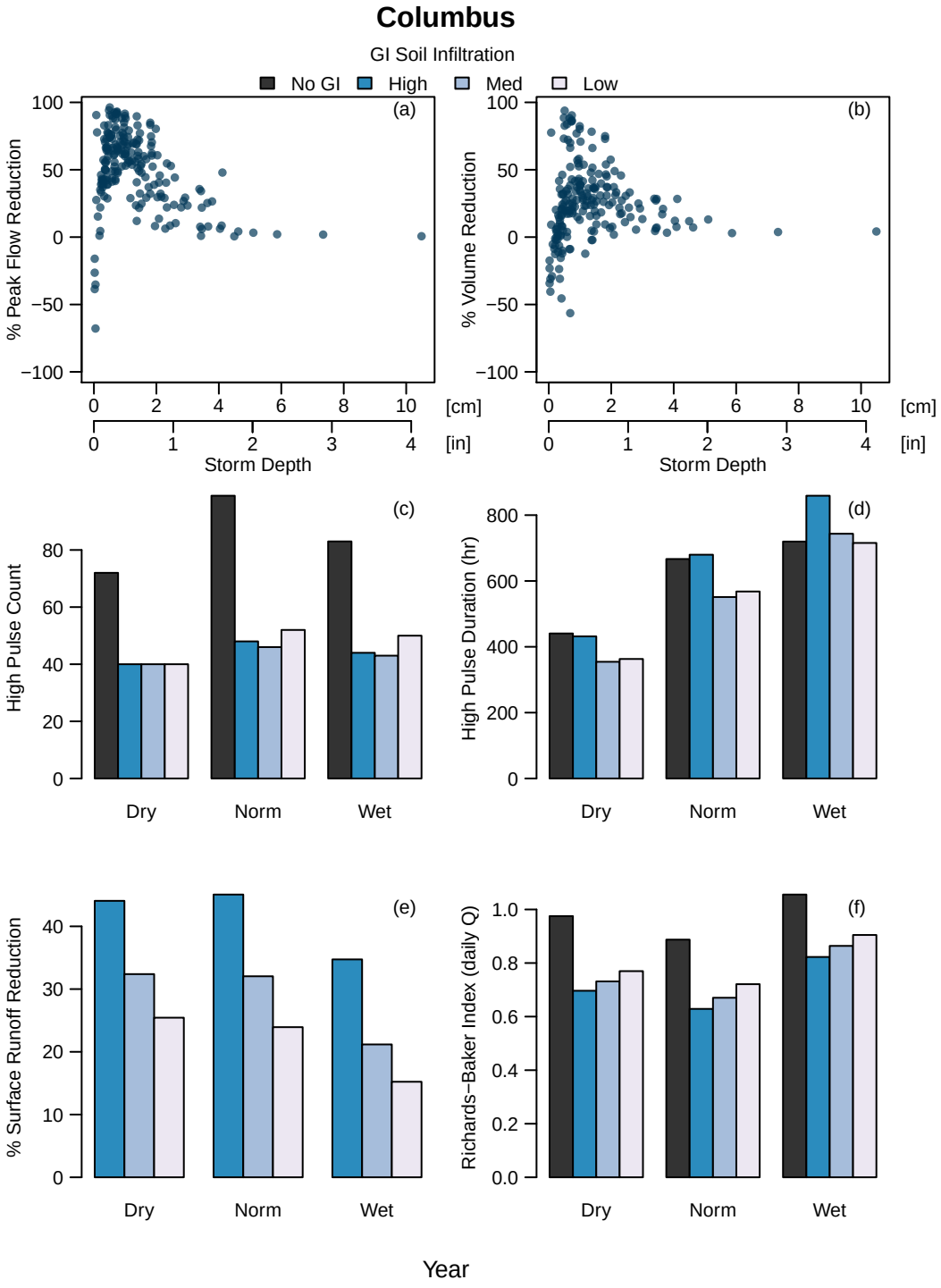

Figure S48: Peak flow reduction (a) and runoff volume reduction (b) by event, high pulse count (c), high pulse duation (d), surface runoff volume reduction (e), and flow flashiness (RBI calculated using 15-min flow data; f) for Columbus. Plots (a) and (b) show only results for high infiltration soils to improve readability.

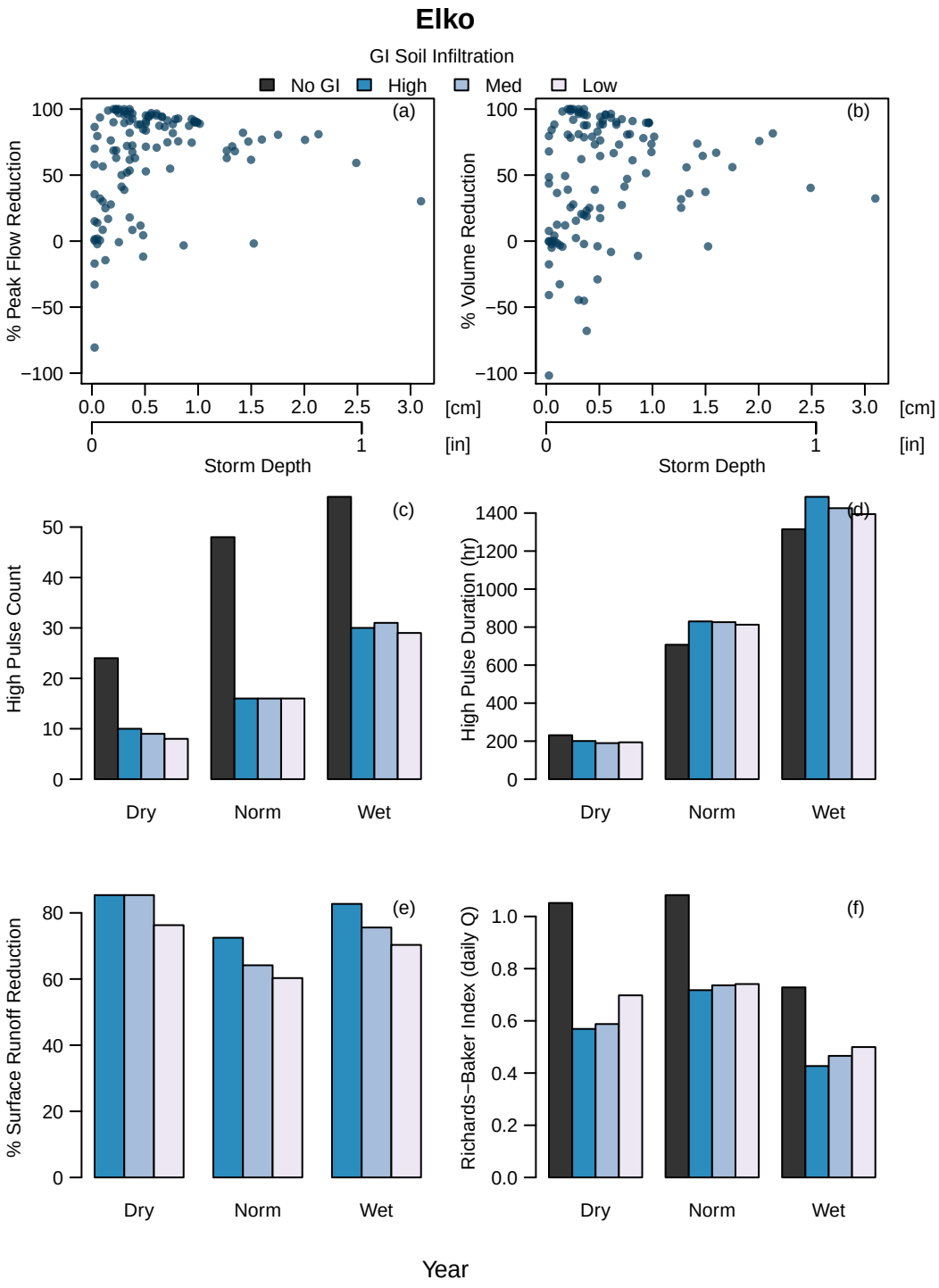

Figure S49: Peak flow reduction (a) and runoff volume reduction (b) by event, high pulse count (c), high pulse duation (d), surface runoff volume reduction (e), and flow flashiness (RBI calculated using 15-min flow data; f) for Elko. Plots (a) and (b) show only results for high infiltration soils to improve readability.

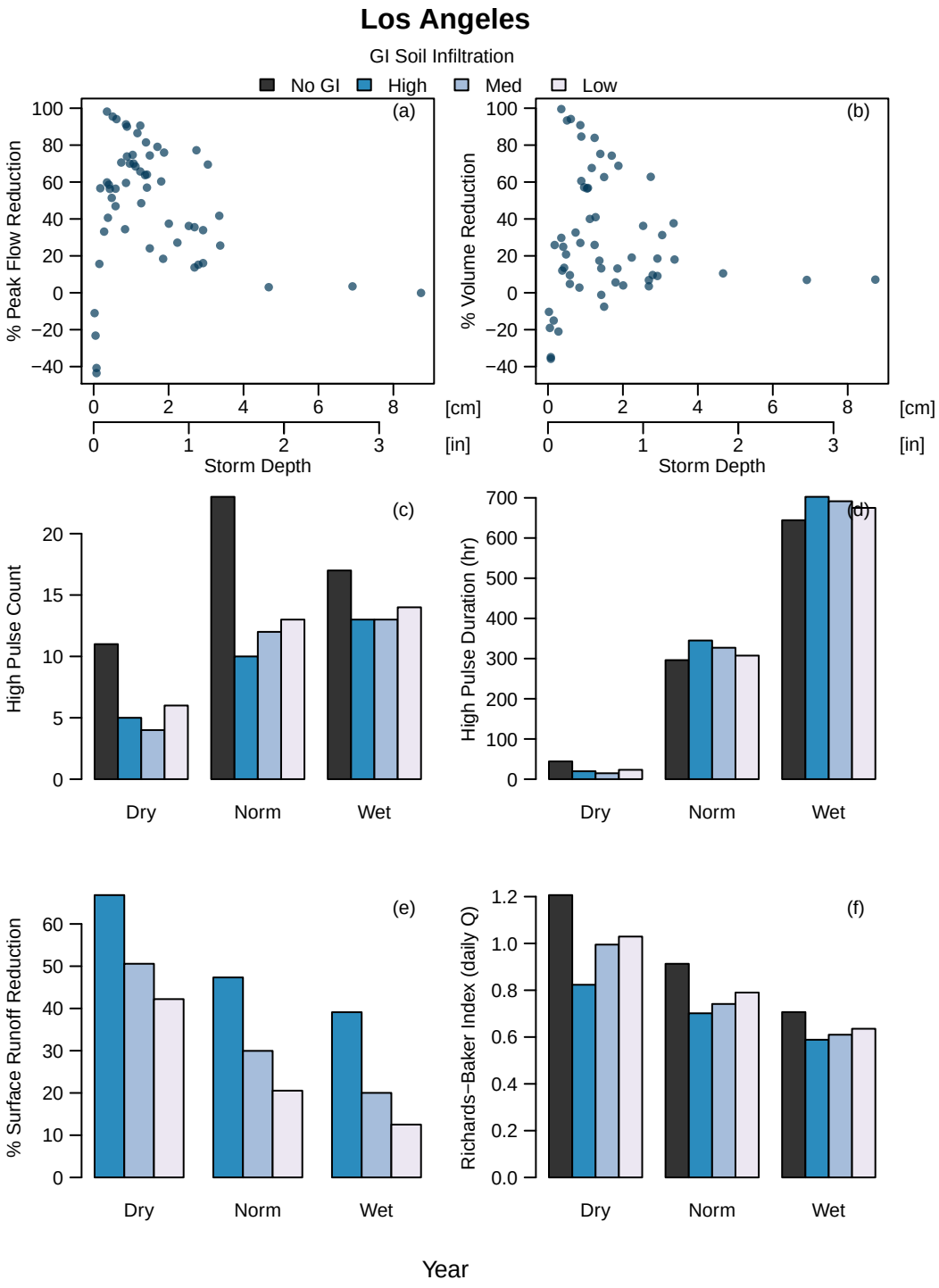

Figure S50: Peak flow reduction (a) and runoff volume reduction (b) by event, high pulse count (c), high pulse duation (d), surface runoff volume reduction (e), and flow flashiness (RBI calculated using 15-min flow data; f) for Los Angeles. Plots (a) and (b) show only results for high infiltration soils to improve readability.

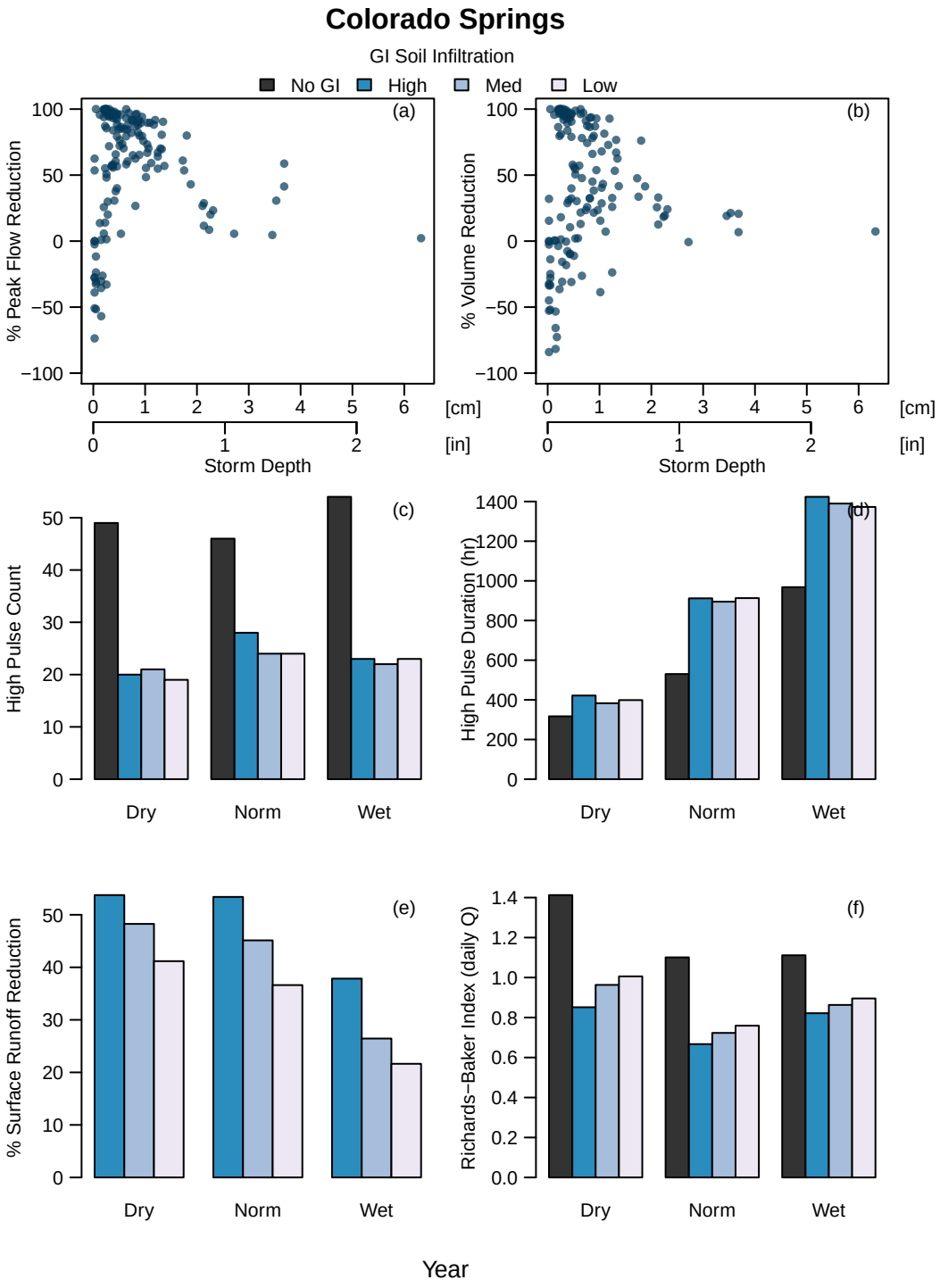

Figure S51: Peak flow reduction (a) and runoff volume reduction (b) by event, high pulse count (c), high pulse duation (d), surface runoff volume reduction (e), and flow flashiness (RBI calculated using 15-min flow data; f) for Colorado Springs. Plots (a) and (b) show only results for high infiltration soils to improve readability.

Green Stormwater Infrastructure Performance

Plots of outflow from of bioretention areas for each city for each of the three years and three soil types simulated. Plots show the percentage of inflow volume, percentage of events, and seasonality of outflow from the bioretention areas associated with high intensity rainfall/runoff and back-to-back storm events.

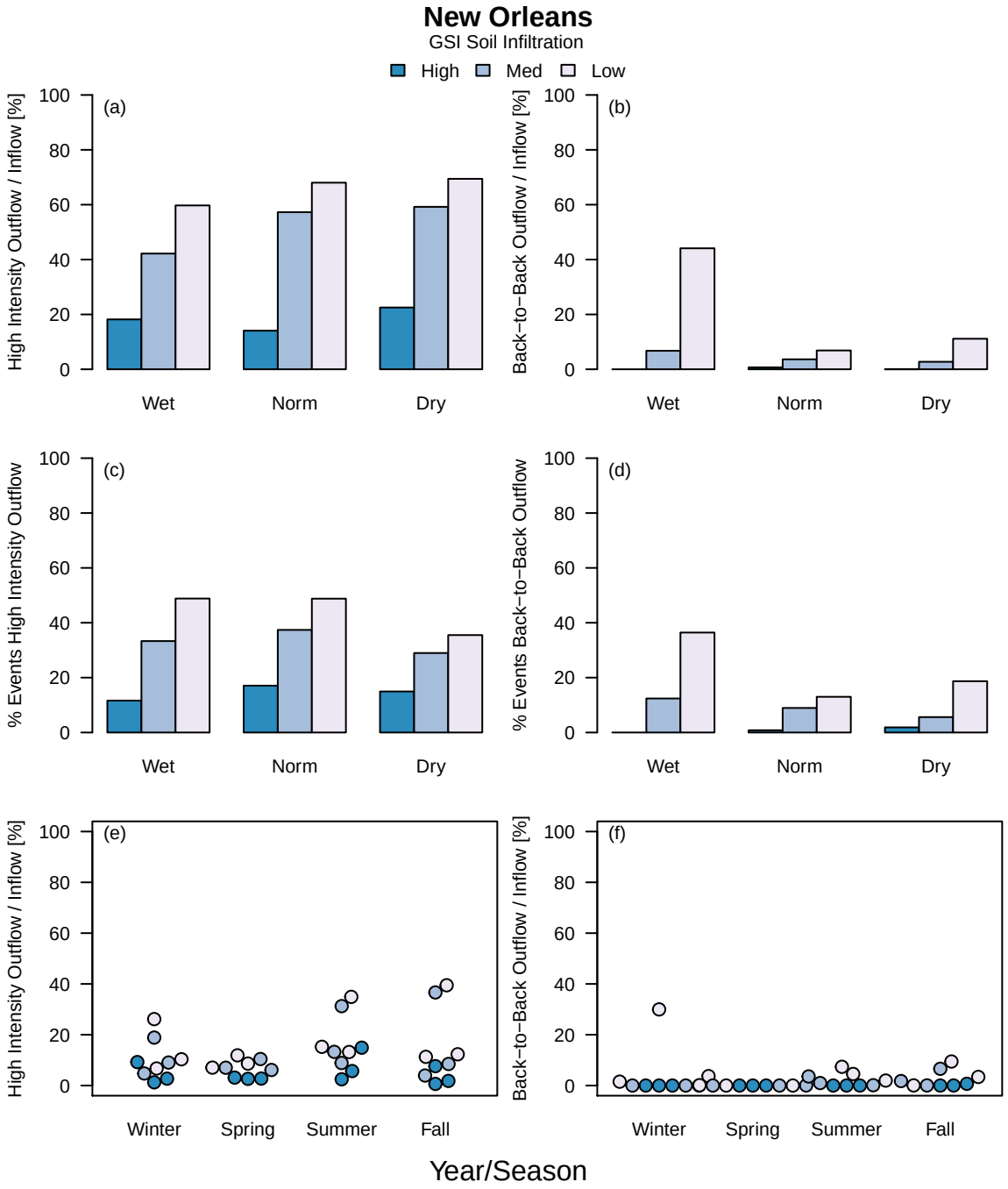

Figure S52: Outflow from high intensity events (a) and back-to-back events (b) as a percent of inflow, percent of storm events with high intensity outflow (c) and back-to-back outflow (d), and otflow from high intensity events (e) and back-to-back events (f) as a percent of inflow, by season, for New Orleans.

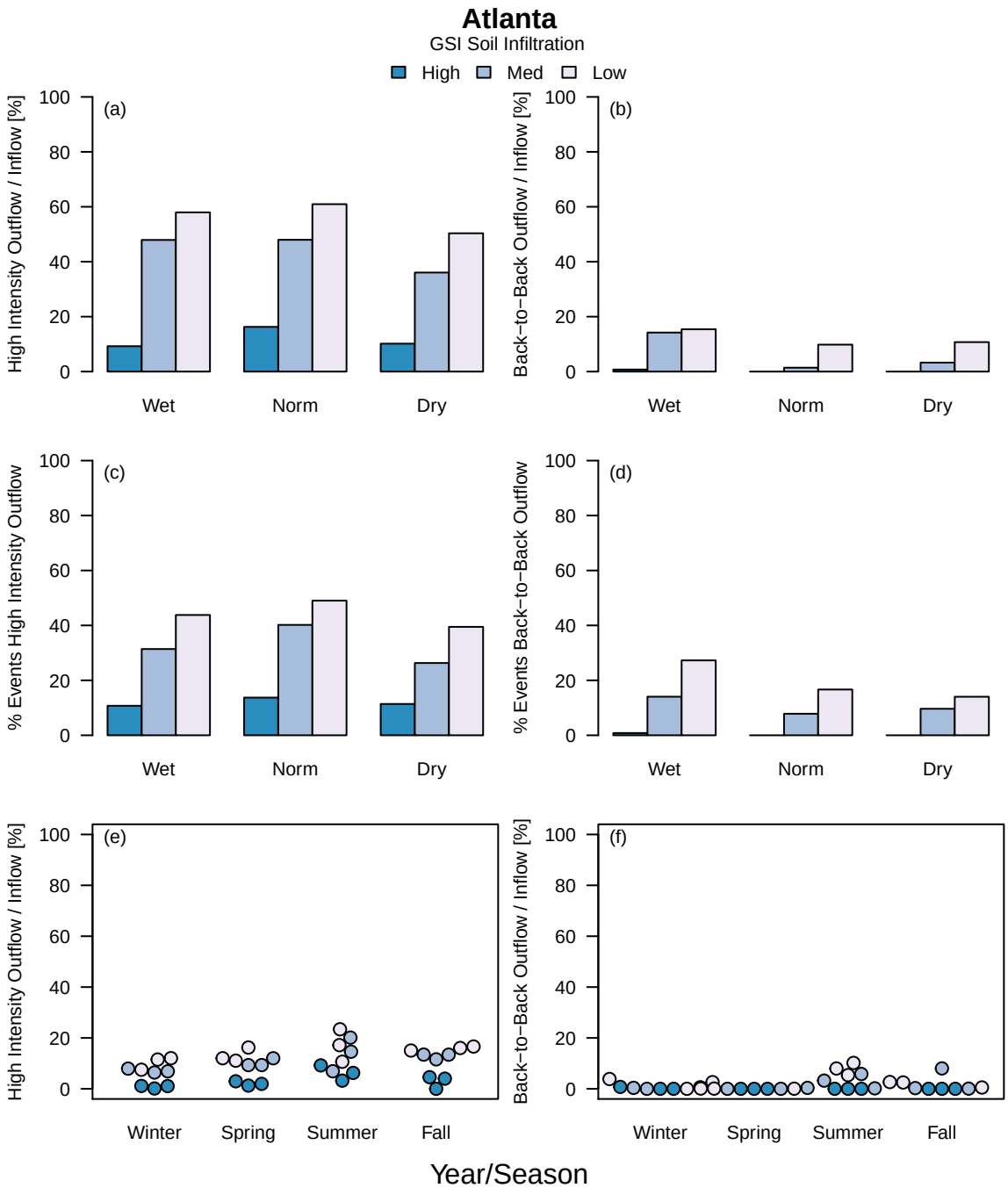

Figure S53: Outflow from high intensity events (a) and back-to-back events (b) as a percent of inflow, percent of storm events with high intensity outflow (c) and back-to-back outflow (d), and otflow from high intensity events (e) and back-to-back events (f) as a percent of inflow, by season, for Atlanta.

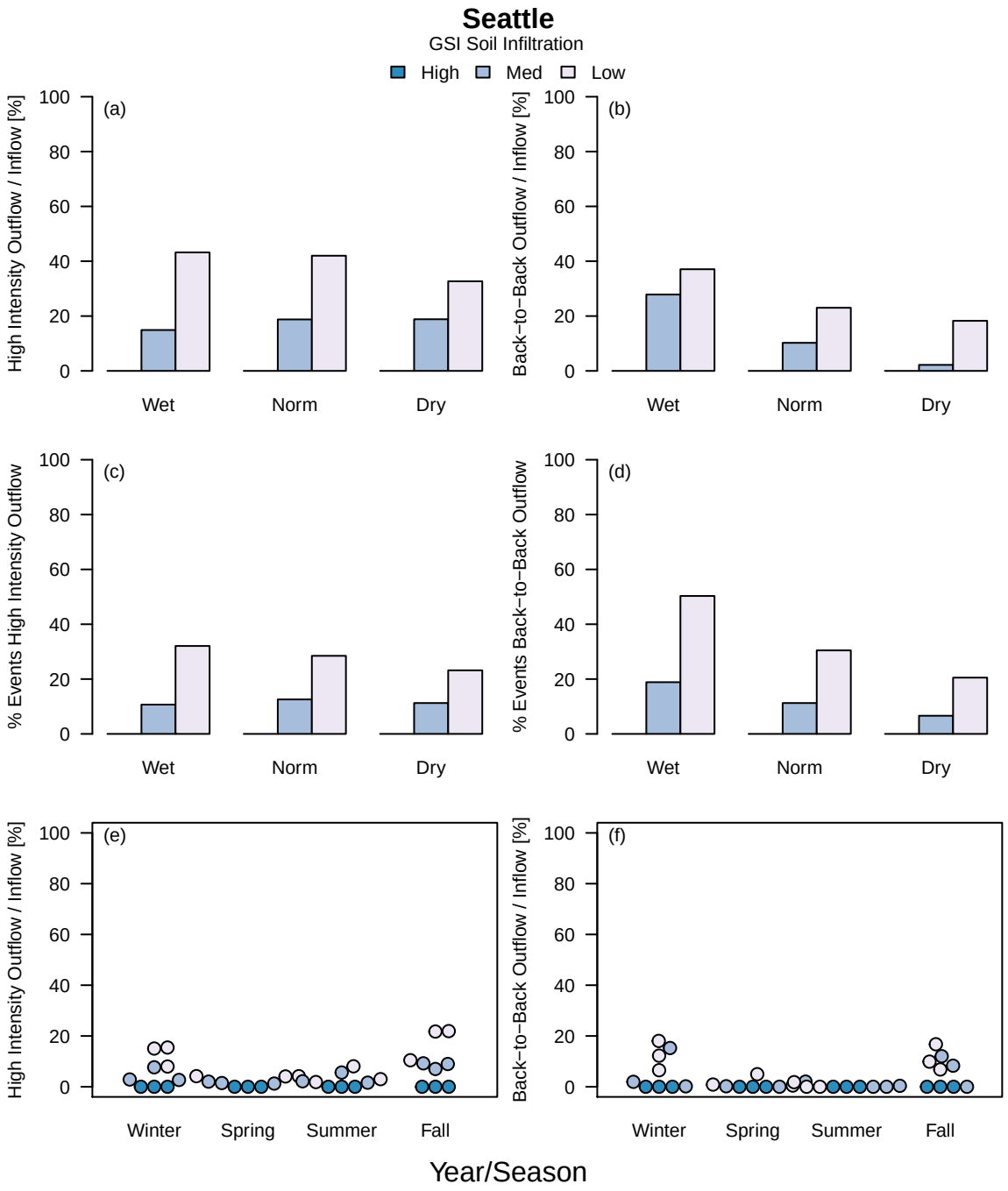

Figure S54: Outflow from high intensity events (a) and back-to-back events (b) as a percent of inflow, percent of storm events with high intensity outflow (c) and back-to-back outflow (d), and otflow from high intensity events (e) and back-to-back events (f) as a percent of inflow, by season, for Seattle.

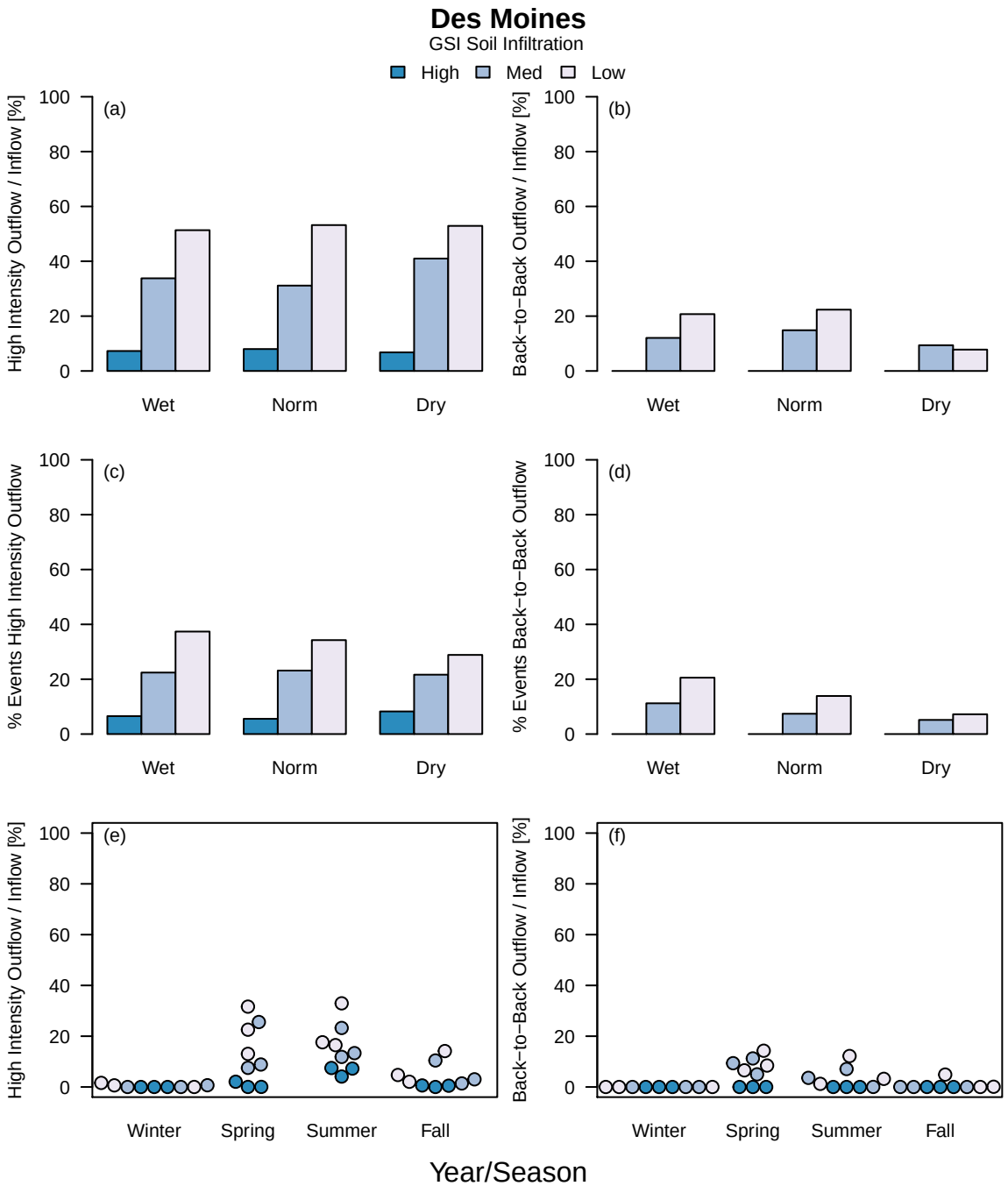

Figure S55: Outflow from high intensity events (a) and back-to-back events (b) as a percent of inflow, percent of storm events with high intensity outflow (c) and back-to-back outflow (d), and otflow from high intensity events (e) and back-to-back events (f) as a percent of inflow, by season, for Des Moines.

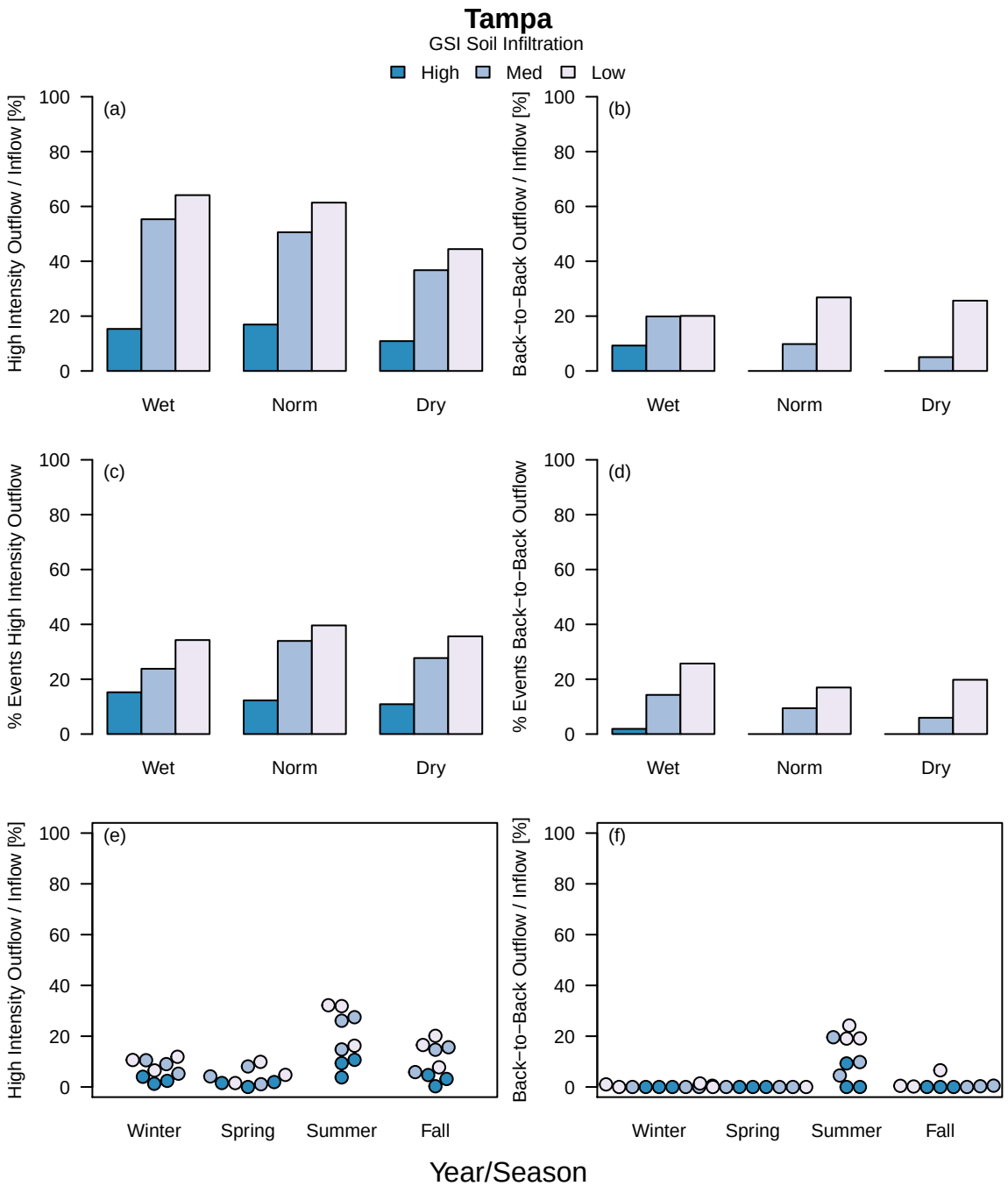

Figure S56: Outflow from high intensity events (a) and back-to-back events (b) as a percent of inflow, percent of storm events with high intensity outflow (c) and back-to-back outflow (d), and otflow from high intensity events (e) and back-to-back events (f) as a percent of inflow, by season, for Tampa.

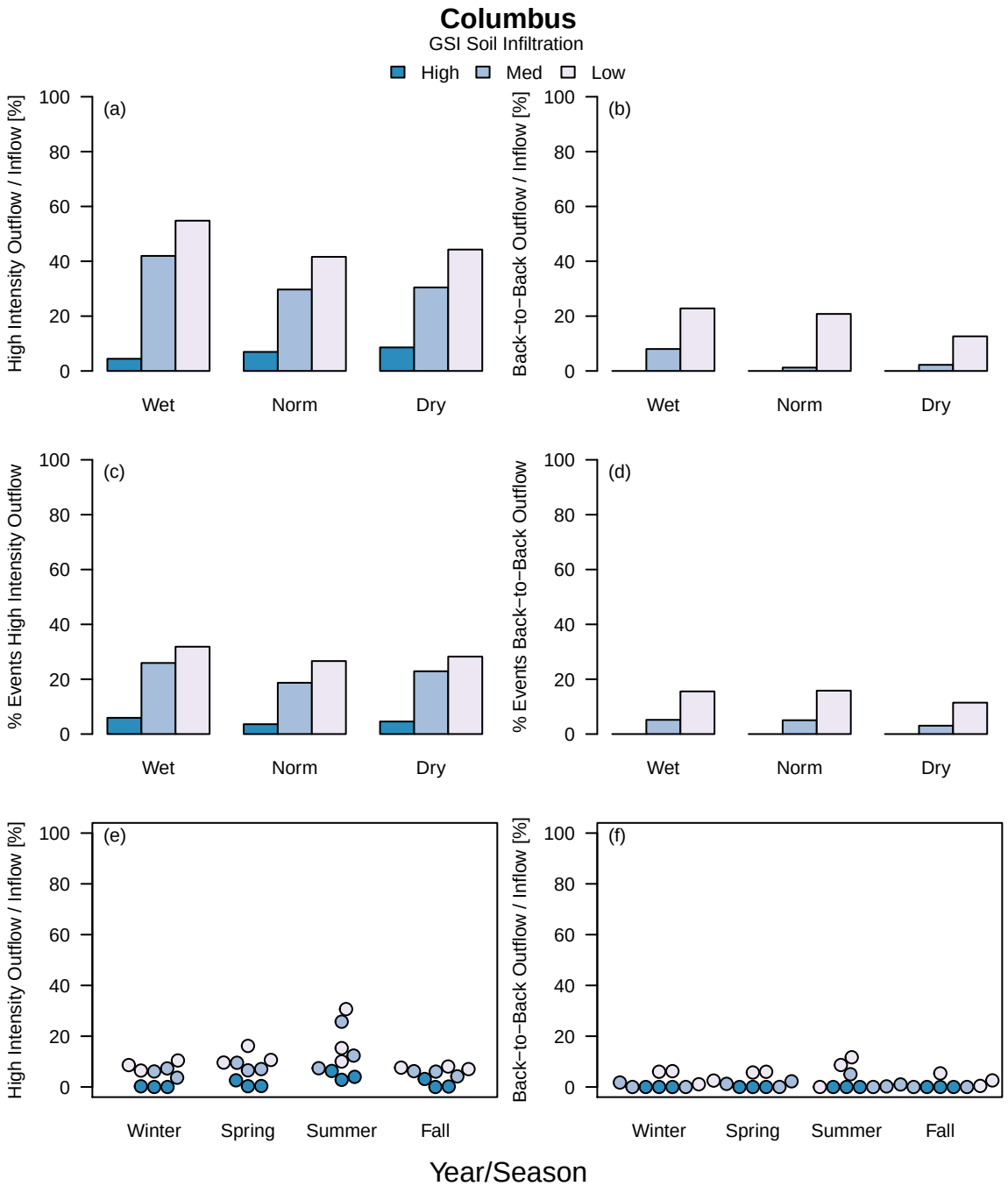

Figure S57: Outflow from high intensity events (a) and back-to-back events (b) as a percent of inflow, percent of storm events with high intensity outflow (c) and back-to-back outflow (d), and otflow from high intensity events (e) and back-to-back events (f) as a percent of inflow, by season, for Columbus.

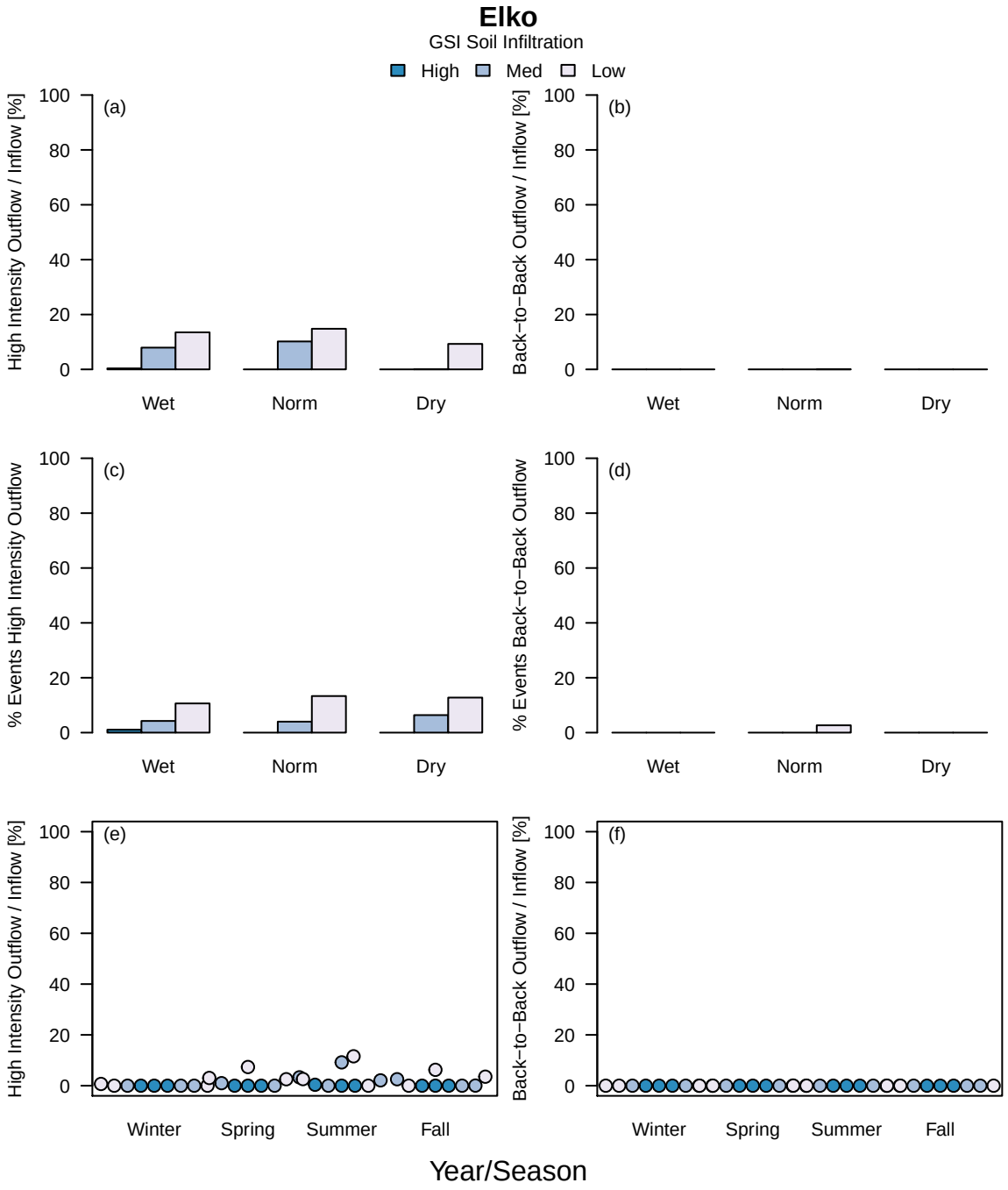

Figure S58: Outflow from high intensity events (a) and back-to-back events (b) as a percent of inflow, percent of storm events with high intensity outflow (c) and back-to-back outflow (d), and otflow from high intensity events (e) and back-to-back events (f) as a percent of inflow, by season, for Elko.

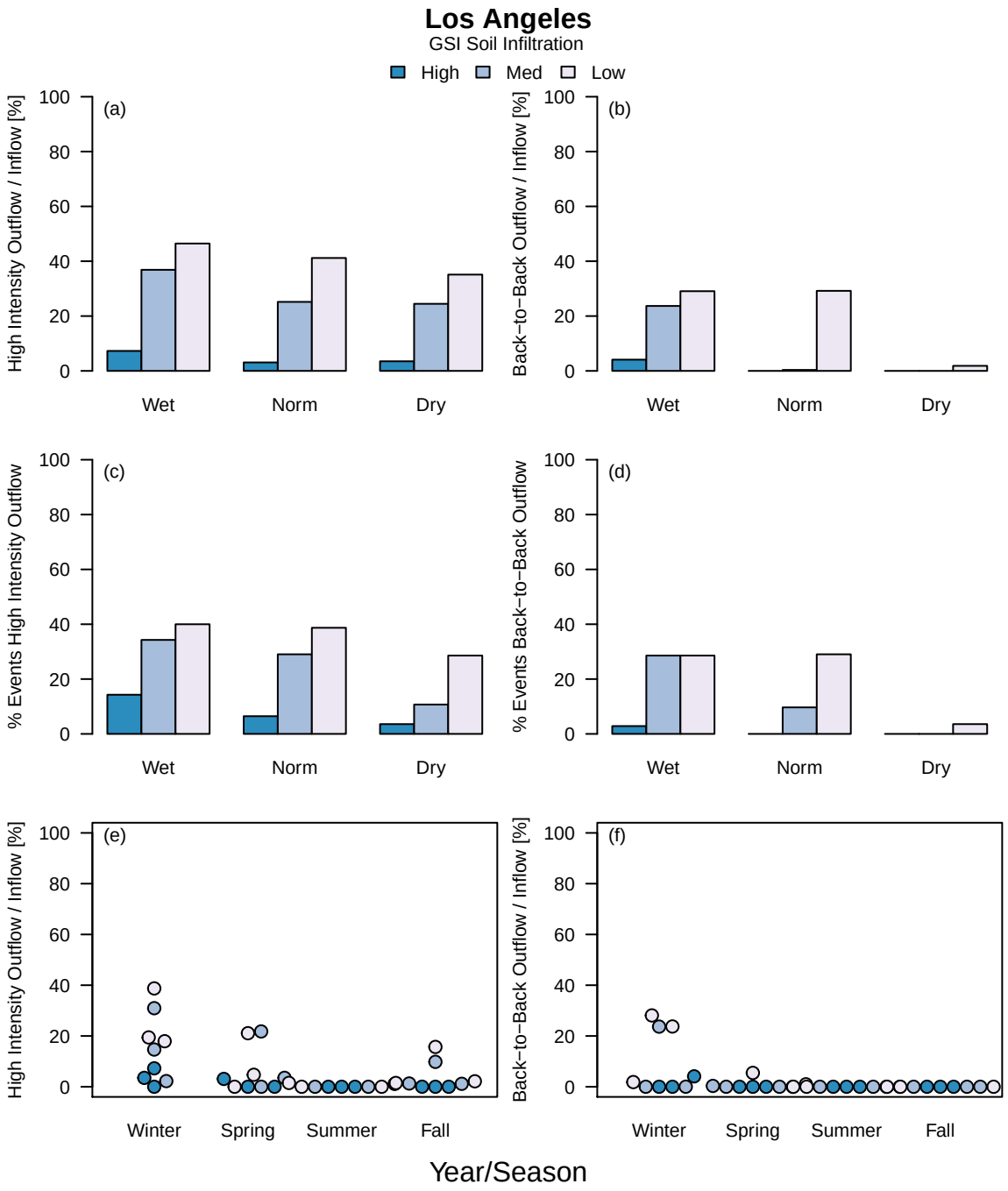

Figure S59: Outflow from high intensity events (a) and back-to-back events (b) as a percent of inflow, percent of storm events with high intensity outflow (c) and back-to-back outflow (d), and otflow from high intensity events (e) and back-to-back events (f) as a percent of inflow, by season, for Los Angeles.

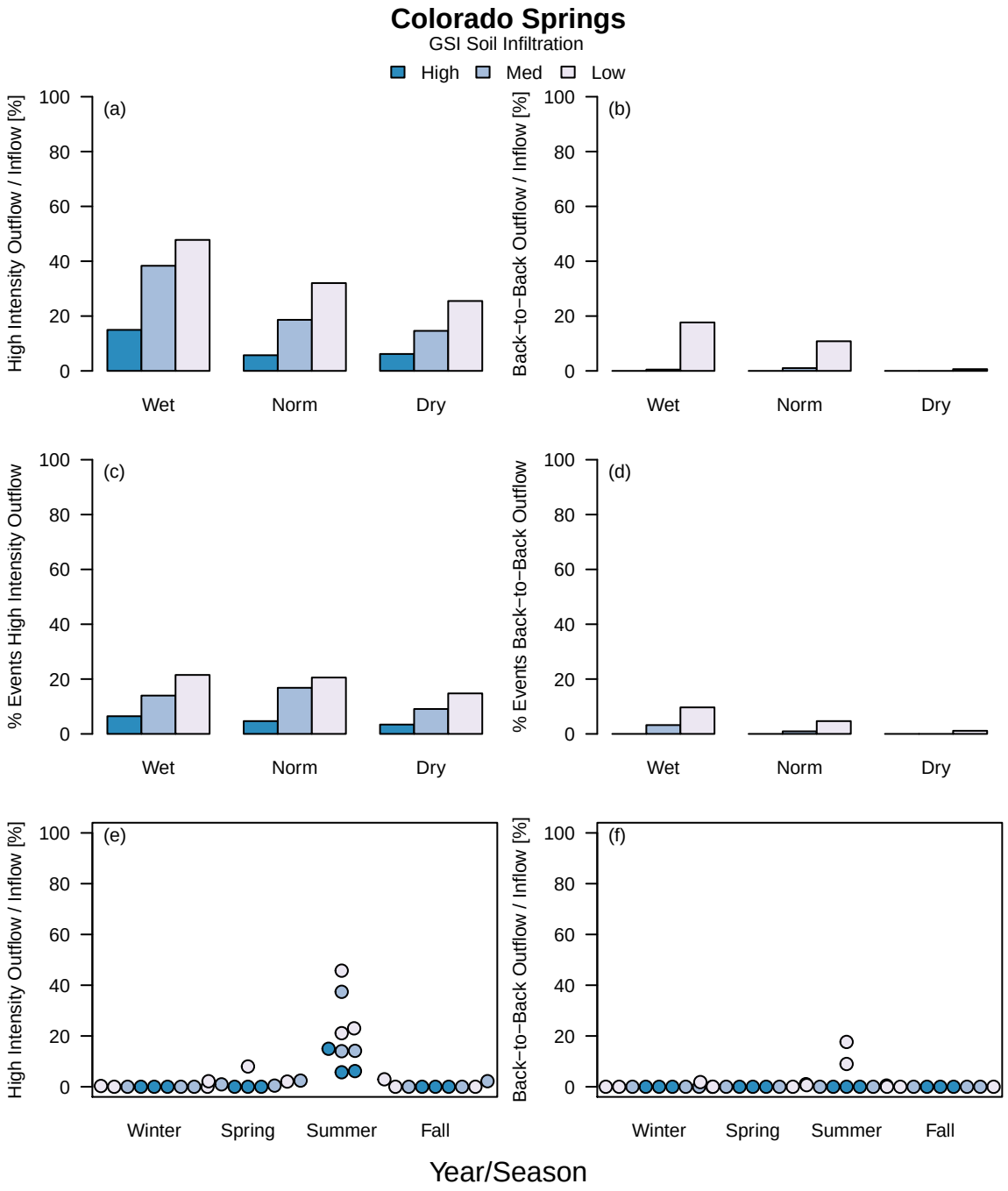

Figure S60: Outflow from high intensity events (a) and back-to-back events (b) as a percent of inflow, percent of storm events with high intensity outflow (c) and back-to-back outflow (d), and otflow from high intensity events (e) and back-to-back events (f) as a percent of inflow, by season, for Colorado Springs.

References

Corripio, J. G. (2019). insol: Solar radiation.

Dourte, D. R., Fraisse, C. W., & Bartels, W. L. (2015). Exploring changes in rainfall intensity and seasonal variability in the Southeastern U.S.: Stakeholder engagement, observations, and adaptation. *Climate Risk Management*, *7*, 11–19. https://doi.org/10.1016/j.crm.2015.02.001

Hamon, W. R. (1960). *Estimating potential evapotranspiration*. *Journal of Irrigation and Drainage Engineering*. Massachusetts Institute of Technology.

Lee, J. G., Nietch, C. T., & Panguluri, S. (2018). Drainage area characterization for evaluating green infrastructure using the Storm Water Management Model. *Hydrology and Earth System Sciences*, *22*(5), 2615–2635. https://doi.org/10.5194/hess-22-2615-2018

Lu, J., Sun, G., McNulty, S. G., & Amatya, D. M. (2005). A comparison of six potential evapotranspiration methods for regional use in the southeastern United States. *Journal of the American Water Resources Association*, *41*(3), 621–633. https://doi.org/10.1111/j.1752-1688.2005.tb03759.x

Maechler, M., Rousseeuw, P., Struyf, A., Hubert, M., & Hornik, K. (2019). cluster: Cluster analysis basics and extensions.

Walsh, R. P. D., & Lawler, D. M. (1981). Rainfall Seasonality: Description, Spatial Patterns and Change Through Time. *Weather*, *36*(7), 201–208. https://doi.org/10.1002/j.1477-8696.1981.tb05400.x